UNIVERSITA' VITA-SALUTE SAN RAFFAELE

CORSO DI DOTTORATO DI RICERCA INTERNAZIONALE

IN MEDICINA MOLECOLARE

Curriculum in Experimental and Clinical Medicine

TARGETING TRANSFERRIN RECEPTOR 2: A NOVEL ERYTHROPOIESIS STIMULATING APPROACH IN ANEMIA OF CHRONIC KIDNEY DISEASE AND OTHER ANEMIAS

DoS: Dr. Antonella Nai

Second Supervisor: Dr. Igor Theurl

Tesi di DOTTORATO di RICERCA di Violante Olivari

matr. 015846

Ciclo di dottorato XXXV

SSD MED/15

Anno Accademico 2021/2022

UNIVERSITA' VITA-SALUTE SAN RAFFAELE

CORSO DI DOTTORATO DI RICERCA INTERNAZIONALE

IN MEDICINA MOLECOLARE

Curriculum in Experimental and Clinical Medicine

TARGETING TRANSFERRIN RECEPTOR 2: A NOVEL ERYTHROPOIESIS STIMULATING APPROACH IN ANEMIA OF CHRONIC KIDNEY DISEASE AND OTHER ANEMIAS

DoS: Dr. Antonella Nai

Second Supervisor: Dr. Igor Theurl

Tesi di DOTTORATO di RICERCA di Violante Olivari

matr. 015846

Ciclo di dottorato XXXV

SSD MED/15

Anno Accademico 2021/2022

CONSULTAZIONE TESI DI DOTTORATO DI RICERCA

La sottoscritta / *I* Violante Olivari

Matricola / *registration number* 015846

nata a/ *born at* Alzano Lombardo (BG)

il/*on* 07/11/1993

autore della tesi di Dottorato di ricerca dal titolo / *author of the PhD Thesis titled*

TARGETING TRANSFERRIN RECEPTOR 2:

A NOVEL ERYTHROPOIESIS STIMULATING APPROACH

IN ANEMIA OF CHRONIC KIDNEY DISEASE AND OTHER ANEMIAS

☐ AUTORIZZA la Consultazione della tesi / AUTHORIZES *the public release of the thesis*

☒ NON AUTORIZZA la Consultazione della tesi per 12 mesi /DOES NOT AUTHORIZE *the public release of the thesis for* 12 *months*

a partire dalla data di conseguimento del titolo e precisamente */ from the PhD thesis date, specifically*

Dal / *from* ...../...../..... Al / *to* ...../...../.....

Poiché /*because*:

□ l'intera ricerca o parti di essa sono potenzialmente soggette a brevettabilità/ *The whole project or part of it might be subject to patentability;*

☒ ci sono parti di tesi che sono già state sottoposte a un editore o sono in attesa di pubblicazione/ *Parts of the thesis have been or are being submitted to a publisher or are in press;*

□ la tesi è finanziata da enti esterni che vantano dei diritti su di esse e sulla loro pubblicazione/ *the thesis project is financed by external bodies that have rights over it and on its publication.*

Data /Date 01/11/2022 Firma /Signature Violante Oliver

DECLARATION

This thesis has been:

- composed by myself and has not been used in any previous application for a degree. Throughout the text I use both 'I' and 'We' interchangeably.
- has been written according to the editing guidelines approved by the University.

Permission to use images and other material covered by copyright has been sought and obtained (Italian legislative Decree no. 68/2003).

All the results presented here were obtained by myself, except for:

1) FACS analysis of erythroid differentiation (Results, chapter 3.1.2; 3.2.2; 3.3.3 and 3.5.3, Figure 16, 21, 29, 39) were processed by Dr. Maria Rosa Lidonnici, Gene Transfer into Stem Cell Unit, SR-TIGET, San Raffaele Scientific Institute, Milan, Italy.
2) μ-Computed Tomography analysis (Results, chapter 3.4, Figure 34, 35, 36) were performed in collaboration with by Sandra Hippauf, Bone Lab, Department of Medicine III, Technische Universität Dresden, Dresden, Germany.
3) Malaria experiments (Results, chapter 3.5, Figure 41, 42, 43) were performed in collaboration with Simona Maria Di Modica, Regulation of Iron Metabolism Unit, Division of Genetics and Cell Biology, San Raffaele Scientific Institute, Milan, italy.
4) Histology and urea biochemistry analyses (Results, chapter 3.1.1, 3.1.3, 3.2.3 and 3.3.4, Figure 13, 18, 23, 32) were processed by Amleto Fiocchi and Michele Raso respectively, OSR Mouse Clinic, San Raffaele Scientific Institute, Milan, Italy.

Part of the work presented in this thesis has been submitted as original article.

All sources of information are acknowledged by means of reference.

Images were created with Biorender.com

ACKNOWLEDGEMENTS

I am extremely grateful to my Director of Study Dr. Antonella Nai for the precious advice and mentoring, and for support and patience. I appreciate everything she taught me and all the great opportunities she gave me during these years.

I acknowledge my second supervisor Dr. Igor Theurl for criticisms and suggestions and my tutor Dr. Stefano Crippa.

I am deeply thankful to Professor Clara Camaschella for her inspiring guidance and support during these years.

I am thankful Dr. Maria Rosa Lidonnici, Francesca Tiboni and Dr. Giuliana Ferrari (Gene Transfer into Stem Cell Unit, SR-TIGET, San Raffaele Scientific Institute, Milan, Italy) for murine erythropoiesis analysis.

I thank Dr. Jessica Bordini and Dr. Alessandro Campanella (Division of Experimental Oncology, San Raffaele Scientific Institute, Milan, Italy) for support on the malaria project.

I thank Michele Raso for biochemistry analyses and Amleto Fiocchi for histological analyses (OSR Mouse Clinic, Milan, Italy).

I am grateful to Dr. Martina Rauner for her hospitality and cordiality during the three months she hosted me in her lab. I thank all the members of the Bone Lab, especially Sandra Hippauf for the help with μ-Computed Tomography analysis (Department of Medicine III, Technische Universität Dresden, Dresden, Germany).

I acknowledge Dr. Shuling Guo and Dr. Mariam Aghajan (Ionis Pharmaceutical Inc., Carlsbad CA, USA) for providing ASOs.

I would like to acknowledge Società Italiana di Ematologia Sperimentale (SIES) for the “Borsa di perfezionamento 2020-2021” that allowed me to work on the bone part of this study. I would like to thank the grants that supported this work: Ospedale San Raffaele (OSR) Seed Grant 2017 and American Society of Hematology (ASH) Global Research Award.

I am extremely grateful to all the members of the Regulation of Iron Metabolism Unit, in particular to Simona Maria Di Modica, for her help with the malaria project, and to Dr. Laura Silvestri and Dr. Alessia Pagani for criticisms and suggestions.

Finally, I would like to honor and acknowledge all the animals that served in this study.

ABSTRACT

Anemia is a pathologic condition caused by the reduced production of red blood cells (RBCs) and hemoglobin. After iron-deficiency, systemic inflammation is the second contributor to the worldwide burden of anemia. Proinflammatory cytokines decrease erythroblast sensitivity to erythropoietin (EPO) on one side, and increase hepcidin levels on the other, sequestering iron in stores and leading to iron restriction. Anemia of inflammation can be caused both by chronic infections and by systemic diseases. Malaria anemia is a peculiar form of anemia of inflammation due to *Plasmodium* infection in which systemic inflammation coexists with prominent hemolysis, while anemia of Chronic Kidney Disease (CKD) is characterized by impaired EPO production and iron loss in urine, which follow progressive renal damage, associated to sustained inflammation.

Standard therapy for anemia based on EPO-mimetics (in combination with iron supplementation for renal anemia) is associated to several off-target effects due to EPO interaction with its receptor in non-erythroid organs, calling for the identification of novel therapeutic strategies.

Transferrin Receptor 2 (TFR2) is a recently identified regulator of the iron-erythropoiesis crosstalk. *Tfr2* deletion in the liver reduces hepcidin production increasing iron absorption, while its inactivation in the bone marrow (BM) increases erythroid EPO sensitivity and RBCs production.

In this study, we proved that BM specific *Tfr2* deletion promotes erythropoiesis and ameliorates anemia in mice with CKD, sterile inflammation and malaria, without increasing EPO levels per se. In CKD, characterized by a real, rather than a functional, iron-deficiency, the combined erythroid and hepatic *Tfr2* deletion represented an effective tool to simultaneously promoting RBCs production and iron absorption, thus leading to a more prolonged amelioration of anemia.

Overall, our results provide the proof of principle that *Tfr2* targeting, in the erythroid and hepatic compartments based on the pathophysiology of the disease, is a promising therapeutic option for balancing erythropoiesis and iron availability in different forms of anemia, without affecting EPO levels.

TABLE OF CONTENTS

ACRONYMS AND ABBREVIATIONS

AKT	Protein Kinase B
ALAS2	δ-aminolevulinic acid synthase-2
ASOs	Antisense Oligonucleotides
BasoEry	Basophilic Erythroblast
BCLXL	B cell lymphoma extra large
BFU-e	Burst Forming Unit erythroid
BM	Bone Marrow
BMP	Bone Morphogenetic Protein
BMPR	BMP Receptor
BMP-RE	BMP Responsive Element
BMT	Bone Marrow Transplantation
CD45	Cluster of differentiation 45
CFU-e	Colony-forming unit erythroid
CKD	Chronic Kidney Disease
CLP	Common Lymphoid Progenitor
CMP	Common Myeloid Progenitor
CTRL	Control
DMT1	Divalent Metal Transporter 1
EPO	Erythropoietin
EPOR	Erythropoietin Receptor
ERFE	Erythroferrone
ERK	Extracellular signal Regulated Kinase
ESA	Erythropoiesis Stimulating Agents
FACS	Fluorescent Activated Cell Sorter
FDA	Food and Drugs Administration
Fe	Iron
Fe-S	Iron-Sulfur
FLVCR1	Feline Leukemia Virus Subgroup Receptor 1
FPN	Ferroportin
GAlNAc	N-acetilgalactosamine
GAPDH	Glyceraldehyde-3-Phosphate Dehydrogenase
HAMP	Hepcidin encoding gene
HB	Hemoglobin
HEPH	Hephaestin
HFE	High Ferro
HH	Hereditary Hemochromatosis
HIF	Hypoxia Inducible Factor
HIR	Heme Regulated Inhibitor of translation
HJV	Hemojuvelin
HLA	Human Leucocyte Antigens
HMOX1	Hemoxygenase 1
Holo-TF	Iron-loaded Transferrin
HPRT1	Hypoxanthine Phosphoribosyl Transferase 1
HRE	Hypoxia Responsive Elements
HSCs	Hematopoietic Stem Cells

ID1	Inhibitor of DNA Binding 1
IE	Ineffective Erythropoiesis
IL-1b	Interleukin 1-β
IL-6	Interleukin 6
IRE	Iron Responsive Element
IRIDA	Iron Refractory Iron Deficiency Anemia
JAK2	Janus Kinase 2
KIC	Kidney Iron Content
KIM-1	Kidney Injury Molecule 1
KO	Knock-out
LCKO	Liver Conditional Knock-Out
LCN2	Lipocalin 2
LIC	Liver Iron Content
LPS	Lipopolysaccharides
LSECs	Liver Sinusoidal Endothelial Cells
MAPK	Mitogen Activated Protein Kinase
MCH	Mean Corpuscular Hemoglobin
MCV	Mean Corpuscular Volume
MEL	Myeloid Erythro-Leukemia
MEP	Megakaryocyte Erythroid Precursor
MFRN1	Mitoferrin
MHC	Major Histocompatibility Complex
MPP	Megakaryocyte Potent Precursor
NCOA4	Nuclear Receptor Coactivator 4
NF-kB	Nuclear Factor Kappa- light-chain-enhancer of activated B cells
NTBI	Non-Transferrin Bound Iron
NTD	Non-Transfusion Dependent
OrthoEry	Orthochromatic Erythroblast
PAI-1	Plasminogen Activator Inhibitor 1
PCC	Plasmodium chabaudi chabaudi
PI3K	Phosphatidyl-Inositol 3-Kinase
PHDs	Prolyl hydroxylase domain containing enzymes
PHIs	Prolyl hydroxylase inhibitors
PIC	Pancreas Iron Content
PolyEry	Polychromatic Erythroblast
ProEry	Pro Erythroblast
RBCs	Red Blood Cells
REPCs	Renal Erythropoietin Producing Cells
RET	Reticulocytes
SAA1	Serum Amyloid A1
SIC	Spleen Iron Content
SMAD	Small Mother Against Decapentaplegic
STAT	Signal Transducer And Activator Of Transcription
TF	Transferrin
TFR1	Transferrin Receptors 1
TFR2	Transferrin Receptor 2
$TFR2^{BMKO}$	Transferrin Receptor 2 Bone Marrow Knock-out

$TFR2^{BMWT}$	Transferrin Receptor 2 Bone Marrow Wild-type
TGF-β	Transforming Growth Factor β
TMPRSS6	Transmembrane Serine Protease 6
TNF-α	Tumor Necrosis Factor-α
UTR	Untranslated Region
VHL	von Hippel-Lindau
WT	Wild Type
μ-CT	μ-Computed Tomography

LIST OF FIGURES AND TABLES

1. INTRODUCTION

1.1 Mammalian erythropoiesis

1.1.1 Early and terminal erythropoiesis: a brief overview

Two-hundred billions red blood cells (RBCs) are produced daily in the bone marrow (BM) of healthy adults and then released in the peripheral blood (Higgins, 2015) through a tightly regulated multi-step process named erythropoiesis.

During early erythropoiesis, hematopoietic stem cells (HSCs) differentiate to multi-potent progenitors (MPPs), that lack self-renewal capacity but preserve full lineage differentiation potential. MPPs generate common lymphoid progenitors (CLPs) and common myeloid progenitors (CMPs), and the latter give rise to megakaryocyte/erythroid progenitors (MEPs) (Palis, 2014; Zivot *et al*, 2018; Fathman *et al*, 2011). MEPs differentiate into burst-forming unit-erythroid (BFU-E) and colony-forming unit-erythroid (CFU-E) cells. During terminal erythropoiesis, CFU-E evolve into pro-erythroblasts (ProEry), basophilic (BasoEry), polychromatic (PolyEry) and orthochromatic (OrthoEry) erythroblasts and then into reticulocytes and mature RBCs (Palis, 2014; Zivot *et al*, 2018) (**Figure 1**). These final phases are characterized by gradual reduction of cell size, progressive hemoglobin accumulation, decreased RNA content and nuclear condensation, culminating into enucleation at the stage of late OrthoEry (Hattangadi *et al*, 2011). In the BM, erythroblasts maturation occurs within structures named “erythroblastic islands”, composed by a central “nurse macrophage” surrounded by several erythroblasts at various differentiation stages. Macrophages promote erythroblasts proliferation and ingest nuclei extruded by late OrthoEry to form reticulocytes, characterized by reduced cell volume, loss of residual organelles and a biconcave shape (Korolnek & Hamza, 2015; Zivot *et al*, 2018). Production of mature RBCs is the final step occurring in the bloodstream, where erythrocytes circulate for 120 and 45 days in humans and mice, respectively (An *et al*, 2015).

The balance between reticulocytes production and senescent RBCs removal is maintained primarily by splenic macrophages, that sustain steady-state RBCs levels

replacing an average of $2.2x10^{11}$ RBCs/day (Palis, 2014; Korolnek & Hamza, 2015; Hattangadi *et al*, 2011).

Murine erythropoiesis is characterized by the same differentiation stages. However, while in humans the BM is the predominant erythropoietic organ, in mice the spleen also plays a key role, mainly in stress conditions. Moreover, together with longer life span, human erythrocytes have greater mean corpuscular volume (90 *vs* 52 fL) and higher oxygen affinity (P50 25 *vs* 40 mm Hg) (An *et al*, 2015).

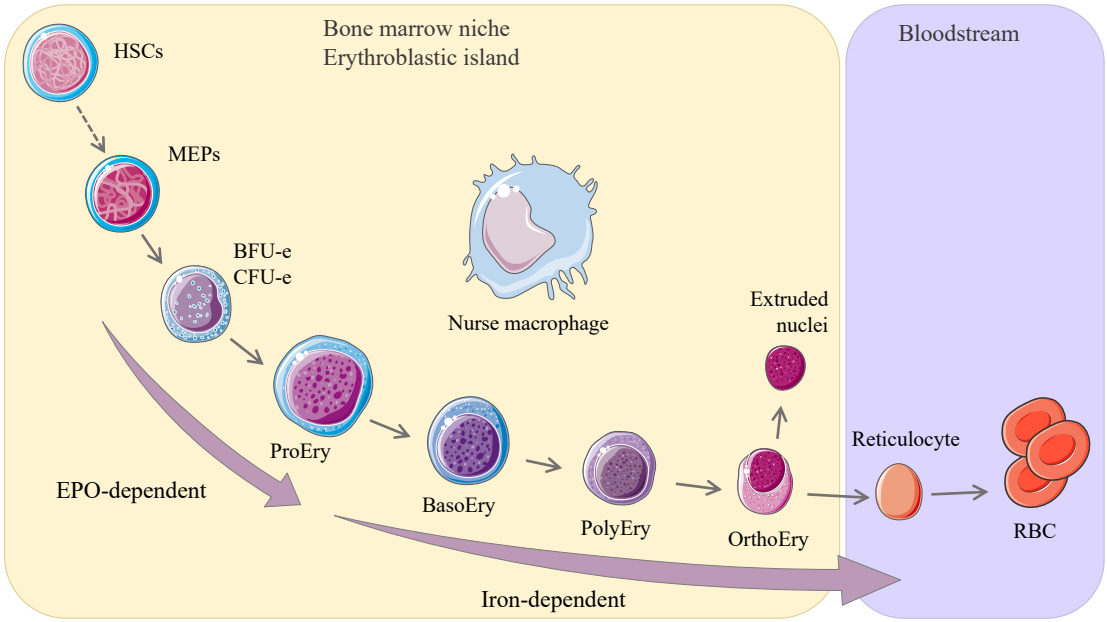

Figure 1. Schematic overview of erythroid differentiation. *Progression from hematopoietic stem cells (HSCs) to red blood cells (RBCs). Megakaryocyte/erythrocyte progenitor (MEPs) derive from HSCs and give raise to burst-forming unit- erythroid (BFU-e) and colony-forming unit-erythroid (CFU-e) cells. CFU-e differentiate into pro-erythroblasts (ProEry), basophilic (BasoEry), polychromatic (PolyEry) and orthochromatic (OrthoEry) erythroblasts and then into reticulocytes and mature RBCs. Nurse macrophages located in the bone marrow niche support erythroid cells proliferation and maturation. Erythropoietin (EPO)- and iron-dependent phases are indicated. Final maturation from reticulocytes to mature erythrocytes occurs in the bloodstream.*

1.1.2 Erythropoietin and its pathway

Erythropoietin (EPO), the master regulator of erythropoiesis, is a glycoprotein cytokine produced by the liver during fetal development. After birth, the main site of EPO production is the kidney (Bondurant & Koury, 1986), in specialized fibroblast-like cells located in the interstitium of outer medulla and cortex, named renal erythropoietin producing cells (REPCs) (Koury *et al*, 1988, 1989; Maxwell *et al*, 1993).

Hypoxia is the main physiological condition that regulates EPO production (Haase, 2010; Wenger & Kurtz, 2011) through the hypoxia inducible factor (HIF), a heterodimeric nuclear transcription factor composed by an O_2-dependent α subunit (isoforms 1α, 2α or 3α) and a constitutive β subunit.

During normoxia, prolyl hydroxylase domain containing enzymes (PHDs) hydroxylate conserved proline residues in HIF-α subunits, leading to von Hippel-Lindau tumor suppressor protein (VHL) binding and to the subsequent E3 ligase complex-mediated HIF-α degradation. When cellular oxygen levels are low, PHDs' function is inhibited and VHL binding to HIF prevented. In this way, α subunits are stabilized and bind the hypoxia responsive elements (HRE) on *EPO* promoter, inducing its transcription (Shah & Xie, 2014). HIF-2α induces *Epo* expression also in the liver (Rankin *et al*, 2007; Warnecke *et al*, 2004; Haase, 2010).

Importantly, EPO production is regulated not only by oxygen levels, but also by iron availability through the iron regulatory proteins (IRPs) system. When iron is low, IRP1 and IRP2 bind iron responsive elements (IRE) on untranslated regions (UTRs) of mRNAs encoding for proteins involved in systemic iron modulation. IRPs-IRE binding increases mRNA stability when occurs at 3'-UTR, while blocks translation when at 5'-UTR. Thus, if systemic iron levels are low and not adequate to sustain enhanced erythropoiesis, IRP1 binds the IRE sequence in *HIF-2α* 5'-UTR, inhibiting its translation and *EPO* transcription (Shah & Xie, 2014; Muckenthaler *et al*, 2017).

EPO regulates erythropoiesis mainly at the stages between early committed erythroid precursors and proEry. EPO receptor (EPOR) is a transmembrane homodimeric glycoprotein present at low levels on the surface of BFU-E. Its expression gradually increases until BasoEry, and then decreases during erythroid differentiation being absent on reticulocytes and RBCs (Bhoopalan *et al*, 2020).

EPO binding to its receptor leads to conformational changes critical for Janus kinase 2 (JAK2) association to the complex and phosphorylation. Phosphorylated JAK2 activates several intracellular signaling pathways among which Signal transducer and activator of transcription 5 (STAT5) (Socolovsky *et al*, 1999; Cui *et al*, 2004), that translocates into the nucleus and activates the transcription of genes involved in erythroid

cells survival, proliferation and differentiation, as B-cell lymphoma extra-large (*Bcl-xl*) (Silva *et al*, 1996; Cui *et al*, 2004; Watowich, 2011). EPO-EPOR interaction also activates the phosphatidylinositol 3-kinase (PI3K)/AKT pathway, that phosphorylates GATA1, a transcription factor critical to erythroid differentiation, and the nuclear factor kappa-light-chain-enhancer of activated B cells (NF-kB) pathway, that activates antioxidant and protective targets (**Figure 2**) (Watowich, 2011; Digicaylioglu & Lipton, 2001; Morgan & Liu, 2011; Zhang & Sun, 2015).

Overall, EPO/EPOR signaling increases the proliferation, differentiation and survival rate of erythroblasts and prevents their apoptosis, increasing circulating RBCs. Thus, oxygen levels augment in tissues activating a negative feedback-loop on EPO production (Wenger & Kurtz, 2011; Bunn, 2013).

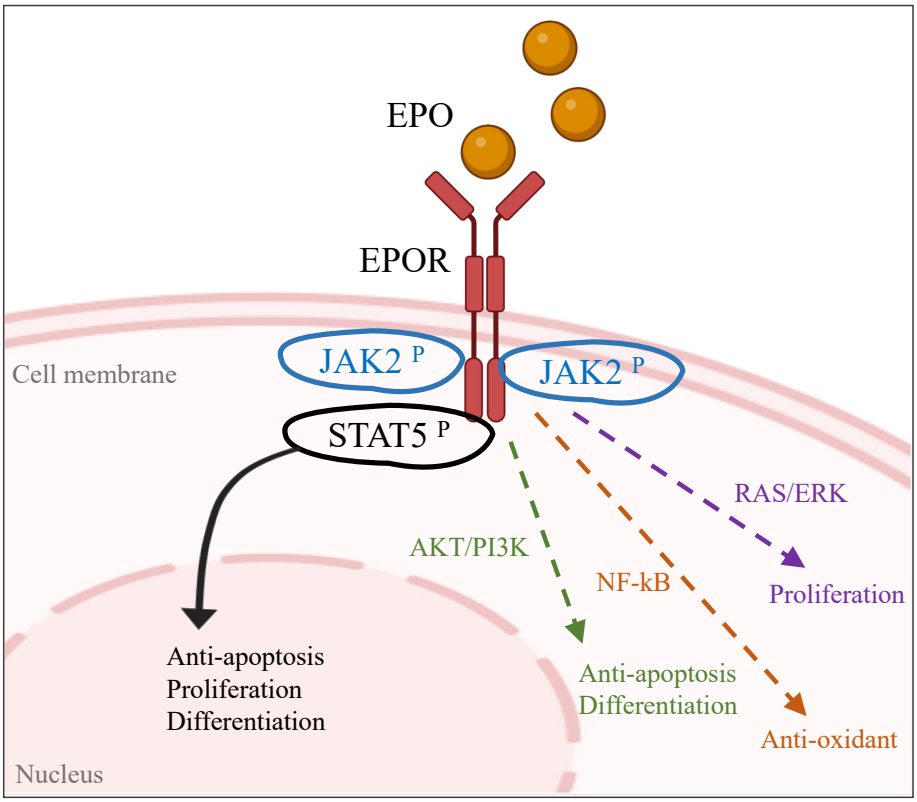

Figure 2. Simplified overview of the EPO-EPO receptor pathway. *Upon erythropoietin (EPO) binding to its receptor (EPOR), conformational changes lead to JAK2 phosphorylation and activation of several intracellular signaling pathways, among which STAT5. Phosphorylated STAT5 dimerizes and translocates into the nucleus inducing the transcription of genes involved in anti-apoptosis, proliferation and differentiation. Other pathways activated by EPO-EPOR signaling are AKT/PI3K, NF-kB and RAS/ERK, implicated in the control of anti-apoptosis and differentiation, anti-oxidant response and proliferation, respectively.*

1.1.3 Heme and hemoglobin

The principal function of RBCs is the transport of gases (O_2, CO_2), but additional roles have been described in redox regulation, nitric oxide metabolism (Kuhn *et al*, 2017) and immune response (Anderson *et al*, 2018; Lam *et al*, 2021).

Hemoglobin, the most abundant protein in RBCs, allows oxygen binding and transport from the lung to peripheral tissues and vice-versa, to sustain cellular respiration and maintain acid/base equilibrium. Hemoglobin is a tetramer composed by 2 α and 2 β globin chains. Each subunit contains heme, a complex formed by an organic protoporphyrin ring and a central ion of iron in the ferrous state (Fe^{2+}), responsible for O_2 binding.

Heme and globin synthesis, necessary for hemoglobin formation, occur in mitochondria and cytosol of erythrocytes though complex steps. Heme availability is highly controlled both at cellular and systemic levels. The first rate-limiting step of heme synthesis is catalyzed by the 5-aminolevulinic acid (ALA) synthase 2 (ALAS2). ALAS2 is regulated by iron, while ALAS1 (the non-erythroid isoform) is regulated by heme itself (Chiabrando *et al*, 2014). Indeed, Iron Regulatory Protein 1 (IRP1, see below) inhibits ALAS2 translation in conditions of low iron availability (Chiabrando *et al*, 2014; Muckenthaler *et al*, 2017).

Globin synthesis is regulated by heme availability through Heme-Regulated Inhibitor of translation (HRI). In conditions of heme deficiency, HRI activates and phosphorylates eIF2α, inhibiting globin synthesis, while when heme is abundant, HRI is maintained inactive by heme itself (Levin *et al*, 1976; Han *et al*, 2001; Chen, 2007; Burwick & Aktas, 2017) , promoting hemoglobin production.

Since hemoglobin synthesis requires about 25 mg of iron/day, an adequate amount of iron is needed to properly sustain erythropoiesis.

1.2 Iron metabolism

1.2.1 Systemic iron metabolism

Since iron plays a pivotal role in several biological processes, as mitochondrial function, enzymatic reactions, DNA synthesis and repair, and erythropoiesis, its amount in the body is regulated both at systemic and cellular levels (Hentze *et al*, 2010).

Dietary non-heme iron is absorbed through the apical membrane of duodenal enterocytes via the divalent metal transporter 1 (DMT1) and reduced mainly by the membrane-associated ferrireductase DcytB. HIF-2α positively regulates iron absorption from enterocytes transcriptionally activating *Dmt1* (Mastrogiannaki *et al*, 2009; Shah *et al*, 2009), while inhibition occurs through sequestration into the iron-storage protein ferritin (FTH). The mechanism of heme uptake is still under investigation, but heme oxygenase 1 (HMOX1) is responsible for its intracellular degradation and iron release. Iron is then exported from the basolateral side into the bloodstream via ferroportin (FPN) (McKie *et al*, 2000; Donovan *et al*, 2000), the only known iron exporter. Hephaestin (HEPH) oxidizes Fe^{2+} to Fe^{3+} to allow iron binding to Transferrin (TF), the carrier that renders iron bioavailable in the circulation, avoiding toxic radical formation and iron utilization by pathogens. Iron is then delivered to organs and tissues for storage (liver) and utilization (muscle and BM). Body iron is predominantly utilized for erythropoiesis, mainly obtained from recycling of senescent erythrocytes by macrophages (about 25 mg/day), which store iron into FT and release it in the circulation via FPN when needed (Muckenthaler *et al*, 2017).

Since there is no active mechanism for iron excretion, dietary iron absorption is tightly controlled and limited to 1-2 mg/day to compensate for iron losses (e.g., skin desquamation, blood loss, sloughing of intestinal epithelial cells) (Hentze *et al*, 2010). The master regulator of systemic iron metabolism is hepcidin (Pigeon *et al*, 2001; Roetto *et al*, 2003), a peptide hormone produced by hepatocytes that regulates cellular iron efflux acting on FPN, abundant on duodenal enterocytes, hepatocytes and macrophages. After FPN binding, hepcidin blocks iron export both directly occluding the channel (Aschemeyer *et al*, 2018) and inducing FPN internalization and degradation (Nemeth *et al*, 2004b), thus reducing circulating iron levels (**Figure 3**).

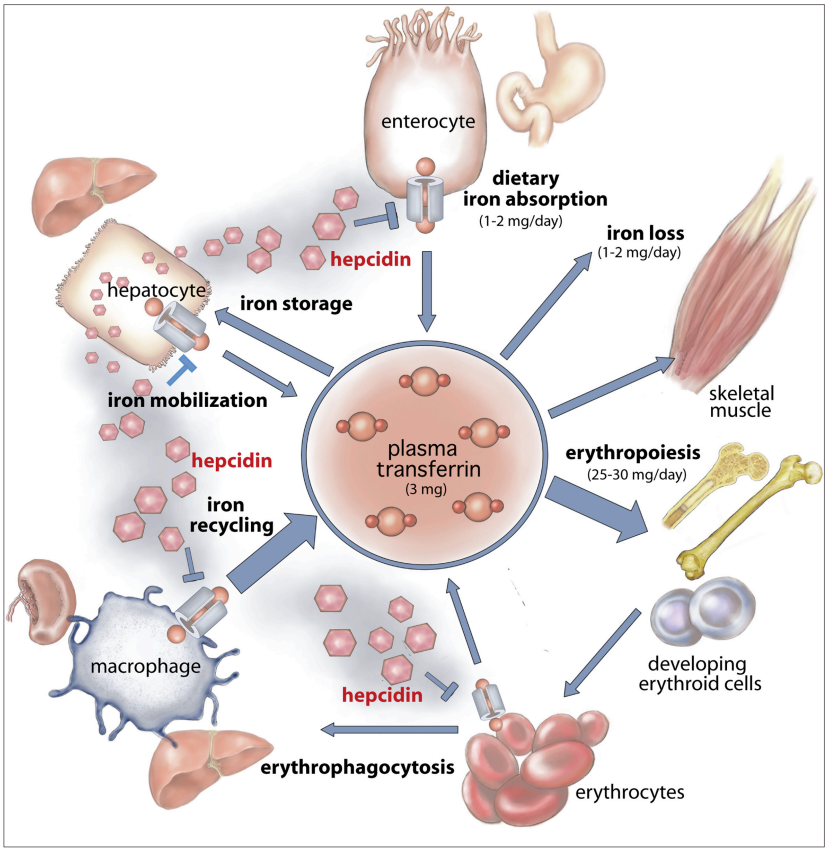

Figure 3. Overview of systemic iron utilization. *Transferrin binds plasma iron for distribution to bone marrow and other tissues. The bone marrow is the main site of iron utilization for erythropoiesis, and then iron is recycled from senescent erythrocytes by macrophages. Iron physiological loss is compensated by dietary iron absorption. Hepcidin, a peptide hormone produced by hepatocytes, regulates iron efflux in the circulation blocking the iron exporter ferroportin on the surface of duodenal enterocytes, hepatocytes and reticuloendothelial macrophages. (Katsarou & Pantopoulos, 2020), license number 5401940129617.*

HAMP is transcriptionally regulated by different stimuli. Inflammation or infection and iron overload upregulate hepcidin transcription, thus blocking FPN activity and limiting iron release in the circulation. In conditions of iron deficiency and increased iron demand, as in erythropoiesis expansion, hepcidin expression is inhibited and FPN stabilized to boost iron export in the bloodstream (Muckenthaler *et al*, 2017).

Hepcidin expression is modulated in response to liver iron stores by the bone morphogenetic protein (BMP)-Son of mother against decapentaplegic (SMAD) pathway (Silvestri *et al*, 2019) (**Figure 4**). BMP2 and BMP6, expressed in liver sinusoidal endothelial cells (LSECs), are involved in hepcidin activation *in vivo*, in a paracrine fashion. When iron levels are sufficient, BMP2 maintains basal hepcidin (Koch *et al*,

2017), while BMP6 strongly contributes to hepcidin activation in iron-overload conditions (Kautz *et al*, 2008; Canali *et al*, 2017). BMP2 and BMP6 bind BMP type I and II receptors, leading to SMAD1/5/8 phosphorylation and SMAD4 binding. Then the complex translocates into the nucleus activating the transcription of genes carrying a BMP responsive element in their promoter, among which hepcidin (Silvestri *et al*, 2019).

The BMP-SMAD pathway is modulated by several proteins and stimuli. The human homeostatic regulatory protein HFE, the second transferrin receptor (TFR2) and the BMP co-receptor hemojuvelin (HJV) contribute to activate the pathway and, when mutated, cause Hereditary Hemocromatosis (HH) (Feder *et al*, 1996; Camaschella *et al*, 2000; Papanikolaou *et al*, 2004). HH is an autosomal recessive disease characterized by low hepcidin levels, that lead to systemic iron overload and related complications in several organs. The traditional treatment is based on iron depletion via phlebotomy.

The transmembrane serine protease matriptase-2 (encoded by the *TMPRSS6* gene) cleaves HJV inhibiting the BMP-SMAD pathway thus reducing hepcidin levels. This occurs in conditions of iron deficiency, when hepcidin has to be downregulated to allow iron release from the stores (Silvestri *et al*, 2008a, 2008b; Finberg *et al*, 2010). When *TMPRSS6* is mutated or inhibited, hepcidin levels are inappropriately increased, leading to iron refractory iron deficient anemia (IRIDA) (Finberg *et al*, 2008).

Hepcidin is upregulated also by inflammation (**Figure 5**), to restrict iron availability to pathogens and avoid worsening of inflammatory status (Nemeth *et al*, 2004b). Lipopolysaccharide (LPS) induces the production of proinflammatory cytokines, like interleukin 6 (IL-6), interleukin 1 β (IL-1β) and tumor necrosis factor α (TNF-α). IL-6 binds to its receptor GP130 on the surface of hepatocytes, activating the JAK2-STAT3 signaling pathway. Phosphorylated STAT3 translocates into the nucleus where binds its responsive element on hepcidin promoter, inducing its transcription (Verga Falzacappa *et al*, 2007). Moreover, LPS further contributes to BMP-SMAD activation stabilizing SMAD4 (Layoun *et al*, 2018).

The control exerted by erythropoiesis on hepcidin occurs through an "erythroid regulator" (Finch, 1994) identified in the secreted protein erythroferrone (ERFE) (Kautz *et al*, 2014). ERFE is produced by erythroid precursors in response to EPO stimulation and transcriptionally downregulates hepcidin. The ERFE-mediated hepcidin modulation involves sequestration of BMPs, mainly BMP6, and interference with the BMP/SMAD pathway (Arezes *et al*, 2018; Nai *et al*, 2016), but the precise mechanism is still incompletely understood.

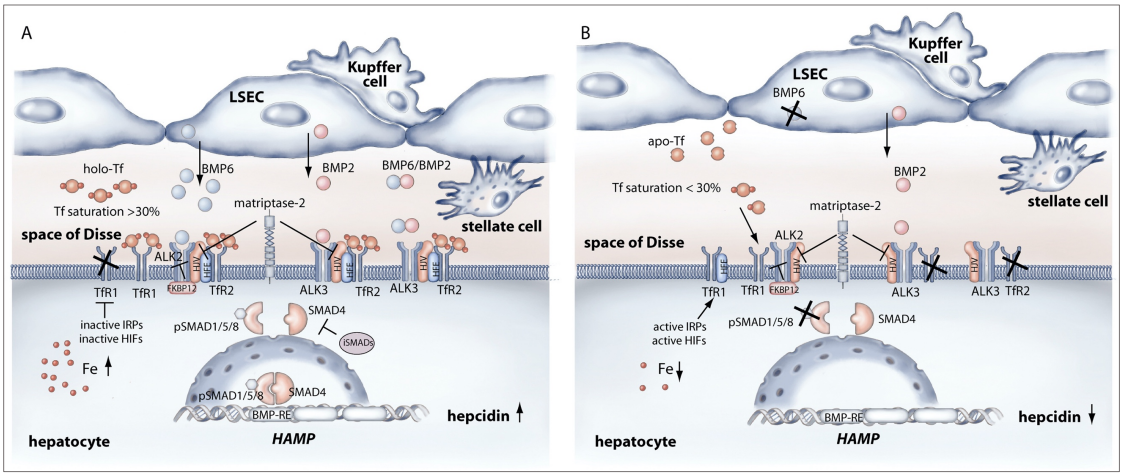

Figure 4. Overview of hepcidin regulation by iron. ***A)*** *When body iron is high, transferrin saturation increases (>30%), stabilizing Transferrin Receptor 2 (TFR2) and contributing to the activation of the BMP/SMAD signaling cascade. Moreover, while bone morphogenetic protein 2 (BMP2) is constitutively expressed, BMP6 production increases in response to iron overload in liver sinusoidal endothelial cells (LSEC) and is released in the space of Disse. BMP6 binds type I BMP receptor ALK2, while BMP2 to ALK3, activating the BMP/SMAD cascade. Phosphorylated SMAD1/5/8 recruit SMAD4 and then the complex translocates into the nucleus and promotes the transcription of hepcidin (HAMP) upon binding to BMP-responsive elements. The BMP co-receptor Hemojuvelin (HJV) and the Hemochromatosis protein HFE are required for signaling initiation.* ***B)*** *Iron deficiency leads to decreased transferrin saturation (<30%), that destabilizes TFR2. In response to low intracellular iron, TFR1 expression and production are increased through activation of Hypoxia Inhibitory Factors (HIFs) and Iron Regulatory Proteins (IRPs), respectively. As a consequence, TFR1 promotes iron uptake and sequesters HFE to attenuate the BMP/SMAD signaling. Moreover, inhibition of the pathway occurs through the enhanced production of matriptase-2, that cleaves HJV, inhibitory SMADs, that bind and sequester SMAD4, and FKBP12, which binds ALK2. (Katsarou & Pantopoulos, 2020), license number 5401940129617.*

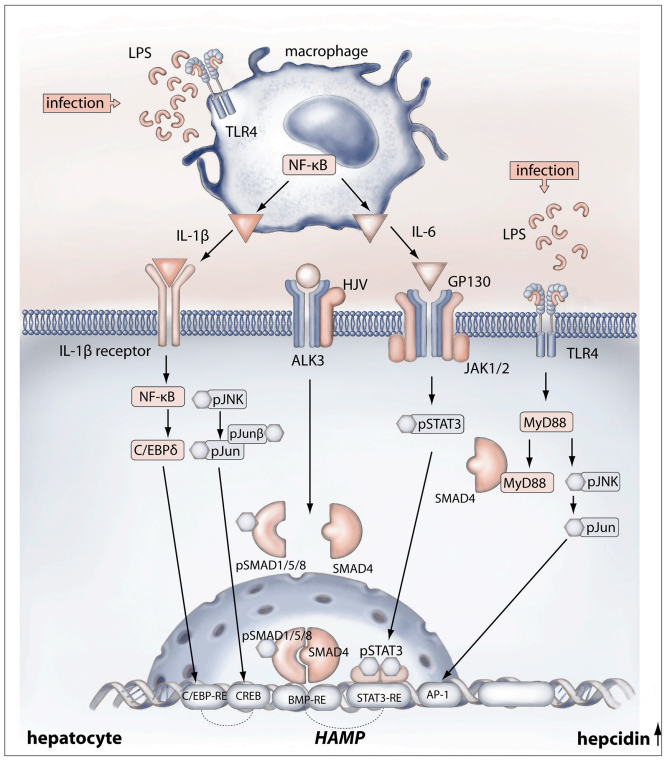

Figure 5. Hepcidin regulation by inflammation. *Pro-inflammatory cytokines, as interleukin 6 (IL-6) and interleukin 1β (IL-1β), are released by activated macrophages and other immune cells in response to inflammation/infections to induce hepcidin transcription. On hepatocytes, IL-6 binds GP130 and signals via the JAK/STAT3 pathway, while IL-1β binds its receptor, activating NF-kB and c-Jun N-terminal kinase (JNK) signaling pathways as depicted in the figure. Moreover, lipopolysaccharides (LPS) deriving from bacteria membranes bind toll-like receptor 4 (TLR4) and activates hepcidin (Hamp) expression through JNK. (Katsarou & Pantopoulos, 2020), license number 5401940129617.*

1.2.2 Cellular iron metabolism

Iron uptake, utilization and storage are finely coordinated in cells to prevent toxicity, and, at difference with systemic metabolism, cells are able to excrete iron in a regulated manner through FPN (Hentze *et al*, 2010) (**Figure 6**).

Plasma iron is generally uptaken by TF receptor 1 (TFR1) through the binding of iron-loaded TF (holo-TF), followed by a clathrin-dependent endocytosis. Iron is then released from TF thanks to the acidic environment in early endosomes, while TF remains bound to TFR1. This complex is recycled to the cell surface and TF is released in the circulation. Inside the cell, iron is reduced to Fe^{2+} by STEAP metalloreductase and transported by DMT1 into the cytosol, where it is available for storage, export or utilization (Muckenthaler *et al*, 2017).

Other mechanisms of iron uptake are erythrophagocytosis by macrophages and import of non-transferrin bound iron (NTBI) through dedicated transporters such as ZIP14, ZIP8, and TRPC6. Moreover, free heme in the circulation binds hemopexin and then the complex can be endocytosed from macrophages, hepatocytes and other cells through the low-density lipoprotein receptor-related protein (LRP)/CD91 (Muckenthaler *et al*, 2017).

After uptake, iron constitutes the so-called "labile iron pool" and is utilized for protein incorporation or mitochondria utilization. Mitoferrin (MFRN1) transports iron in mitochondria for incorporation into heme and/or Fe-S cluster prosthetic groups (important for electron transfer in respiratory complexes and ROS production). Heme is then exported to the cytoplasm by the mitochondrial isoform of Feline Leukemia Virus Subgroup Receptor 1 (FLVCR1) (Chiabrando *et al*, 2012).

Unutilized iron is exported via FPN or stored into ferritin. Ferritin is an heteropolymer constituted of 24 subunits of heavy (FTH1) and light (FTL) chains, ubiquitously expressed but with different FTH1/FTL ratios depending on tissues and physiological conditions. Ferritin stores iron in a non-toxic form, which can be mobilized through ferritin degradation (Hentze *et al*, 2010). Nuclear Receptor Coactivator 4 (NCOA4) mediates ferritinophagy in iron-deficient cells, allowing iron recovery. On the contrary, NCOA4 turnover is increased in iron-loaded cells to limit ferritinophagy (Mancias *et al*, 2014, 2015; An *et al*, 2014).

When a cell faces iron deficiency, IRP1 and IRP2 bind IREs in the 3' UTR of *TFR1* mRNA, increasing its stability, and in the 5' UTR of ferritin and *FPN* mRNAs, blocking their translation. Thus, iron uptake is enhanced, and iron storage and export are prevented. The opposite occurs in conditions of iron-loading, when the binding of IRPs to IREs is suppressed (Hentze *et al*, 2010).

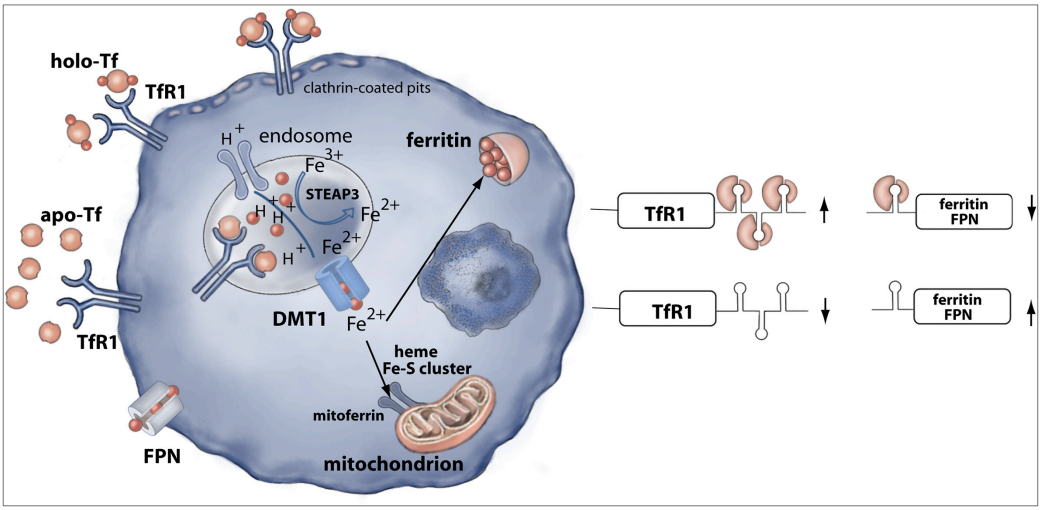

Figure 6. Cellular iron metabolism. *Iron-loaded Transferrin (holo-TF) binds Transferrin Receptor 1 (TFR1) on cell surface, promoting its internalization through clathrin-mediated endocytosis. Endosome acidification releases iron from TF. Then, the metal is reduced by STEAP3 and exported in the cytosol via the Divalent Metal Transporter 1 (DMT1), while TFR1 is recycled on the cell membrane and TF is released in the circulation. Intracellular iron is either utilized by the mitochondria for heme and Fe-S cluster synthesis, stored in ferritin or exported via ferroportin (FPN). TFR1, ferritin and FPN expression is post-transcriptionally regulated by the Iron Regulatory Element (IRE)/ Iron Regulatory Protein (IRP) system. (Katsarou & Pantopoulos, 2020), license number 5401940129617.*

1.2.3 Transferrin Receptor 2

Transferrin Receptor 2 (TFR2) was firstly reported in 1999 as a second mammalian receptor for TF (Kawabata *et al*, 1999). *TFR2* gene, present on chromosome 7 in humans, is transcribed into two isoforms, *TFR2*-α and *TFR2*-β. *TFR2*-α is a type 2 transmembrane glycoprotein (90-105 kDa), mainly expressed in hepatocytes and erythroid precursors, while *TFR2*-β is ubiquitously expressed but at low levels (Kawabata *et al*, 1999; Deaglio *et al*, 2002). *TFR2*-α binds holo-TF similarly to the homologous TFR1, but with a lower affinity (about 1/25) (West *et al*, 2000; Kawabata *et al*, 2000). Conversely to *TFR1*, *TFR2* expression is not regulated by iron availability, but holo-TF binding stabilizes TFR2-α protein on the cell surface (Robb & Wessling-Resnick, 2004; Johnson & Enns, 2004) decreasing lysosomal degradation (Johnson *et al*, 2007) and reducing receptor shedding from plasma membrane (Pagani *et al*, 2015). Several transcription factors bind and activate *TFR2* promoter as GATA1 and C/EBP-a, expressed in erythroid and myeloid cells respectively, hepatocytes and adipose tissues (Kawabata *et al*, 2001), and hepatocyte nuclear factor 4α (Matsuo *et al*, 2015).

Mutations in *TFR2* lead to HH (Camaschella *et al*, 2000), a genetic iron overload disorder, because of hepcidin down-regulation (Kawabata *et al*, 2005; Wallace, 2005; Nemeth *et al*, 2005) . Indeed, in the liver, TFR2 positively regulates hepcidin transcription modulating the BMP-SMAD pathway as described above.

An erythroid role for TFR2 has been proposed several years after the elucidation of the hepatic one. Indeed, TFR2 and EPOR are co-expressed and interact during erythroid progenitors differentiation (Forejtnikovà *et al*, 2010). Moreover, Genome Wide Association Studies identified *TFR2* single nucleotide polymorphisms associated with RBC count, hematocrit and MCV in normal subjects (Ganesh *et al*, 2009; Soranzo *et al*, 2009; Lo *et al*, 2011; van der Harst *et al*, 2012; Auer *et al*, 2014).

In mice, germline *Tfr2* deletion leads to iron overload and a moderate hemoglobin increase compared to wild-type. Mice with specific deletion of *Tfr2* in the liver display a similar iron-overload (**Figure 7**), but interestingly hemoglobin levels are not increased in these animals (Wallace, 2005; Roetto *et al*, 2010). Moreover, *Tfr2-Tmprss6* double KO mice develop erythrocytosis despite iron-deficiency, conversely to *Tmprss6*-KO mice with *Tfr2* hepato-specific deletion (Nai *et al*, 2014). Overall, these findings suggested a specific role for *Tfr2* in erythroid cells in the control of RBCs and hemoglobin levels.

In line with this assumption, mice lacking *Tfr2* in the hematopoietic compartment (BM and spleen, $Tfr2^{BMKO}$), obtained through BM transplantation, show increased RBC count, enhanced terminal erythroid differentiation and reduced erythroid precursors apoptosis. This effect is not due to increased serum EPO levels, but rather to higher EPO responsiveness of erythroid cells (Nai *et al*, 2015). Thus, TFR2 acts as negative regulator of the EPO-EPOR pathway (**Figure 7**), sensing iron levels and adapting hepcidin and erythropoiesis mutual needs, balancing RBCs production and iron availability (Nai *et al*, 2015).

The potential beneficial effect of erythroid *Tfr2* deletion in the amelioration of anemia has been proven by our lab in murine models of transfusion independent ($Hbb^{th3/+}$) (Artuso *et al*, 2018) and transfusion dependent ($Hbb^{th1/th2}$) (Di Modica *et al*, 2022) β-thalassemia. Indeed, $Tfr2^{BMKO}/Hbb^{th3/+}$ mice maintain higher Hb levels, RBC count and enhanced erythropoiesis for at least 21 weeks after transplantation compared to controls (Artuso *et al*, 2018). The same effect is observed also in $Hbb^{th1/th2}$ mice, in which BM

Tfr2 deletion avoids long-term blood transfusions and related complications, too (Di Modica *et al*, 2022).

Recently, Rauner and collegues described a role for TFR2 also in the bone. *Tfr2*$^{-/-}$ mice have higher bone volume, strength and turnover, independently from the iron status (Rauner *et al*, 2019). In detail, the effect on bone metabolism is driven by *Tfr2* deletion in osteoblasts, that reduces BMP-SMAD signaling and the expression of WNT inhibitors. As a consequence, WNT promotes bone formation (Rauner *et al*, 2019). These findings open the possibility that TFR2 might be a mediator of the erythropoiesis-bone crosstalk (**Figure 7**).

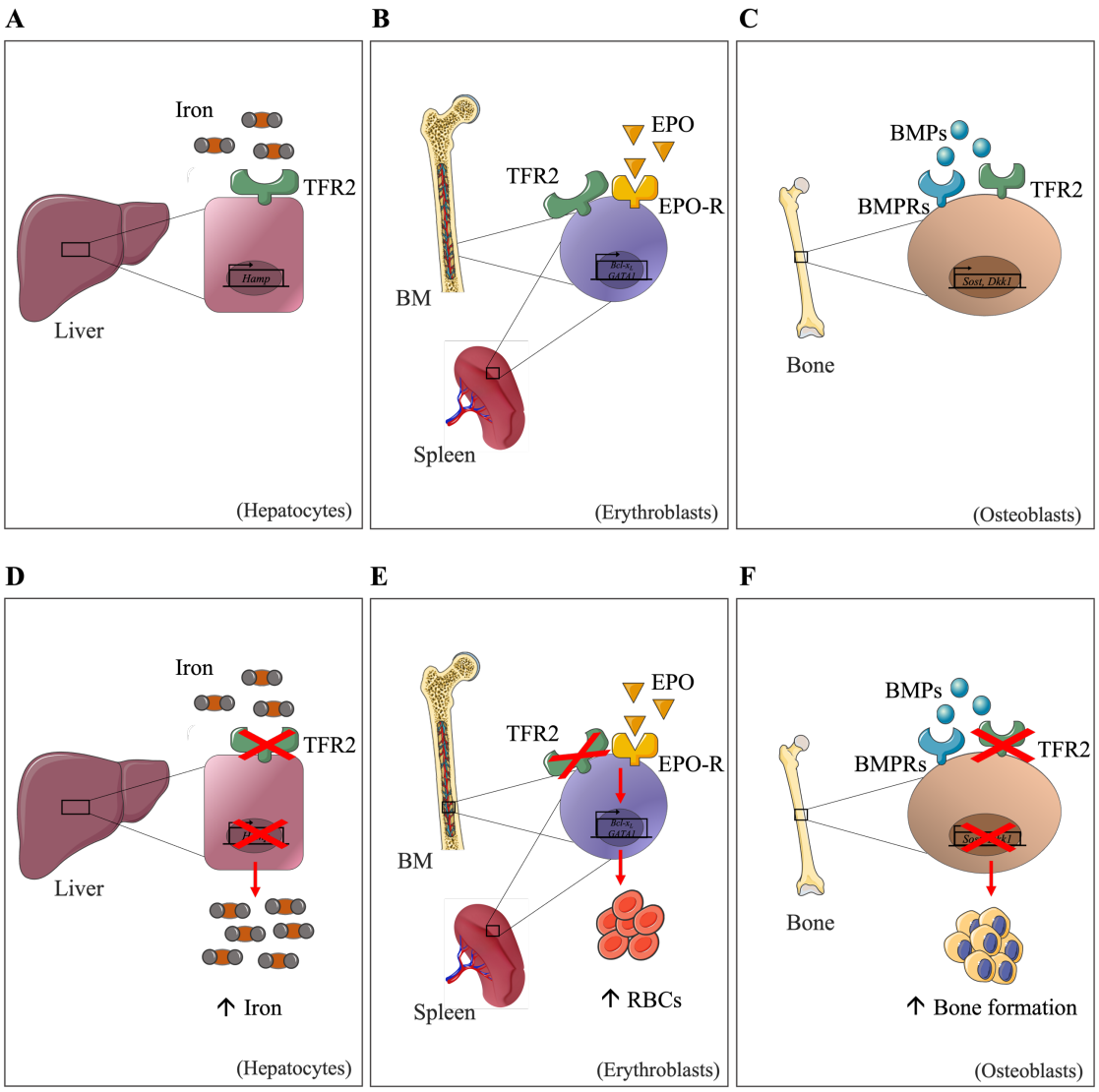

Figure 7. Simplified scheme of Transferrin Receptor 2 (TFR2) function in the liver, hematopoietic compartment and bone.
A-D*) In the liver, TFR2 acts as a positive regulator of hepcidin, activating its transcription through a partially unknown mechanism. When Tfr2 is deleted in total body or in the liver of mice, hepcidin (Hamp) expression is reduced and thus iron absorption and release in the circulation are increased.*
B-E*) In the hematopoietic compartment, TFR2 interacts with Erythropoietin Receptor (EPOR) and modulates erythropoiesis. When Tfr2 is deleted in BM-derived cells (and consequently in the spleen) in mice, the EPO-EPOR pathway is enhanced, increasing the expression of genes involved in proliferation and differentiation of erythroid cells, despite unchanged EPO levels. Thus, TFR2 is a negative regulator of the EPO-EPOR pathway, whose inactivation boosts Red Blood Cells (RBCs) production increasing erythroid responsiveness to EPO, through a still unknown mechanism.*
C-F*) In osteoblasts, TFR2 binds Bone Morphogenetic Protein 2 (BMP2) and activates the BMP/SMAD pathway to induce the transcription of Dickkopf WNT Signaling Pathway Inhibitor 1 (Dkk1) and Sclerostin (Sost), a WNT antagonist, thus inhibiting bone formation. On the contrary, when Tfr2 is deleted in osteoblasts, WNT is not inhibited, increasing bone formation.*

1.3 Erythropoiesis-bone crosstalk

1.3.1 Bone organization and functions

Bone is a dynamic mineralized connective tissue that supports and protects vital organs, maintains mineral homeostasis, serves as a calcium and phosphate storage, allows locomotion and harbors the BM, providing proper environment for hematopoiesis (Robling *et al*, 2006; Datta *et al*, 2008; Florencio-Silva *et al*, 2015).

The cortical bone, thick and robust, surrounds the marrow, while the trabecular bone is the spongy, honeycomb-like system of trabeculae in which the BM is disseminated. The human skeleton is formed of eighty-percent cortical bone and twenty-percent trabecular bone, and the cortical/trabecular ratio is variable in different bones. The four main groups of bones are long, short, flat and irregular (Clarke, 2008). The BM is located in the mid-diaphyseal portion of fat and long bones in adults. The adipose and hematopoietic tissues coexist in equal proportion, with the adipose volume adapting accordingly to changes in the hematopoietic activity (Gurkan & Akkus, 2008).

Bone is composed by osteoblasts and osteoclasts, that coordinate bone remodeling, osteocytes and bone lining cells. Osteoblasts form new bone, while osteoclasts resorb it, osteocytes have mechanosensitive functions and bone lining cells help maintaining

physiological homeostasis (Nakamura, 2007; Florencio-Silva *et al*, 2015). The equilibrium between bone resorption and bone formation is pivotal to preserve homeostasis. When one of these two process prevails, osteoporosis or osteopetrosis may occur. Importantly, osteoblasts derive from mesenchymal stem cells (MSC), while osteoclasts derive from mononuclear cells of hematopoietic lineage, sharing their origin with erythrocytes (**Figure 8**) (Florencio-Silva *et al*, 2015).

In addition to anatomic connections, bone and BM are also functionally linked, and alterations in one of these compartments affect the other one (Del Fattore *et al*, 2010).

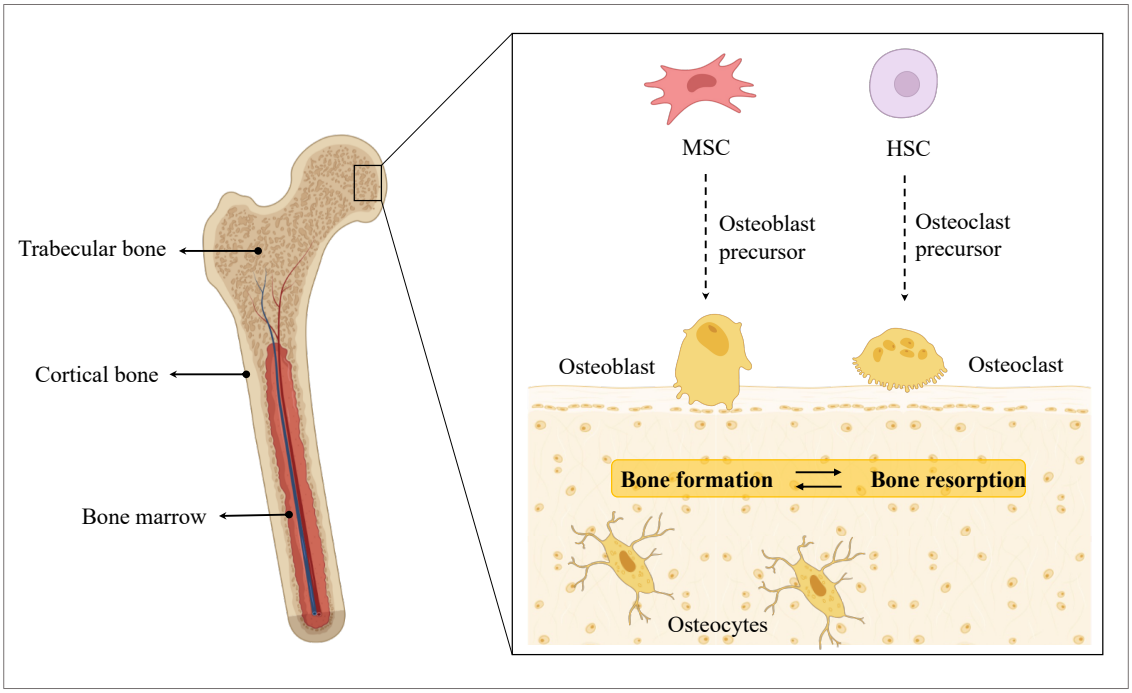

Figure 8. Schematic representation of bone structure and composition. *The bone is constituted by two types of tissues: the cortical bone and the trabecular bone. The first is the hard, protective part of the bone, while the latter is the spongy honeycomb-like tissue in which the BM resides. Bone undergoes a continuous remodeling, required to balance bone mass and mineral homeostasis. Osteoclasts, deriving from hematopoietic stem cells, resorb old or damaged bone, while osteoblasts, of mesenchymal origin, replace the removed bone. Osteocytes, which derive from osteoblasts, support this process.*

1.3.2 Bone impairment in erythroid disorders

Some forms of anemia, malignant diseases and storage or infiltrative disorders often present coexistence of alterations in bone homeostasis and erythropoietic defects, suggesting a functional link between these 2 systems. For example, β-thalassemia patients suffer from reduced bone mass, bone pain and frequent fractures, due to BM expansion and concomitant medullary cavity widening, together with iron overload and endocrine complications (Vogiatzi *et al*, 2009).

Moreover, anemia of chronic kidney disease (CKD) often leads to secondary hyperparathyroidism associated to bone and mineral abnormalities (called CKD-BMD), that cause higher fracture frequency compared to the general population (Fried *et al*, 2007; Pimentel *et al*, 2021). CKD is characterized by inappropriately low EPO levels because of renal damage, that may contribute to bone impairment (Wei *et al*, 2016). Indeed, EPO has a regulatory role in bone homeostasis and several studies in mice showed that EPO increases bone volume and repair increasing cell proliferation, Vascular Endothelial Growth Factor-mediated angiogenesis and cartilaginous callus formation (Holstein *et al*, 2011; Wan *et al*, 2014). Also, osteoclastogenesis and osteoblastogenesis are activated by EPO both directly (through EPOR) and indirectly (BMPs expression by HSCs is stimulated by EPO to promote bone formation) (Shiozawa *et al*, 2010). The pro-angiogenic capacity of EPO may also increase BM microenvironment vascular density and direct bone precursors to bone formation sites (Kertesz *et al*, 2004). Conversely, EPO has also been linked to bone loss, probably acting on osteoclasts (Deshet-Unger *et al*, 2016; Hiram-Bab *et al*, 2015). In this way, EPO might enhance bone turnover while promoting erythropoiesis, thus widening space in the BM for hematopoietic expansion (Eggold & Rankin, 2019).

Nevertheless, EPO effect on bone formation depends on experimental conditions and is still under debate, requiring further mechanistic insights.

Overall, the exact mechanisms and players involved in the bone-erythropoeisis crosstalk remain to be clearly elucidated. Interestingly, TFR2 might be involved in this process as a negative regulator of both erythropoiesis and bone mass and turnover (Rauner *et al*, 2019), and possibly targeted for therapeutic purposes.

1.4 Defective erythropoiesis

1.4.1 Erythropoiesis-related disorders: a brief overview

During normal erythropoiesis, approximately 2.5 x 10^6 erythroblasts are released in the circulation every second. When defects in erythroid precursors' proliferation or maturation or in circulating RBCs survival occur, anemia develops. Erythroid hypoproliferation, ineffective erythropoiesis and peripheral hemolysis are the three causative pathogenetic mechanisms (Cazzola, 2022).

Erythroid hypoproliferation is the inadequate production of erythroid cells due to limiting factors, such as insufficient iron supply, increased cytokine levels and impaired EPO production (Cazzola, 2022). These are common features of anemia of inflammation/infection and anemia of CKD.

Ineffective erythropoiesis is defined as an inadequate production of reticulocytes because of the hyperplasia of early-stage erythroid precursors and the increased apoptosis of late-stage erythroblasts. This expansion in erythroid marrow causes ERFE overproduction (Kautz *et al*, 2014), leading to higher iron release and absorption and eventually to secondary iron overload (Kautz *et al*, 2015; Coffey *et al*, 2022) . Ineffective erythropoiesis is responsible for both inherited and acquired anemic disorders, as thalassemia, sideroblastic anemias, congenital dyserythropoietic anemias, myelodysplastic syndrome and megaloblastic anemia (Cazzola, 2022).

Peripheral hemolysis is the premature destruction of RBCs, that causes anemia when erythropoiesis is not able to compensate for RBCs reduction. Hemolysis may be acquired, as in autoimmune or immune (e.g., during infectious diseases) hemolytic anemias, or inherited, as in enzymopathies and hemoglobinopathies (Dhaliwal *et al*, 2004).

1.4.2 Anemia of inflammation

Anemia of inflammation is one of the most common anemias worldwide, together with iron-deficiency anemia. Anemia of inflammation is often associated with chronic systemic inflammation (e.g., systemic lupus erythematosus, inflammatory bowel disease, rheumatoid arthritis), infections, some types of cancer and anemia of CKD (Ganz, 2019).

The inflammatory response, elicited by the immune system to limit infections and injuries, is the first driver of the cascade that leads to anemia development. Indeed, inflammatory cells produce cytokines as TNF-α, IL-1β, IL-6 and interferon-γ (IFN-γ), that lead to hypoferremia, decreased erythroid cell survival and EPO responsiveness, eventually causing anemia (**Figure 9**).

IL-6 stimulates hepcidin expression as an acute-phase response against infections to reduce pathogens growth and promote their phagocytosis (Arezes *et al*, 2015). Increased hepcidin levels limit iron absorption and sequester iron in stores (Armitage *et al*, 2011; Nemeth *et al*, 2004a; Lee *et al*, 2005; Verga Falzacappa *et al*, 2007; Kim *et al*, 2014; Kanamori *et al*, 2014), impairing hemoglobin and RBCs production (Prince *et al*, 2012).

Moreover, pro-inflammatory cytokines directly inhibit erythroid cells proliferation (Means & Krantz, 1991; Means *et al*, 1992) and impair erythroid responsiveness to EPO (Macdougall & Cooper, 2002; Kimachi *et al*, 2015; Morceau *et al*, 2009). EPO production itself is suppressed, likely because of an inflammatory effect on renal EPO producing cells (Souma *et al*, 2013). Moreover, cytokines activate macrophage-mediated erythrophagocytosis, further decreasing RBCs survival (Libregts *et al*, 2011).

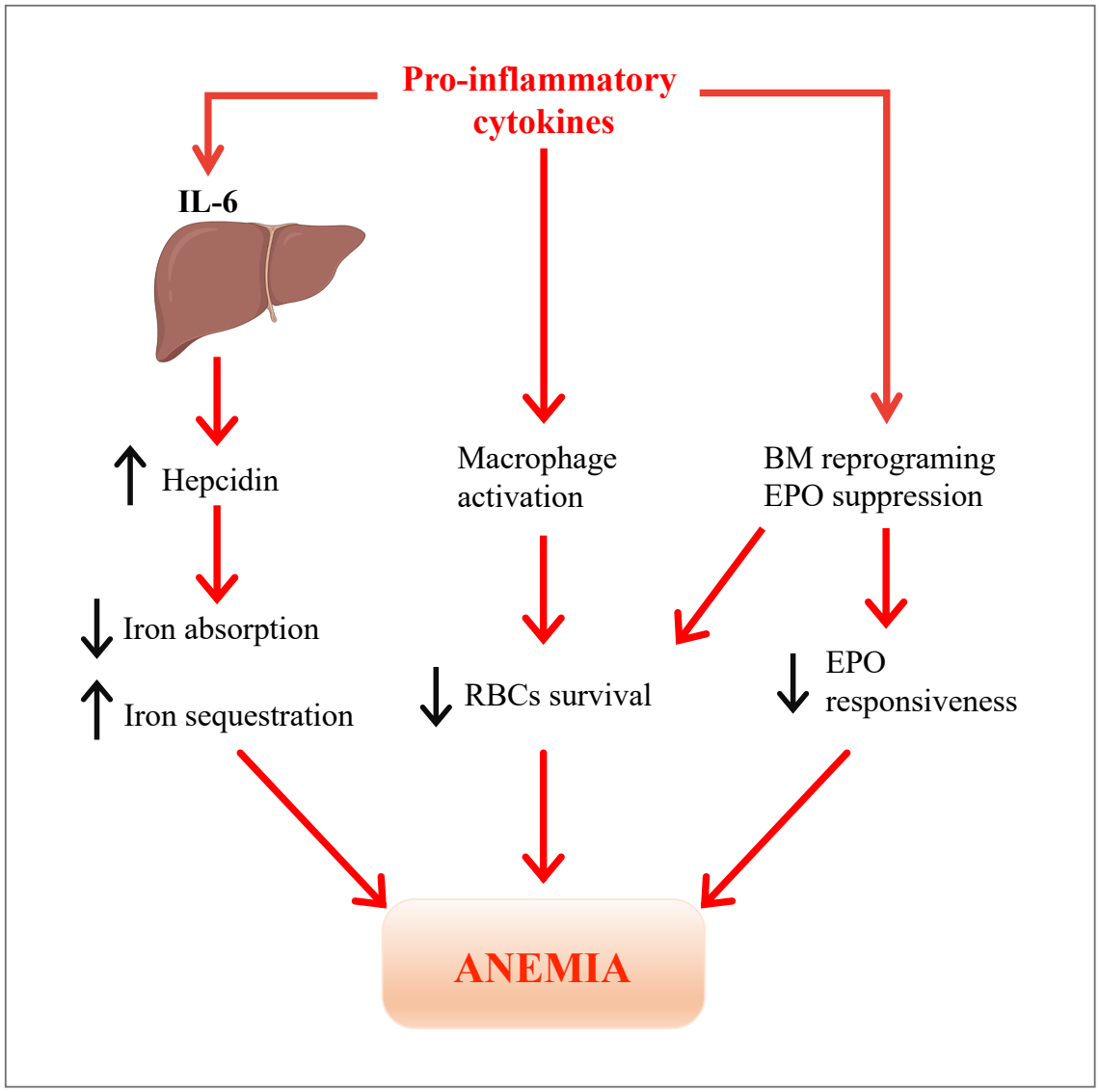

Figure 9. Schematic overview of anemia of inflammation pathophysiology. *Pro-inflammatory cytokines produced by immune cells in response to inflammation or infection lead to hepcidin transcriptional upregulation and, as a consequence, to reduced dietary iron absorption and iron release from stores. Moreover, pro-inflammatory cytokines activate macrophages, promoting Red Blood Cells (RBCs) clearance from circulation, promote BM reprograming toward leukocytosis, decrease Erythropoietin (EPO) responsiveness of erythroid progenitors and limit EPO production. All these factors contribute to the development of anemia of inflammation.*

1.4.3 Malaria anemia

Malaria is caused by the infection from intracellular protozoa of the genus *Plasmodium* (e.g., *Plasmodium falciparum*) and is one of the major causes of mortality and morbidity worldwide, affecting mostly African children and pregnant women (WHO, 2021). Anopheles mosquitos are the parasite' vectors that, during blood meal, release sporozoites into the host bloodstream. The sporozoites proliferate in hepatocytes without causing symptoms, during the so-called liver stage, producing and releasing merozoites into the circulation. Then, merozoites invade RBCs, undergoing three phases: the ring stage, the trophozoite stage and the schizont stage. The parasites consume up to 60-80% of RBCs' cytoplasm and especially hemoglobin. When new merozoites burst to continue the infection, RBCs are eventually destroyed (Francis *et al*, 1997).

Clinical manifestations depend on disease severity. Uncomplicated malaria is characterized by fever, sweats, headaches and general weakness, while severe malaria displays neurologic disabilities, cardiovascular and respiratory complications, hemoglobinuria, kidney injury and severe anemia (Laishram *et al*, 2012). The main cause of anemia is hemolysis of infected RBCs. However, destruction of non-parasitized erythrocytes (White, 2018) and BM dyserythropoiesis caused by the production of erythropoiesis suppressors (e.g., proinflammatory cytokines, nitric oxide, lipoperoxides) (Hassan *et al*, 2009) largely contribute to anemia development (**Figure 10**). The by-product of hemoglobin digestion by malaria parasite, hemozoin, and free heme, released in the circulation as a consequence of hemolysis, play a relevant role in enhancing cytokines production (Casals-Pascual *et al*, 2006; Ferreira *et al*, 2008).

The relationship between iron homeostasis and malaria is complex. Hepcidin is upregulated during infection by proinflammatory cytokines. Moreover, RBCs disruption and hemoglobin consumption by the parasite reduce iron availability. Thus, iron deficiency is a common consequence of malaria (Howard *et al*, 2007; de Mast *et al*, 2009, 2010), that reduces the incidence of severe disease (Gwamaka *et al*, 2012). Indeed, several studies have shown that iron supplementation worsens malaria, likely promoting parasite growth (Sazawal *et al*, 2006; Soofi *et al*, 2013). Recent studies have shown that hepcidin can also be suppressed during malaria infection, mainly because of increased ERFE production (Latour *et al*, 2017).

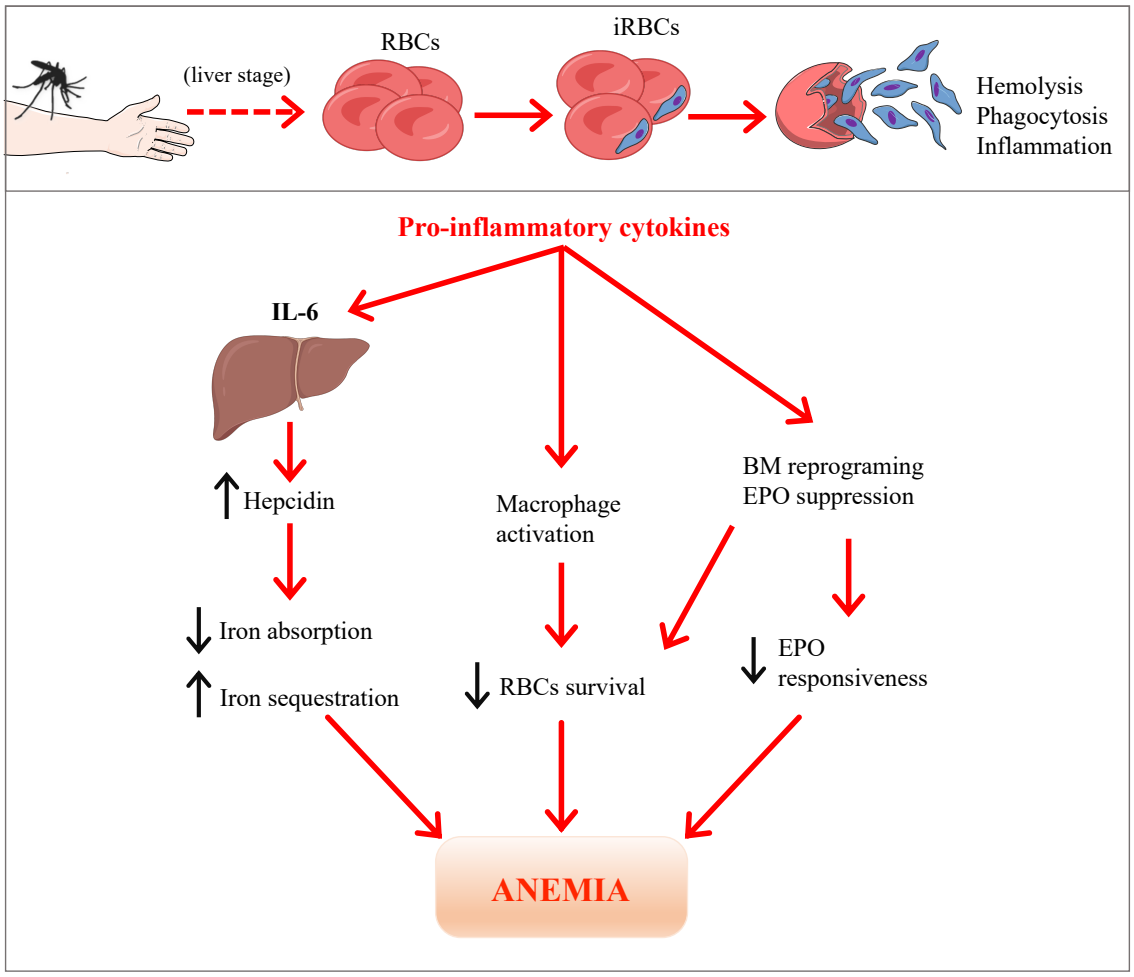

Figure 10. Schematic overview of malaria anemia pathophysiology. *During Anopheles mosquito blood meal, Plasmodium sporozoites are released in the bloodstream. Sporozoites migrate to the liver where they infect hepatocytes and multiply into merozoites, which return into the bloodstream following the rupture of liver cells. Merozoites infect Red Blood Cells (RBCs), where further replicate and produce gametocytes, causing the rupture of the membrane of infected RBCs (iRBCs) to invade circulation and be uptaken by other mosquitos through bite. In mosquito's gut, male and female gametes fuse to form oocysts, able to produce new sporozoites, maintaining Plasmodium infectious life cycle. The timing of each step depends on Plasmodium species. In the host, iRBCs undergo hemolysis and phagocytosis by macrophages, causing the release of pro-inflammatory cytokines and promoting macrophages' activation, further shortening RBCs lifespan. Upon IL-6 signaling, hepcidin levels are increased reducing circulating iron levels. Hemolysis, BM reprograming toward leukocytosis, EPO suppression, decreased EPO responsiveness and iron sequestration contribute to the development of malaria anemia.*

1.4.4 Anemia of Chronic Kidney Disease

Anemia of CKD is a peculiar form of anemia of inflammation, associated with poor quality of life and higher mortality (National Kidney Foundation, 2002; Mujais *et al*, 2009; Palaka *et al*, 2020; Kovesdy *et al*, 2006; Regidor *et al*, 2006; Thorp *et al*, 2009), with an estimated 9.1% global prevalence in 2017 (Bikbov *et al*, 2020). Progressive renal damage impairs EPO synthesis. Indeed, inflammation related to kidney damage promotes differentiation of renal EPO producing cells from fibroblasts to myofibroblasts, that are less able to produce EPO (Shih *et al*, 2018). Also, damaged kidney may have defects in oxygen sensing (Hirakawa *et al*, 2017). So, EPO becomes inappropriately low relative to the degree of anemia, being 10-100 times lower than in anemic patients with normal kidney function (Babitt & Lin, 2012). Moreover, inflammation further impairs RBCs production and survival (McGonigle *et al*, 1984) and stimulates the synthesis of hepcidin, whose levels further increase because of decreased kidney clearance, leading to severe iron restriction (Babitt & Lin, 2010; Ashby *et al*, 2009). Finally, iron loss in urine may occur in CKD patients, especially those undergoing dialysis (**Figure 11**) (Nakatani *et al*, 2018; Besarab & Coyne, 2010).

CKD may be caused by a variety of factors, as diabetes, hypertension, obesity, pre-existing renal dysfunctions (glomerulonephritis, AKI), genetic conditions (Gudbjartsson *et al*, 2010; Köttgen *et al*, 2022) and infectious diseases (National Kidney Foundation, 2002). When glomerular filtration rate (GFR), the volume of plasma filtered from kidneys per unit of time, is reduced for more than three months, together with proteinuria, polyuria or oliguria, fatigue and changes in body weight, CKD is diagnosed. Apart from anemia, common complications of CKD are cardiovascular diseases, and mineral and bone disorders (National Kidney Foundation, 2002).

CKD still does not have a specific treatment, and dialysis and kidney transplant may be necessary in advanced stages (National Kidney Foundation, 2002). However, some therapeutic options are available for CKD complications, as anemia.

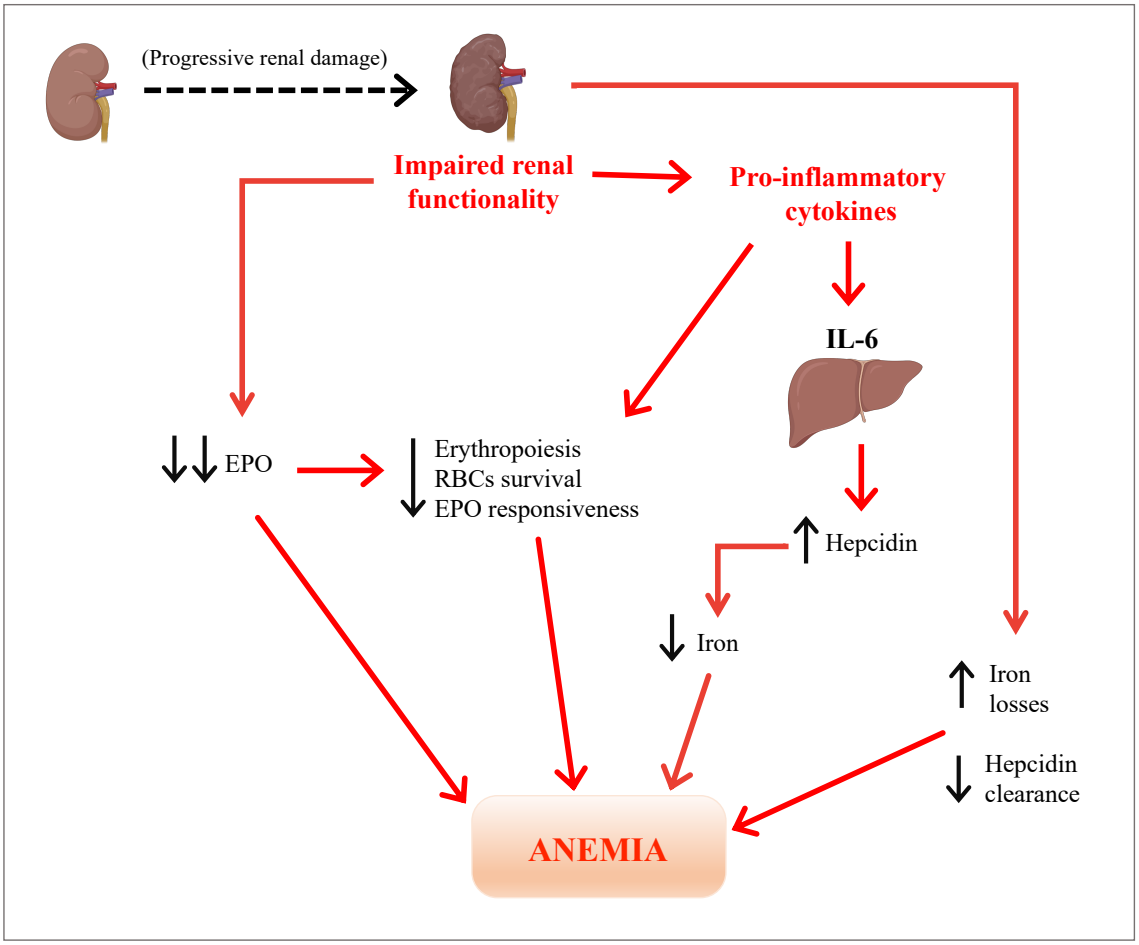

Figure 11. Schematic overview of anemia of CKD pathophysiology. *Progressive renal damage impairs kidney function, resulting in decreased EPO production, iron loss, impaired hepcidin clearance, and local and systemic inflammation. Pro-inflammatory cytokines increase hepcidin thus reducing iron availability and contribute to decreased EPO responsiveness, as described above. Inappropriately low EPO levels impair erythropoiesis, RBCs survival and EPO responsiveness. All these factors contribute to the development of renal anemia.*

1.5 Current therapeutic approaches

1.5.1 Erythropoiesis Stimulating Agents and iron

Administration of exogenous EPO is the gold standard in the treatment of anemia of CKD, and may benefit also some patients affected by anemia of inflammation. EPO α was firstly approved in 1989 for anemia of CKD by FDA, followed by darbepoetin α in 2001, a related erythropoiesis-stimulating agent (ESA). Exogenous EPO enhances erythropoiesis effectively increasing hematocrit, but iron-restricted erythropoiesis often develops because of the elevated hepcidin levels. For this reason, ESAs are usually administered with oral iron supplementation, that, in turn, further increases hepcidin (Lin *et al*, 2007; Zimmermann *et al*, 2009). Moreover, several off-target effects have been described for ESAs, as hypertension, congestive heart failure, myocardial infarction, stroke, thrombotic events or even death. These events are due to EPO interaction with its receptor in non-erythropoietic organs and tissues, that may stimulate platelet activation and endothelial cell proliferation (Besarab *et al*, 1998; Smith, 2003; Unger *et al*, 2010). Also, iron supplementation further increases the risk of adverse outcomes, as infections, inflammation, cardiovascular diseases or even death (Feldman *et al*, 2002; Besarab & Coyne, 2010). Thus, the use of ESAs has been revaluated and other drugs have been developed over the years (Unger *et al*, 2010).

1.5.2 Prolyl Hydroxylase Inhibitors

Prolyl hydroxylase inhibitors (PHIs) are small molecules that, inhibiting PHDs, stabilize HIFs, as HIF-2a, and induce HIF-regulated gene expression. More specifically, they increase endogenous kidney *EPO* production eventually boosting erythropoiesis (Yeh *et al*, 2017). Moreover, PHIs affect transcription of genes involved in iron metabolism, increasing iron uptake and transport in duodenal enterocytes, decreasing hepcidin, and increasing transferrin levels (Dhillon, 2019; Schwartz *et al*, 2018; Barrett *et al*, 2015; Haase, 2021), with the advantage of reducing the need for EPO and iron administration.

Some PHIs have been approved for clinical use, mainly in Asia (Dhillon, 2019), while FDA still raises concern about safety (Astrazeneca Press Releases, 2021). Indeed, since HIFs are implicated in several biologic processes, their activation may induce side effects

as stimulation of VEGF-dependent pathways (Seeley *et al*, 2017), hyperkalemia (Chen *et al*, 2019) and ophthalmology complications (Akizawa *et al*, 2020).

ESAs and PHIs are effective in renal anemia treatment but present some limitation due to possible side-effects and adverse events.

Therapeutic options for anemia of inflammation are mostly restricted to ESAs (Goodnough *et al*, 2000; Weiss & Goodnough, 2005; Weiss *et al*, 2019), while iron administration has to be carefully evaluated in inflammatory status and infections (Ganz, 2019). Malaria treatment is mainly focused on limiting oxidative stress and interfering with parasitic hemoglobin metabolism. Since the BM is unable to properly respond to EPO, malaria anemia still needs effective cures apart from blood transfusions (White, 2018).

Therefore, the identification of a novel, more general therapeutic approach for different forms of anemia would be clinically relevant.

2. AIM OF THE WORK

TFR2 is a key player of the iron-erythropoiesis crosstalk, acting as negative regulator of the EPO-EPOR pathway, able to balance RBCs production and iron availability.
We have already proven that *Tfr2* deletion in the BM ameliorates anemia in β-thalassemic mice, increasing erythroid EPO sensitivity and promoting erythroid differentiation, thus strengthening the critical *Tfr2* erythroid role.

Anemia of CKD is characterized by inappropriately low EPO levels, inflammation, and iron restriction. Our assumption is that *Tfr2* deletion, both at erythroid and hepatic level, may ameliorate anemia and iron deficiency in a murine model of CKD. To address this point, we used germline *Tfr2* KO mice, mice that lack *Tfr2* only in the BM, and mice treated with antisense oligonucleotides anti-*Tfr2* to downregulate hepatic *Tfr2*. Moreover, since TFR2 has been described as a negative regulator of bone formation, we speculate that its deletion may improve also CKD bone defects.

On the contrary, specific *Tfr2* deletion in the BM may be beneficial to anemia of inflammation and malaria anemia, in which inflammation impairs erythroid responsiveness to EPO and RBCs survival, and iron is retained in stores to avoid worsening of inflammatory status and infection. To test this assumption, we induced sterile inflammation and malaria in a model with BM specific *Tfr2* deletion.

Importantly, our approach is based on enhancing erythroid EPO responsiveness rather than increasing EPO levels per se, thus avoiding off-target effects of current EPO-based treatments.

Thus, overall, we aim at obtaining the proof-of-principle that TFR2 targeting may represent a valuable novel tunable therapeutic approach for several forms of anemia.

3. RESULTS

3.1 Bone marrow specific *Tfr2* targeting in a murine model of anemia of CKD

3.1.1 Bone marrow Tfr2 deletion sustains RBC production in CKD

To investigate whether the specific deletion of *Tfr2* in the BM may ameliorate anemia of CKD, as already proved in murine models of β-thalassemia (Artuso *et al*, 2018; Di Modica *et al*, 2022), we induced CKD in mice lacking BM *Tfr2* and relative controls. We exploited an adenine-rich diet (Jia *et al*, 2013), that we confirmed able to recapitulate human features of CKD, inducing anemia (**Figure 12A-E**), iron deficiency (**Figure 12F**) and renal damage (**Figure 13**) in wild-type (wt) animals.

WT recipients were lethally irradiated and received BM from wt or *Tfr2*$^{-/-}$ mice to generate *Tfr2*^{BMWT} and *Tfr2*^{BMKO} mice, respectively. Donor/host chimerism evaluated at the end of the protocol was superior to 90% both in the BM and in the spleen in all animals. Ten weeks after transplantation, when erythropoiesis was fully recovered, mice were fed the adenine-rich diet as indicated in **Figure 14A**.

Following CKD induction, *Tfr2*^{BMWT} mice showed progressive decrease of RBCs and hemoglobin (Hb) levels (**Figure 14B-C**), as expected. On the contrary, *Tfr2*^{BMKO} mice maintained higher RBCs for the entire protocol (**Figure 14B**). Hb was higher for 6 weeks but reached levels comparable to controls at 8 weeks (**Figure 14C**), indicating the development of iron-restricted erythropoiesis. In agreement, mean corpuscular volume (MCV, **Figure 14D**) and mean corpuscular hemoglobin (MCH, **Figure 14E**) showed a trend to be reduced in *Tfr2*^{BMKO} mice.

Figure 12

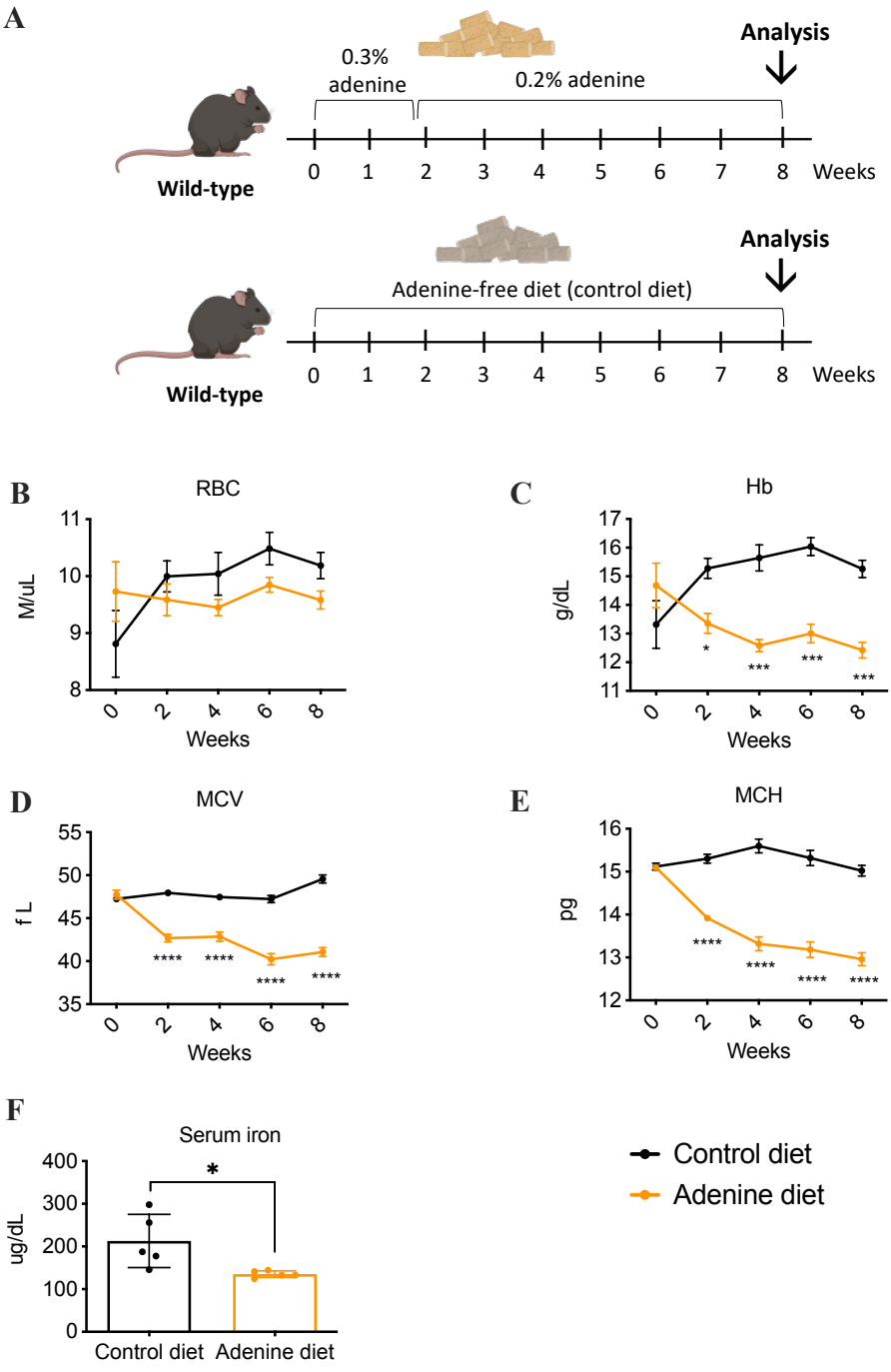

Figure 12. The adenine diet induces anemia and iron deficiency. *Eight-week-old wt mice were fed the adenine diet and the control diet (with the same composition, but adenine-free) for 8 weeks. In the figure are represented: a scheme of the protocol (**A**); red blood cell count (RBC, **B**); hemoglobin levels (Hb, **C**); mean corpuscular volume (MCV, **D**); mean corpuscular hemoglobin (MCH, **E**) and circulating iron levels (**F**).*
*Mean values of 5 mice per group are represented. Two-way ANOVA for multiple comparisons (correction test Šídák, panels **B-E**) and unpaired 2-tailed Student's t-test (panel **F**) were used. Bars indicate standard deviation (SD). Asterisks refer to statistically significant differences. *P<0.05; ***P<0.001; ****P<0.0001.*

Figure 13

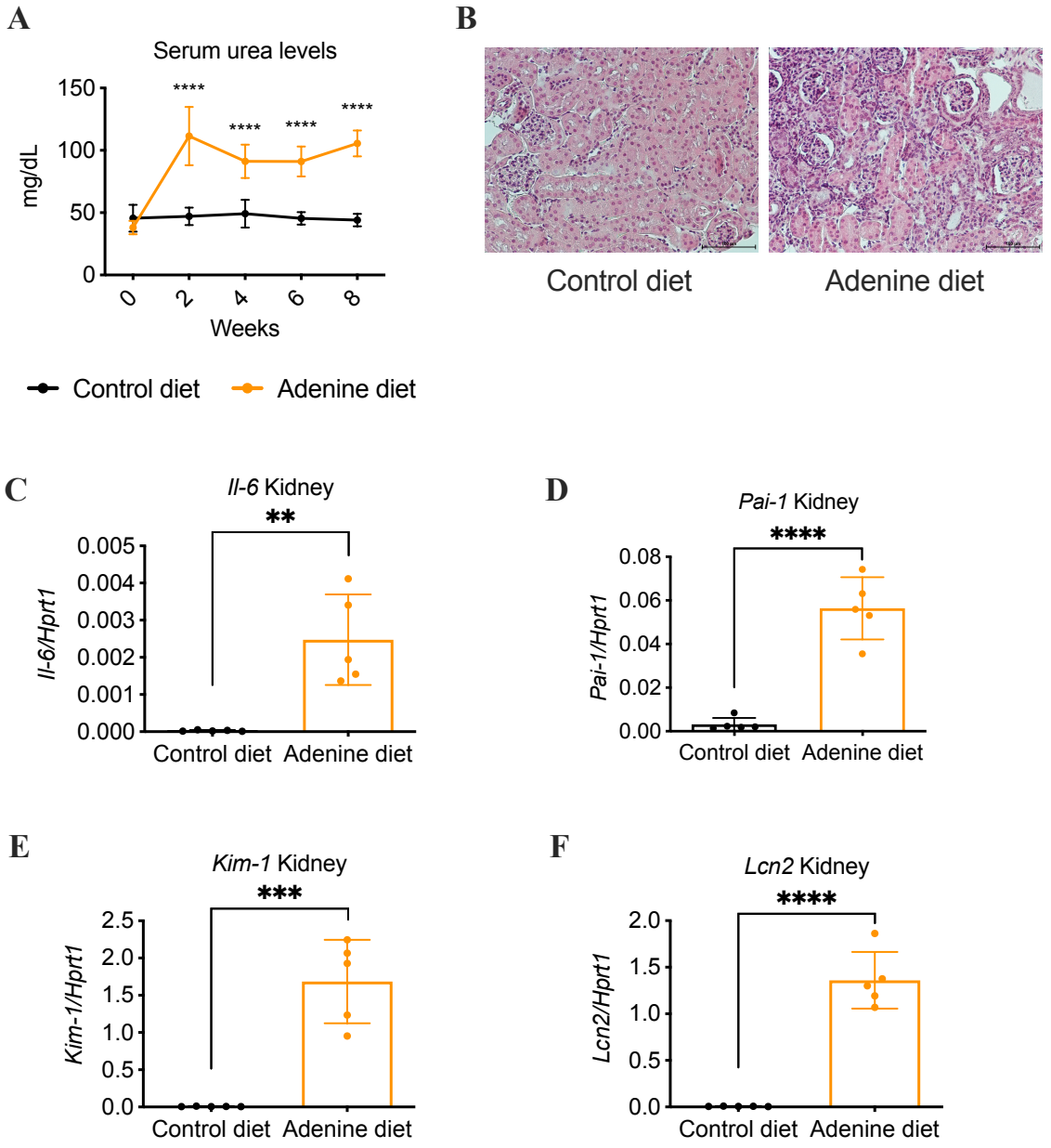

Figure 13. The adenine diet induces renal damage. *Eight-week-old wt mice were fed the adenine diet and the control diet (with the same composition, but adenine-free) for 8 weeks. In the figure are represented: serum urea levels (**A**); representative hematoxylin-eosin staining of kidney sections (magnification 20x, **B**); kidney mRNA levels of Inteleukin-6 (Il-6, **C**), Plasminogen activator inhibitor 1 (Pai-1, **D**), Kidney injury molecule 1 (Kim-1, **E**) and Lipocalin 2 (Lcn-2, **F**) relative to Hypoxanthine Phosphoribosyltransferase1 (Hprt1).*
*Mean values of 5 mice per group are represented. Two-way ANOVA for multiple comparisons (correction test Šídák, panel **A**) and unpaired 2-tailed Student's t-test (panels **C-F**) were used. Bars indicate standard deviation (SD). Asterisks refer to statistically significant differences. **P<0.005; ***P<0.001; ****P<0.0001.*

Figure 14

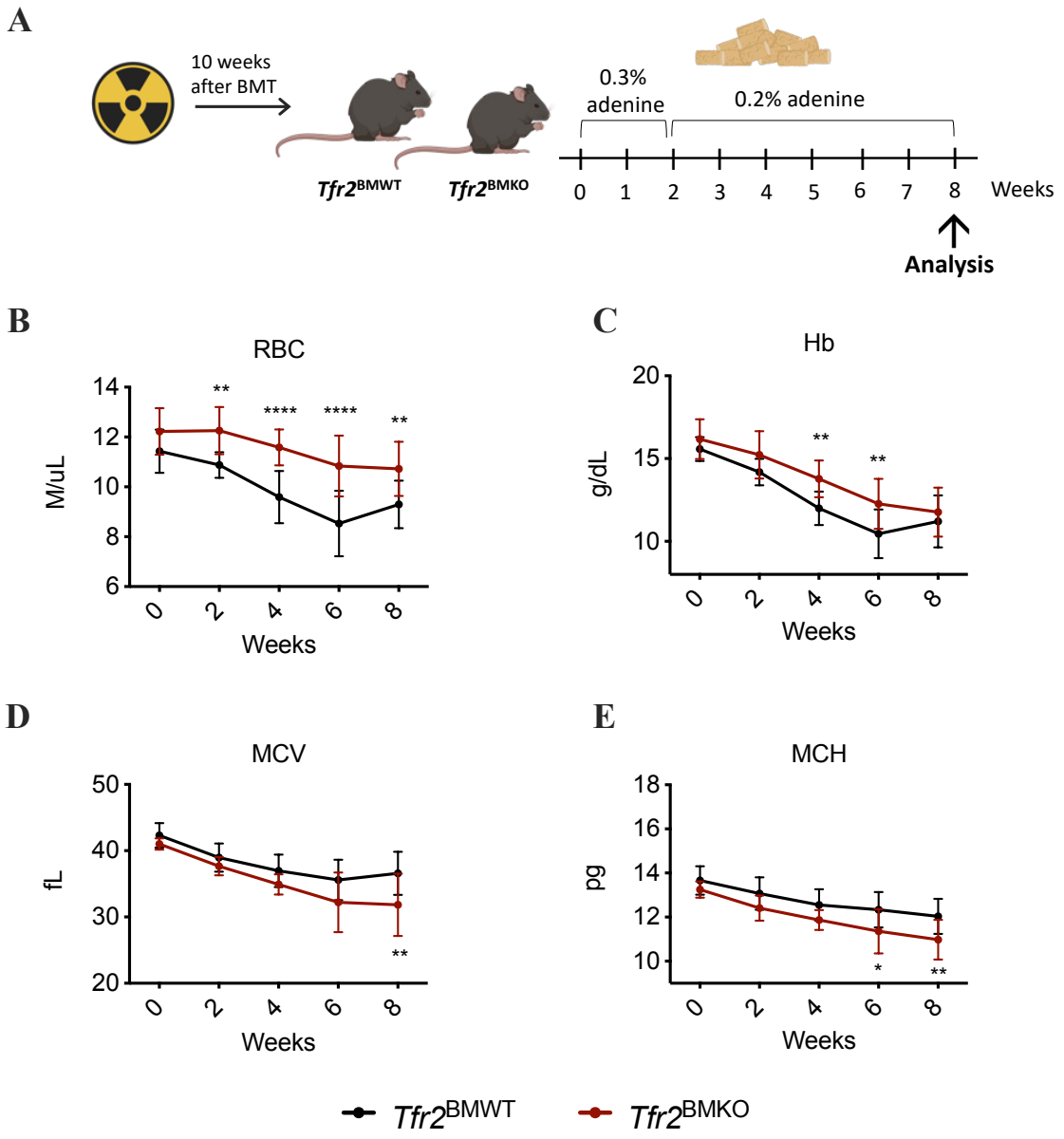

Figure 14. CKD $Tfr2^{BMKO}$ mice show higher RBC count and signs of iron-restricted erythropoiesis compared to controls. *$Tfr2^{BMWT}$ and $Tfr2^{BMKO}$ mice were generated through BM transplantation. Ten weeks later, mice were fed the adenine diet for 8 weeks. In the figure are represented: a scheme of the protocol (**A**); red blood cell count (RBC, **B**); hemoglobin levels (Hb, **C**); mean corpuscular volume (MCV, **D**) and mean corpuscular hemoglobin (MCH, **E**).*
*Mean values of 8-12 mice per group are represented. Two-way ANOVA for multiple comparisons (correction test Šídák, panels **B-E**) was used. Bars indicate standard deviation (SD). Asterisks refer to statistically significant differences. *P<0.05; **P<0.005; ****P<0.0001.*

3.1.2 Circulating iron levels are inadequate to sustain the enhanced erythropoiesis of CKD Tfr2^{BMKO} mice

Serum iron and transferrin saturation were low in both *Tfr2*^{BMWT} and *Tfr2*^{BMKO} relative to wt healthy mice, but comparable between the two groups (**Figure 15A** and **B**). No differences between *Tfr2*^{BMWT} and *Tfr2*^{BMKO} mice were detected also in liver (LIC), spleen (SIC) and kidney (KIC) iron content (**Figure 15C-E**).

In line with LIC, the expression levels of the hepatic iron-regulatory hormone hepcidin (*Hamp*, **Figure 15F**) were also comparable. Hepatic marker or systemic inflammation Serum Amyloid A1 (*Saa1,* **Figure 15G**) and circulating IL-6 levels (**Figure 15H**) were comparable, indicating similar inflammatory degree.

Despite a comparable degree of iron deficiency between *Tfr2*^{BMWT} and *Tfr2*^{BMKO} mice, *Tfr2*^{BMKO} showed enhanced terminal erythropoiesis, as indicated by the increased percentage of total Ter119^{+} cells both in BM and spleen, mainly due to the expansion of basophilic and polychromatic erythroblasts (**Figure 16A-B**). Thus, we hypothesized that low iron levels were not sufficient to properly sustain on the long-term the enhanced erythropoiesis of *Tfr2*^{BMKO} animals, leading to the decrease in Hb levels observed at the end of the protocol.

The augmented erythropoiesis of *Tfr2*^{BMKO} mice was not due to higher EPO production, but rather to an increased erythroblasts sensitivity to EPO due to BM *Tfr2* deletion. Indeed, serum EPO levels were comparable between the two groups (**Figure 16C**) and *Epo* expression in the kidney was even lower in *Tfr2*^{BMKO} mice (**Figure 16D**). On the contrary, the expression levels of the EPO target gene *Bcl-xl* were increased in BM and spleen of *Tfr2*^{BMKO} mice both as absolute values (**Figure 16E-F**) and when normalized on circulating EPO (**Figure 16G-H**), suggesting an over-activation of the EPO-EPOR pathway.

In agreement, the expression of *Erfe*, another EPO target gene, showed a trend to be higher both in the BM and in the spleen of *Tfr2*^{BMKO} mice (**Figure 17A-B**), and the difference reached statistical significance in the BM when normalized on circulating EPO levels (**Figure 17 C-D**). Also, mRNA levels of *Epor*, which is activated by the signaling in a positive feedback loop, despite similar between the 2 groups both in the BM and in

the spleen as absolute values (**Figure 17 E-F**), were higher in the spleen of *Tfr2*^{BMKO} mice when normalized on circulating EPO levels (**Figure 17G-H**), again confirming that the absence of *Tfr2* promotes EPO signaling in erythroid cells.

Figure 15

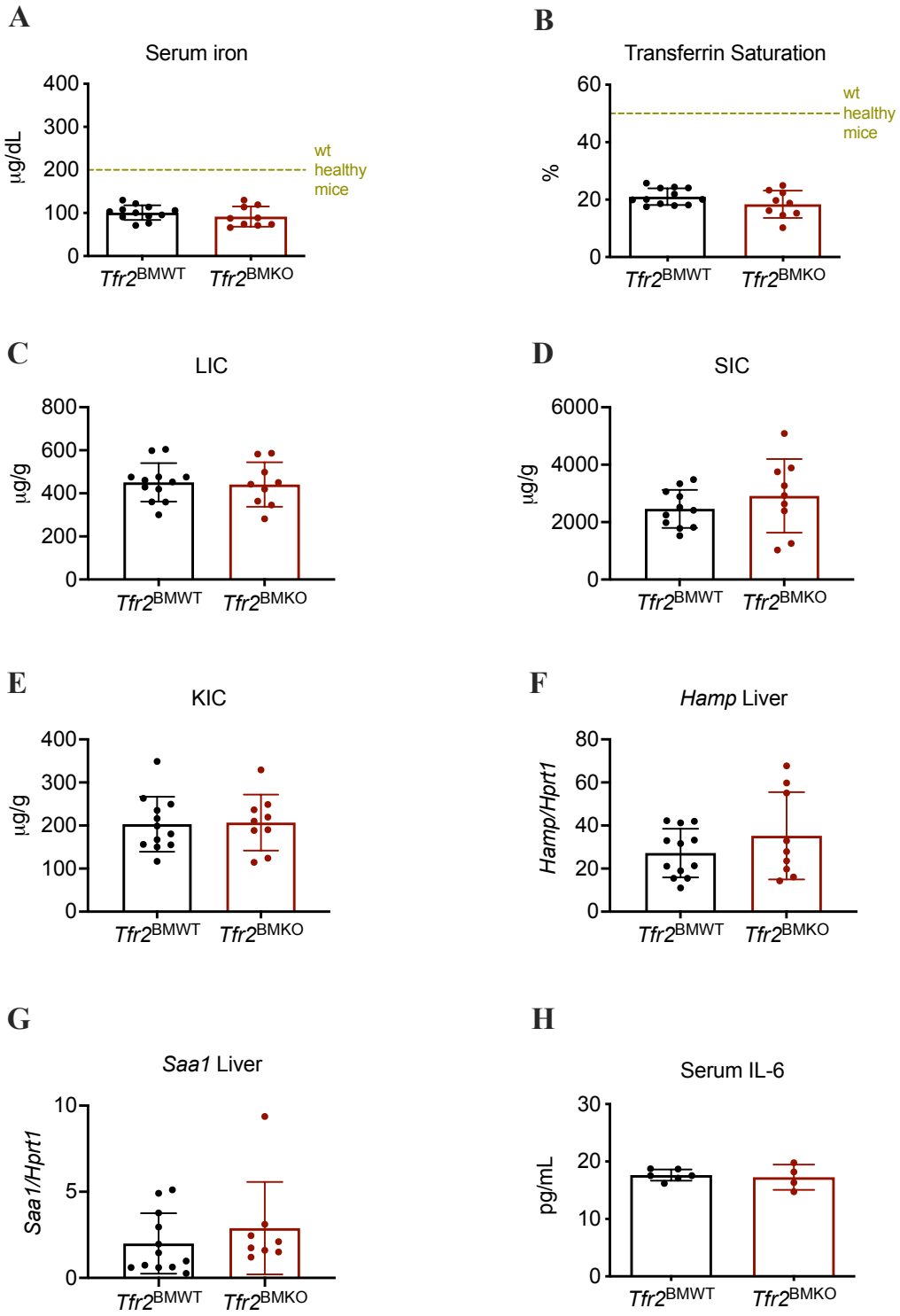

Figure 15. CKD Tfr2^{BMKO} and control mice have comparable iron and inflammatory profile.
*Tfr2^{BMWT} and Tfr2^{BMKO} mice were generated through BM transplantation. Ten weeks later, mice were fed the adenine-rich diet for 8 weeks. In the figure are represented: serum iron levels (**A**); transferrin saturation (**B**); liver iron content (LIC, **C**); spleen iron content (SIC, **D**), kidney iron content (KIC, **E**), hepatic mRNA levels of hepcidin (Hamp, **F**), and of Serum amyloid a-1 (Saa1) relative to Hypoxanthine Phosphoribosyltransferase1(Hprt1) in the liver (**G**); circulating levels of IL-6 (**H**).*
*Mean values of 8-12 mice per group are represented. Unpaired 2-tailed Student's t-test (panels **A-H**) was used. Bars indicate standard deviation (SD).*

Figure 16

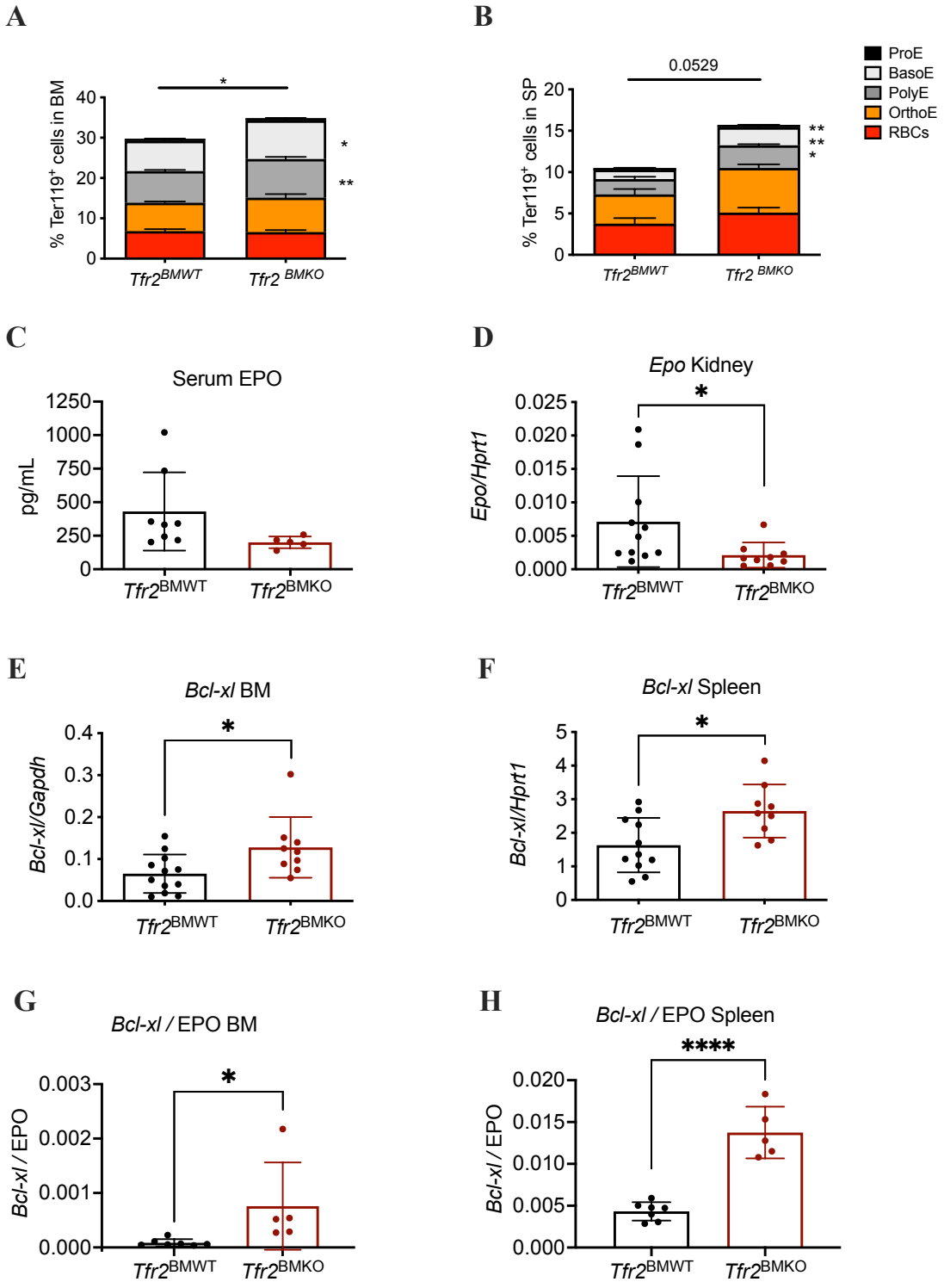
A
% Ter119+ cells in BM
Tfr2BMWT
Tfr2 BMKO
B
0.0529
% Ter119+ cells in SP
ProE
BasoE
PolyE
OrthoE
RBCs
C
Serum EPO
pg/mL
D
Epo Kidney
Epo/Hprt1
E
Bcl-xl BM
Bcl-xl/Gapdh
F
Bcl-xl Spleen
Bcl-xl/Hprt1
G
Bcl-xl / EPO BM
Bcl-xl / EPO
H
Bcl-xl / EPO Spleen

Figure 16. CKD Tfr2^{BMKO} mice show enhanced erythropoiesis and higher activation of the EPO-EPOR pathway than controls. *Tfr2^{BMWT} and Tfr2^{BMKO} mice were generated through BM transplantation. Ten weeks later, mice were fed the adenine-rich diet for 8 weeks. In the figure are represented: the percentage of total Ter119^{+} cells in the BM (**A**) and in the spleen (SP, **B**) and the contribution of the 5 erythroblasts populations [proerythroblasts (ProE), basophilic erythroblasts (BasoE), polychromatic erythroblasts (PolyE), orthochromatic erythroblasts and immature reticulocytes (OrthoE), and mature red cells (RBCs)], identified through the evaluation of cell size and Ter119/CD44 relative expression; serum erythropoietin levels (EPO, **C**); mRNA levels of Epo relative to Hypoxanthine Phosphoribosyltransferase1 (Hprt1) in the kidney (**D**); mRNA levels of B-cell lymphoma extra-large (Bcl-xl) relative to Glyceraldehyde-3-phosphate dehydrogenase (Gapdh) in the BM (**E**) and relative to Hprt1 in the spleen (**F**); B-cell lymphoma extra-large (Bcl-xl) mRNA levels normalized on circulating EPO in the BM (**G**) and in the spleen (**H**).*

*Mean values of 8-12 mice per group are represented. Unpaired 2-tailed Student's t-test (panels **A-H**) was used. Bars indicate standard deviation (SD). Asterisks refer to statistically significant differences. *P<0.05; **P<0.005; ****P<0.0001. P-values close to 0.05 are also shown.*

Figure 17

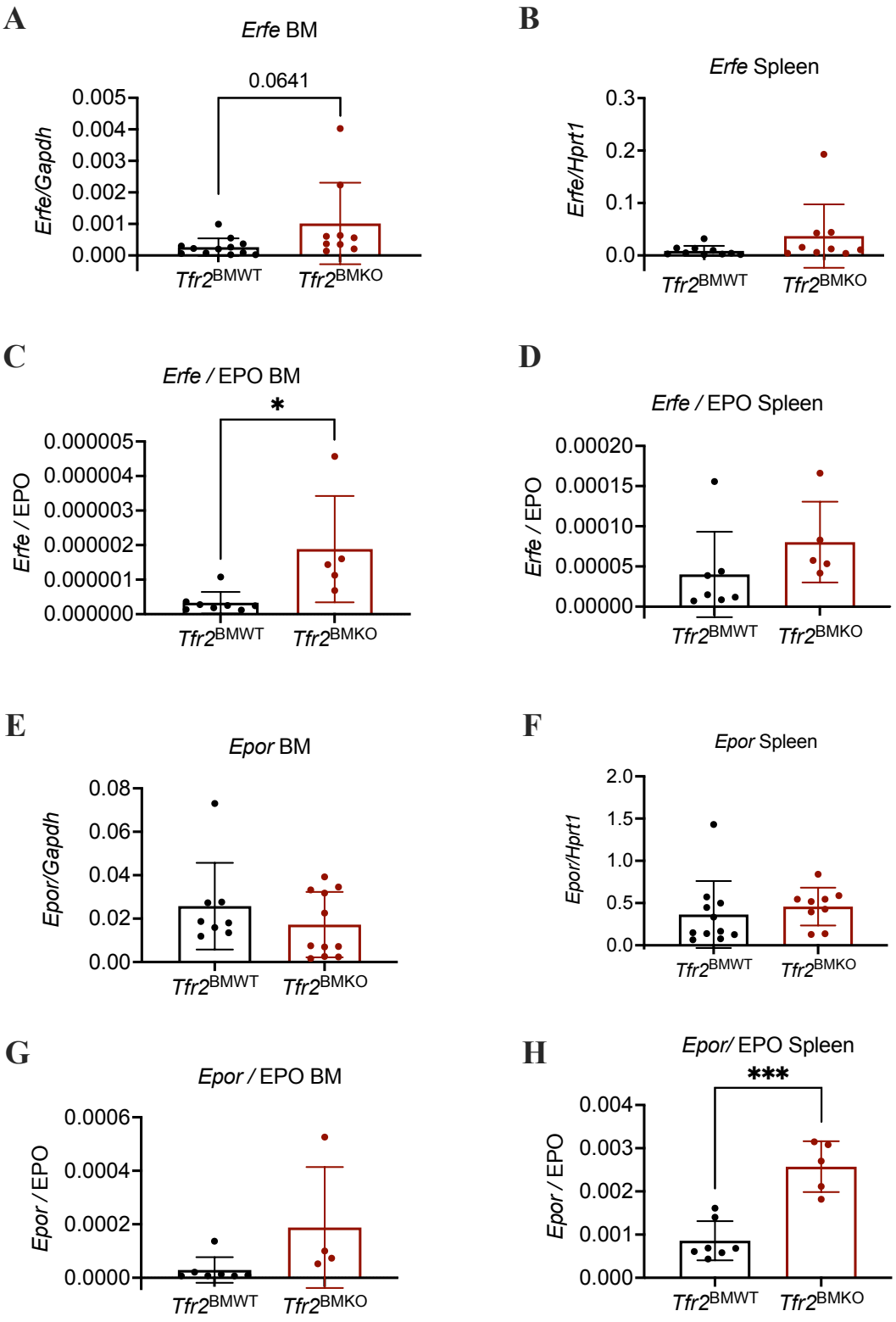
A
Erfe BM
0.0641
Erfe/Gapdh
0.005
0.004
0.003
0.002
0.001
0.000
Tfr2BMWT
Tfr2BMKO
B
Erfe Spleen
Erfe/Hprt1
0.3
0.2
0.1
0.0
Tfr2BMWT
Tfr2BMKO
C
Erfe / EPO BM
*
Erfe / EPO
0.000005
0.000004
0.000003
0.000002
0.000001
0.000000
Tfr2BMWT
Tfr2BMKO
D
Erfe / EPO Spleen
Erfe / EPO
0.00020
0.00015
0.00010
0.00005
0.00000
Tfr2BMWT
Tfr2BMKO
E
Epor BM
Epor/Gapdh
0.08
0.06
0.04
0.02
0.00
Tfr2BMWT
Tfr2BMKO
F
Epor Spleen
Epor/Hprt1
2.0
1.5
1.0
0.5
0.0
Tfr2BMWT
Tfr2BMKO
G
Epor / EPO BM
Epor / EPO
0.0006
0.0004
0.0002
0.0000
Tfr2BMWT
Tfr2BMKO
H
Epor/ EPO Spleen
***
Epor / EPO
0.004
0.003
0.002
0.001
0.000
Tfr2BMWT
Tfr2BMKO

Figure 17. CKD Tfr2^{BMKO} mice show increased expression of EPO-target genes. *Tfr2^{BMWT} and Tfr2^{BMKO} mice were generated through BM transplantation. Ten weeks later, mice were fed the adenine-rich diet for 8 weeks. In the figure are represented: mRNA levels of Erythroferrone (Erfe) relative to Glyceraldehyde-3-phosphate dehydrogenase (Gapdh) in the BM (**A**) and relative to Hypoxanthine Phosphoribosyltransferase1 (Hprt1) in the spleen (**B**); Erfe mRNA levels normalized on circulating EPO in the BM (**C**) and in the spleen (**D**); mRNA levels of Erythropoietin receptor (Epor) relative to Gapdh in the BM (**E**) and relative to Hprt1 in the spleen (**F**); Epor mRNA levels normalized on circulating EPO in the BM (**G**) and in the spleen (**H**). Mean values of 8-12 mice per group are represented. Unpaired 2-tailed Student's t-test (panels **A-H**) was used. Bars indicate standard deviation (SD). Asterisks refer to statistically significant differences. *P<0.05; ***P<0.001. P-values close to 0.05 are also shown.*

3.1.3 CKD Tfr2^{BMKO} mice and controls have comparable renal damage

To exclude a differential effect of the adenine diet on renal damage in the two groups, we analyzed parameters of kidney function, damage and inflammation.

Serum urea, a marker of renal functionality, increased over time in a comparable way between *Tfr2*^{BMWT} and *Tfr2*^{BMKO} mice (**Figure 18A**). The expression levels of Kidney injury molecule 1 (*Kim-1,* **Figure 18B***)* and Lipocalin-2 (*Lcn-2,* **Figure 18C**), markers of proximal and distal tubular damage, respectively (Nakagawa *et al*, 2015), and of Plasminogen activator inhibitor 1 (*Pai-1*, **Figure 18D**), marker of fibrosis (Eddy & Fogo, 2006) were similar between the 2 groups, excluding a different degree of renal damage. Also, the inflammatory phenotype of kidneys from *Tfr2*^{BMWT} and *Tfr2*^{BMKO} animals appears similar. Indeed, no differences were detected in the mRNA levels of *Il-6* (**Figure 18E***)*, a pro-inflammatory cytokine, and of the monocyte infiltration marker Protein Tyrosine Phosphatase Receptor Type C (*Cd45*, **Figure 18F**). Histological analyses of kidney sections confirmed comparable tubules dilatation and local infiltration (**Figure 18G**).

Overall, these data indicate that BM-specific *Tfr2* deletion increases RBCs production in CKD mice, enhancing erythroid EPO responsiveness despite comparable EPO levels. However, low iron availability causes the development of an iron-restricted erythropoiesis, leading to transient anemia amelioration.

Figure 18

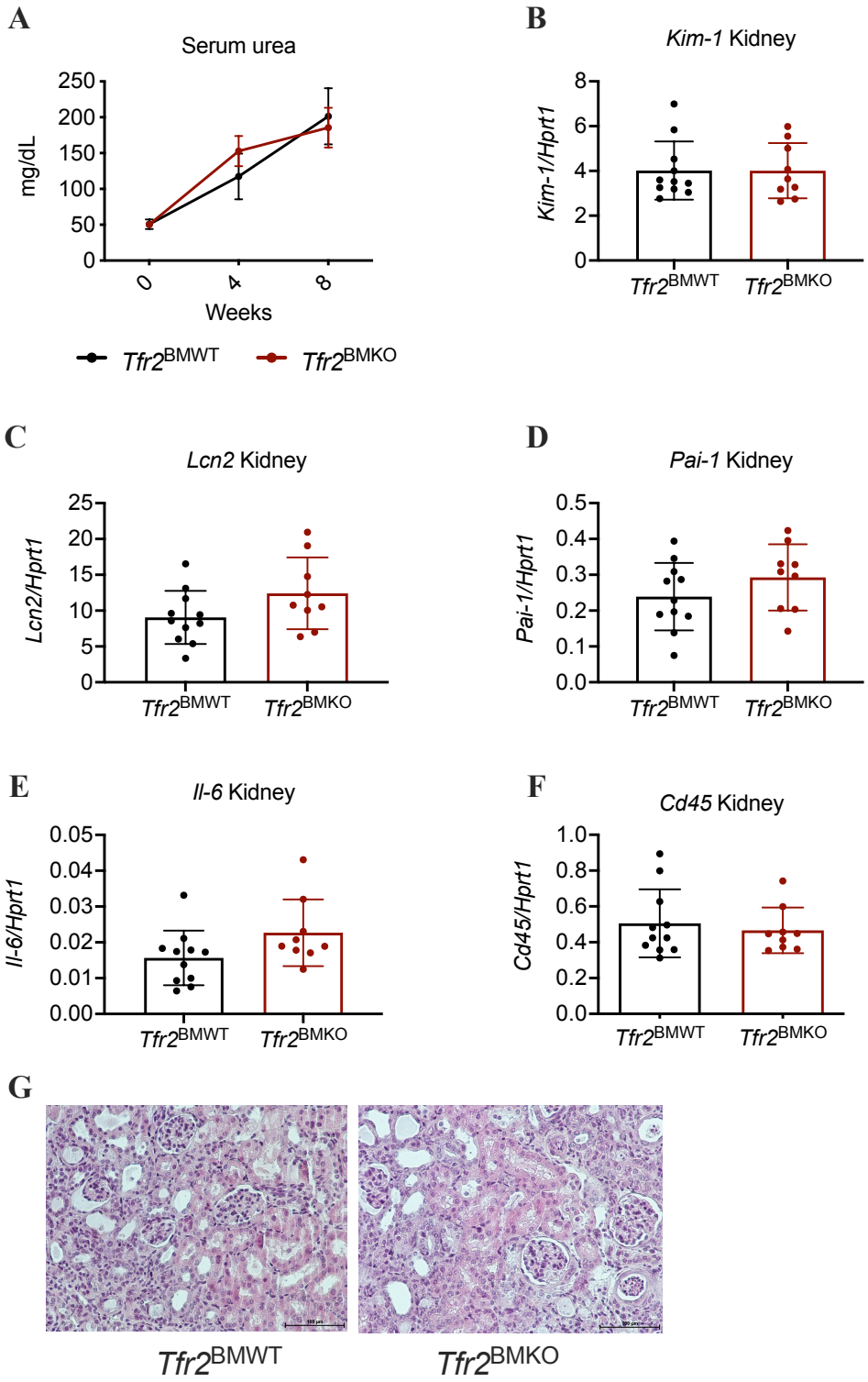
A
Serum urea
mg/dL
250
200
150
100
50
0
0
4
8
Weeks
Tfr2BMWT
Tfr2BMKO
B
Kim-1 Kidney
Kim-1/Hprt1
8
6
4
2
0
Tfr2BMWT
Tfr2BMKO
C
Lcn2 Kidney
Lcn2/Hprt1
25
20
15
10
5
0
Tfr2BMWT
Tfr2BMKO
D
Pai-1 Kidney
Pai-1/Hprt1
0.5
0.4
0.3
0.2
0.1
0.0
Tfr2BMWT
Tfr2BMKO
E
Il-6 Kidney
Il-6/Hprt1
0.05
0.04
0.03
0.02
0.01
0.00
Tfr2BMWT
Tfr2BMKO
F
Cd45 Kidney
Cd45/Hprt1
1.0
0.8
0.6
0.4
0.2
0.0
Tfr2BMWT
Tfr2BMKO
G
Tfr2BMWT
Tfr2BMKO

Figure 18. CKD Tfr2^{BMKO} and control mice show comparable renal damage. *Tfr2^{BMWT} and Tfr2^{BMKO} mice were generated through BM transplantation. Ten weeks later, mice were fed the adenine-rich diet for 8 weeks. In the figure are represented: serum urea levels (**A**); kidney mRNA levels of Kidney injury molecule 1 (Kim-1, **B**), Lipocalin 2 (Lcn-2, **C**), Plasminogen activator inhibitor 1 (Pai-1, **D**), Inteleukin-6 (Il-6, **E**) and Protein Tyrosine Phosphatase Receptor Type C (Cd45, **F**) relative to Hypoxanthine Phosphoribosyltransferase1 (Hprt1); representative images of hematoxylin-eosin staining of kidney sections (magnification 20x, **G**).*
*Mean values of 8-12 mice per group are represented. Two-way ANOVA for multiple comparisons (correction test Šídák, panel **A**) and unpaired 2-tailed Student's t-test (panels **B-F**) were used. Bars indicate standard deviation (SD).*

3.2 Total *Tfr2* targeting in a murine model of anemia of CKD

3.2.1 CKD Tfr2$^{-/-}$ mice maintain higher RBC count, Hb levels and iron availability than wt littermates

To overcome the problem of the low iron availability, we hypothesized that the simultaneous deletion of erythroid and hepatic *Tfr2* would induce a sustained amelioration of anemia of CKD, increasing both circulating iron and RBCs production. To address this point, we induced CKD in germline *Tfr2$^{-/-}$* mice and wt (*Tfr2$^{+/+}$*) littermates as in **Figure 19A**. At the beginning of the protocol, *Tfr2$^{-/-}$* mice were already iron-loaded (Roetto *et al*, 2010), but hematological parameters were comparable to controls (**Figure 19B-E**). However, during CKD development, *Tfr2$^{-/-}$* mice maintained RBC count (**Figure 19B**) and Hb levels (**Figure 19C**) higher than controls for the entire time-span. MCV and MCH were comparable between the two groups (**Figure 19D-E**), suggesting that, in this setting, iron availability is sufficient to sustain the increased RBC output of *Tfr2$^{-/-}$* mice.

Indeed, both serum iron levels and transferrin saturation were higher in *Tfr2$^{-/-}$* mice, reaching values comparable to wt healthy mice (**Figure 20A-B**). As expected, liver iron content (LIC, **Figure 20C**) was higher in *Tfr2$^{-/-}$* mice, while spleen (SIC) and kidney (KIC) iron content (**Figure 20D-E**) were comparable to controls. Pancreas iron content (PIC) showed a trend to be higher in *Tfr2$^{-/-}$* mice (**Figure 20F**), compatibly with an iron-overload phenotype. As expected, this was due to hampered hepcidin production. Indeed, hepatic *Hamp* levels, despite comparable between the 2 genotypes, were inappropriately low in *Tfr2$^{-/-}$* mice relative to the degree of hepatic iron loading (**Figure 20G-H**).

Figure 19

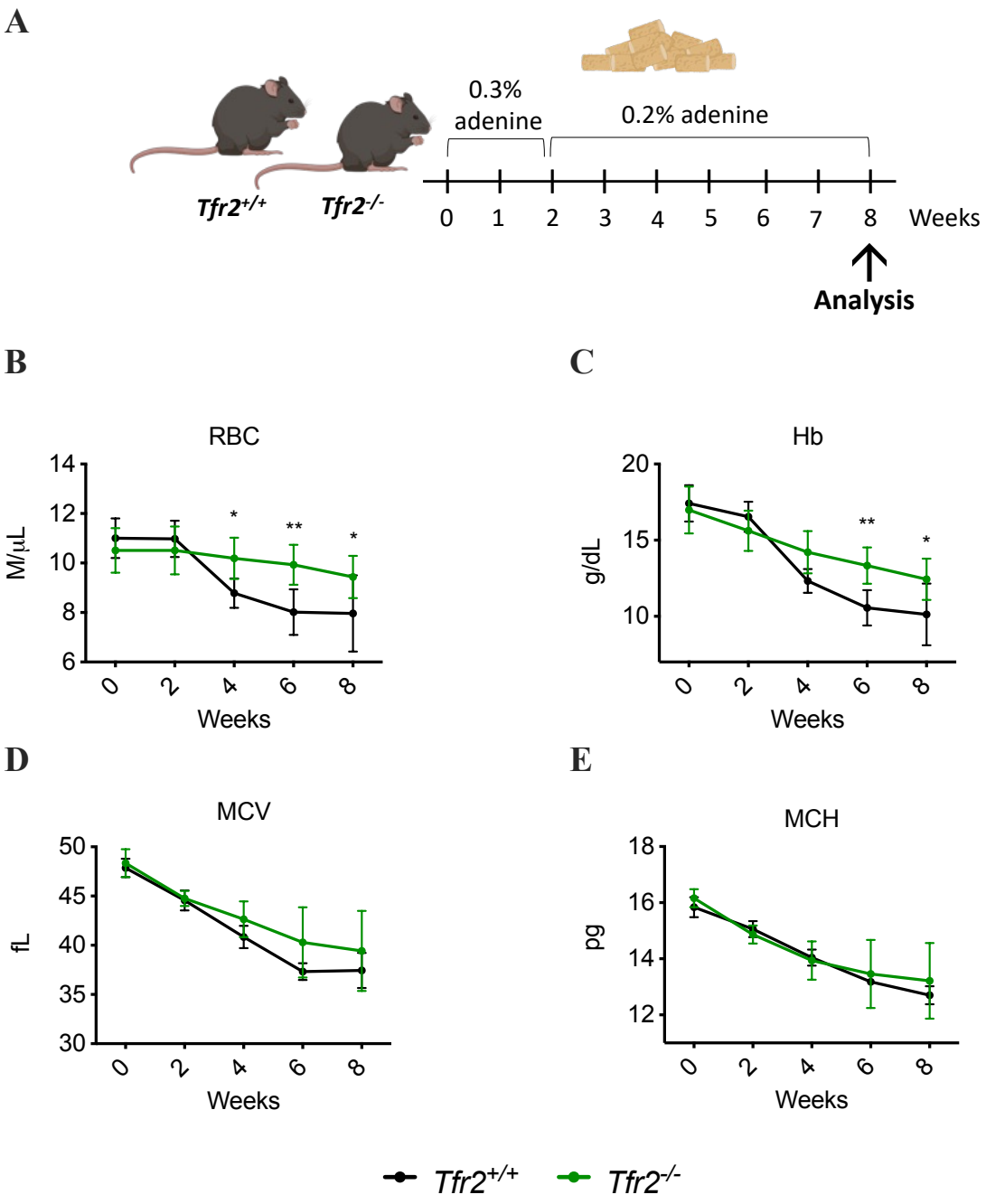

Figure 19. CKD Tfr2$^{-/-}$ mice have higher RBCs and Hb levels than controls. *Eight-week-old Tfr2$^{+/+}$ and Tfr2$^{-/-}$ mice were fed the adenine-rich diet for 8 weeks. In the figure are represented: a scheme of the protocol (**A**); red blood cell count (RBC, **B**); hemoglobin levels (Hb, **C**); mean corpuscular volume (MCV, **D**) and mean corpuscular hemoglobin (MCH, **E**).*
*Mean values of 5-7 mice per group are represented. Two-way ANOVA for multiple comparisons (correction test Šídák, panels **B-E**) was used. Bars indicate standard deviation (SD). Asterisks refer to statistically significant differences. *P<0.05; **P<0.005.*

Figure 20

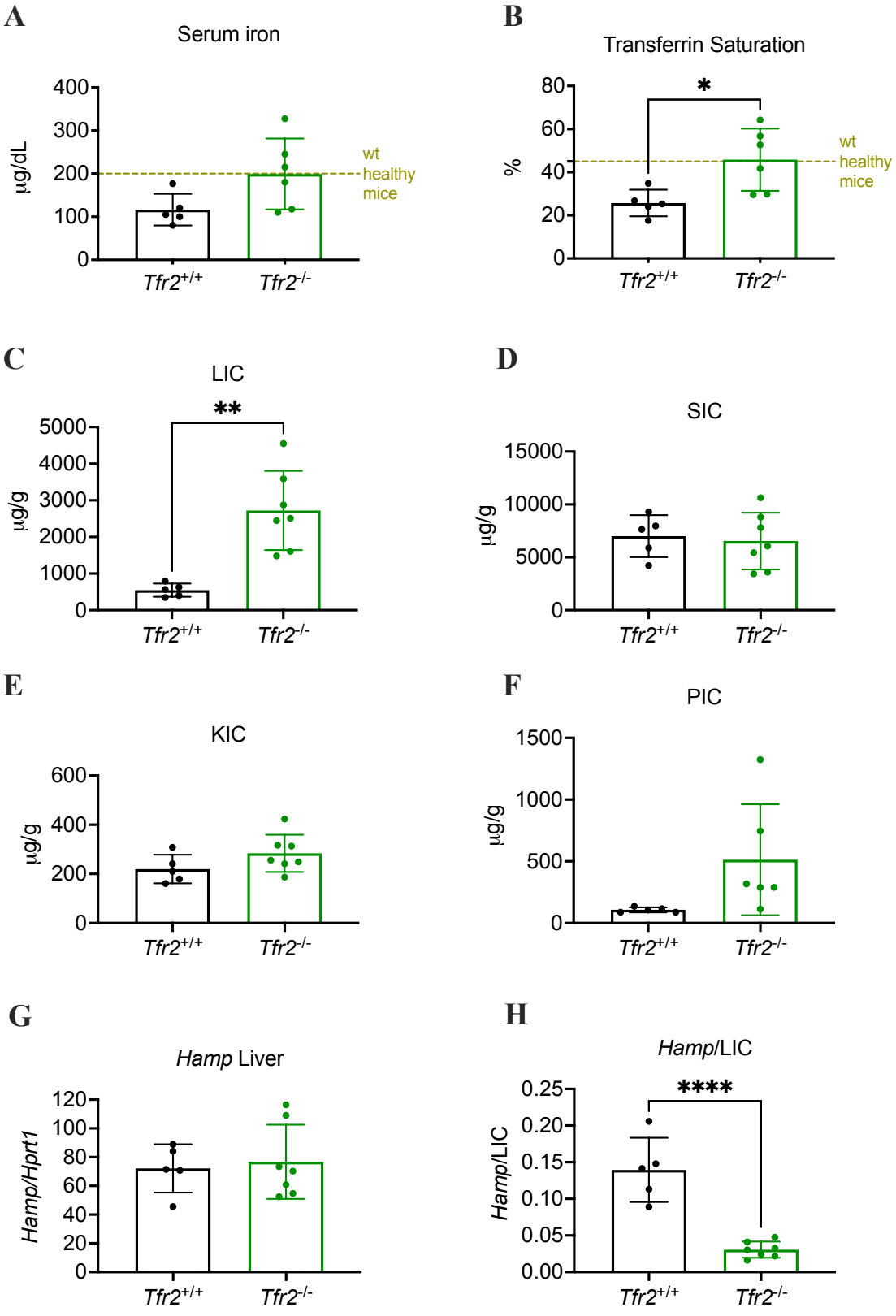
A
Serum iron
µg/dL
400
300
200
100
0
wt
healthy
mice
Tfr2+/+
Tfr2-/-
B
Transferrin Saturation
%
80
60
40
20
0
*
wt
healthy
mice
Tfr2+/+
Tfr2-/-
C
LIC
**
µg/g
5000
4000
3000
2000
1000
0
Tfr2+/+
Tfr2-/-
D
SIC
µg/g
15000
10000
5000
0
Tfr2+/+
Tfr2-/-
E
KIC
µg/g
600
400
200
0
Tfr2+/+
Tfr2-/-
F
PIC
µg/g
1500
1000
500
0
Tfr2+/+
Tfr2-/-
G
Hamp Liver
Hamp/Hprt1
120
100
80
60
40
20
0
Tfr2+/+
Tfr2-/-
H
Hamp/LIC
****
Hamp/LIC
0.25
0.20
0.15
0.10
0.05
0.00
Tfr2+/+
Tfr2-/-

Figure 20. CKD Tfr2$^{-/-}$ mice have higher iron levels than controls. *Eight-week-old Tfr2$^{+/+}$ and Tfr2$^{-/-}$ mice were fed the adenine-rich diet for 8 weeks. In the figure are represented: serum iron levels (**A**); transferrin saturation (**B**); liver (LIC, **C**), spleen (SIC, **D**), kidney (KIC, **E**) and pancreas (PIC, **F**) iron content; hepatic mRNA levels of hepcidin (Hamp, **G**) relative to Hypoxanthine Phosphoribosyltransferase1 (Hprt1) in the liver; ratio between the relative quantification of Hamp mRNA levels and the liver iron content (**H**).*
*Mean values of 5-7 mice per group are represented. Unpaired 2-tailed Student's t-test (panels **A-H**) was used. Bars indicate standard deviation (SD). Asterisks refer to statistically significant differences. *P<0.05; **P<0.005; ****P<0.0001.*

3.2.2 CKD Tfr2$^{-/-}$ mice have increased erythroid EPO sensitivity than controls

Terminal erythropoiesis did not differ between *Tfr2$^{-/-}$* mice and controls at the end of the protocol, both in the BM and in the spleen (**Figure 21A-B**). However, circulating EPO levels were lower in *Tfr2$^{-/-}$* mice (**Figure 21C**) and *Epo* kidney expression showed a trend to be reduced (**Figure 21D**), in line with improved hematological parameters. Transcript levels of the EPO target gene *Bcl-xl* were comparable between *Tfr2$^{-/-}$* and control mice both in the BM and in the spleen (**Figure 21E-F**), but inappropriately high in *Tfr2$^{-/-}$* mice relative to low circulating EPO (**Figure 21G-H**). *Epor* had a similar behavior (**Figure 22A-D**), overall confirming the increased EPO sensitivity of erythroid cells lacking *Tfr2* (Nai *et al*, 2015). Surprisingly, *Erfe* levels were lower in *Tfr2$^{-/-}$* mice relative to controls (**Figure 22E-F**), but comparable when normalized on circulating EPO (**Figure 22G-H**).

Figure 21

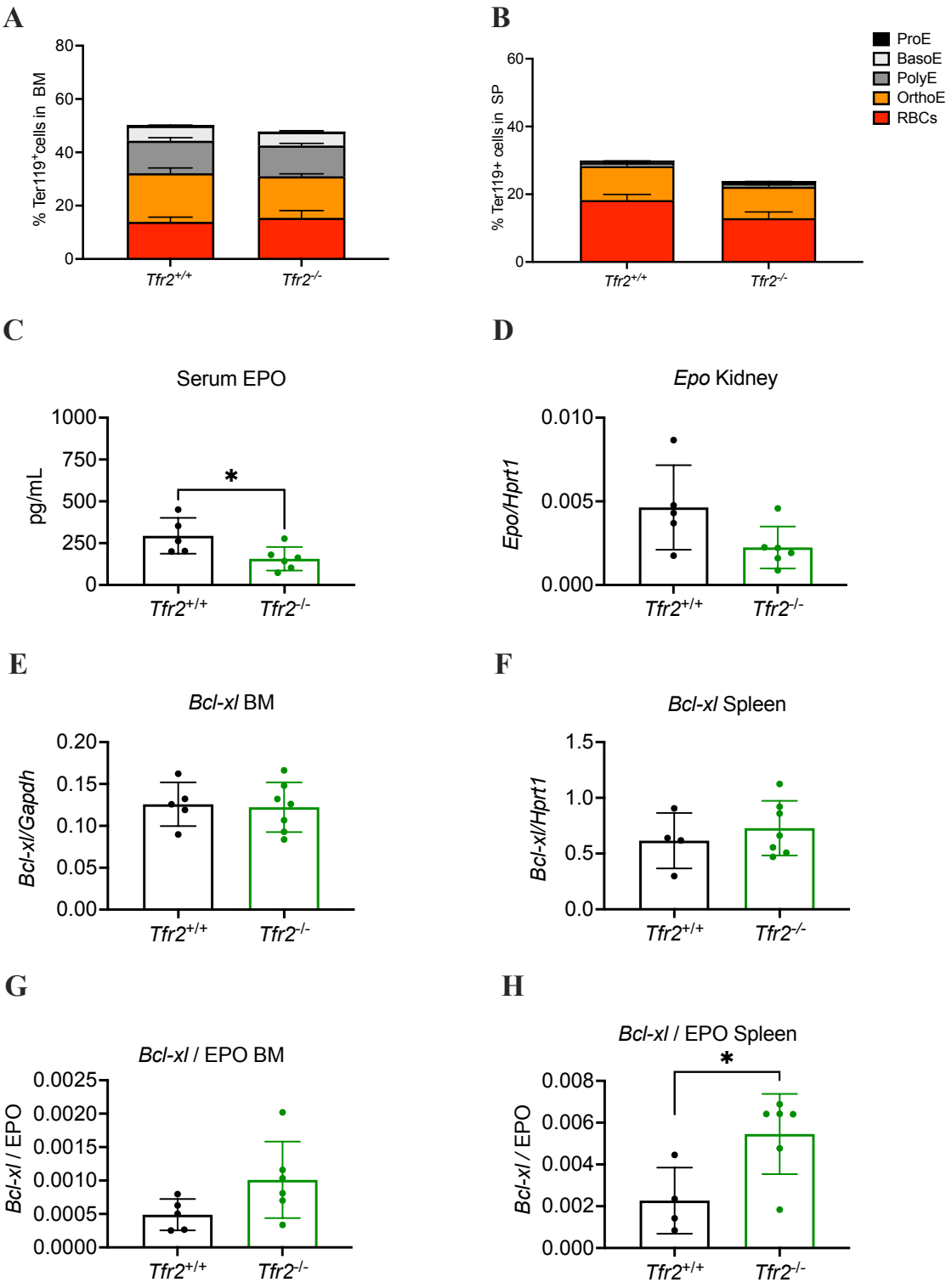
A
% Ter119+cells in BM
80
60
40
20
0
Tfr2+/+
Tfr2-/-
B
% Ter119+ cells in SP
60
40
20
0
ProE
BasoE
PolyE
OrthoE
RBCs
C
Serum EPO
pg/mL
1000
750
500
250
0
*
D
Epo Kidney
Epo/Hprt1
0.010
0.005
0.000
E
Bcl-xl BM
Bcl-xl/Gapdh
0.20
0.15
0.10
0.05
0.00
F
Bcl-xl Spleen
Bcl-xl/Hprt1
1.5
1.0
0.5
0.0
G
Bcl-xl / EPO BM
Bcl-xl / EPO
0.0025
0.0020
0.0015
0.0010
0.0005
0.0000
H
Bcl-xl / EPO Spleen
Bcl-xl / EPO
0.008
0.006
0.004
0.002
0.000
*

Figure 21. CKD Tfr2$^{-/-}$ mice have higher erythroid EPO responsiveness than controls. *Eight-week-old Tfr2$^{+/+}$ and Tfr2$^{-/-}$ mice were fed the adenine-rich diet for 8 weeks. In the figure are represented: the percentage of total Ter119^{+} cells in the BM (**A**) and in the spleen (SP, **B**) and the contribution of the 5 erythroblasts populations [proerythroblasts (ProE), basophilic erythroblasts (BasoE), polychromatic erythroblasts (PolyE), orthochromatic erythroblasts and immature reticulocytes (OrthoE), and mature red cells (RBCs)], identified through the evaluation of cell size and Ter119/CD44 relative expression; serum erythropoietin levels (EPO, **C**); mRNA levels of Epo relative to Hypoxanthine Phosphoribosyltransferase1 (Hprt1) in the kidney (**D**); mRNA levels of B-cell lymphoma extra-large (Bcl-xl) relative to Glyceraldehyde-3-phosphate dehydrogenase (Gapdh) in the BM (**E**) and relative to Hprt1 in the spleen (**F**); B-cell lymphoma extra-large (Bcl-xl) mRNA levels normalized on circulating EPO in the BM (**G**) and in the spleen (**H**).*
*Mean values of 5-7 mice per group are represented. Unpaired 2-tailed Student's t-test (panels **A-H**) was used. Bars indicate standard deviation (SD). Asterisks refer to statistically significant differences. *P<0.05.*

Figure 22

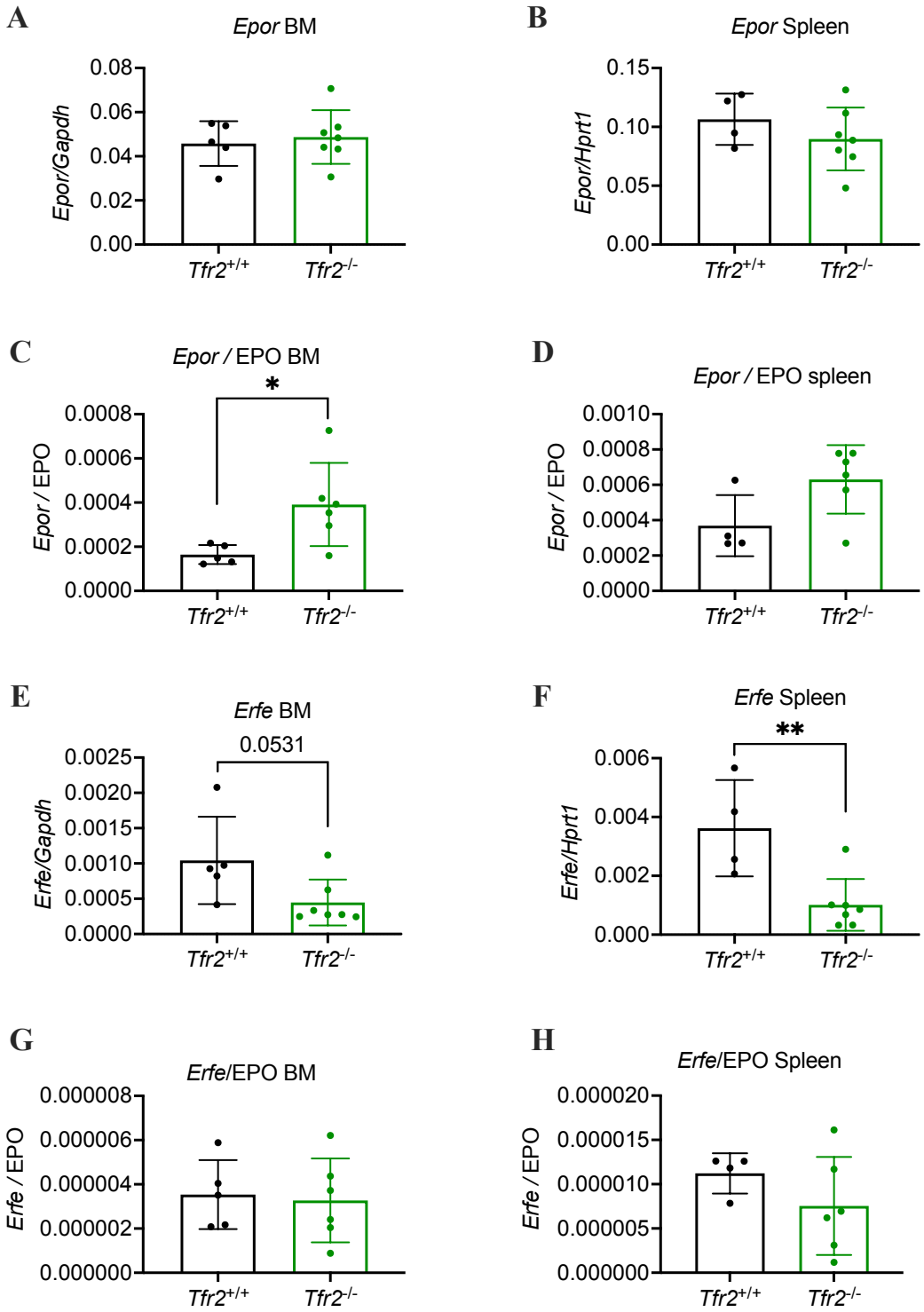
A
Epor BM
Epor/Gapdh
0.08
0.06
0.04
0.02
0.00
Tfr2+/+
Tfr2-/-
B
Epor Spleen
Epor/Hprt1
0.15
0.10
0.05
0.00
Tfr2+/+
Tfr2-/-
C
Epor / EPO BM
*
Epor / EPO
0.0008
0.0006
0.0004
0.0002
0.0000
Tfr2+/+
Tfr2-/-
D
Epor / EPO spleen
Epor / EPO
0.0010
0.0008
0.0006
0.0004
0.0002
0.0000
Tfr2+/+
Tfr2-/-
E
Erfe BM
0.0531
Erfe/Gapdh
0.0025
0.0020
0.0015
0.0010
0.0005
0.0000
Tfr2+/+
Tfr2-/-
F
Erfe Spleen
**
Erfe/Hprt1
0.006
0.004
0.002
0.000
Tfr2+/+
Tfr2-/-
G
Erfe/EPO BM
Erfe / EPO
0.000008
0.000006
0.000004
0.000002
0.000000
Tfr2+/+
Tfr2-/-
H
Erfe/EPO Spleen
Erfe / EPO
0.000020
0.000015
0.000010
0.000005
0.000000
Tfr2+/+
Tfr2-/-

Figure 22. CKD Tfr2$^{-/-}$ mice have increased activation of the erythroid EPO-EPOR pathway than controls. *Eight-week-old Tfr2$^{+/+}$ and Tfr2$^{-/-}$ mice were fed the adenine-rich diet for 8 weeks. In the figure are represented: mRNA levels of Erythropoietin receptor (Epor) relative to Glyceraldehyde-3-phosphate dehydrogenase (Gapdh) in the BM (**A**) and relative to Hypoxanthine Phosphoribosyltransferase1 (Hprt1) in the spleen (**B**); Epor mRNA levels normalized to circulating EPO in the BM (**C**) and in the spleen (**D**); mRNA levels of Erythroferrone (Erfe) relative to Gapdh in the BM (**E**) and relative to Hprt1 in the spleen (**F**); Erfe mRNA levels normalized to circulating EPO in the BM (**G**) and in the spleen (**H**).*
*Mean values of 5-7 mice per group are represented. Unpaired 2-tailed Student's t-test (panels **A-H**) was used. Bars indicate standard deviation (SD). Asterisks refer to statistically significant differences. *P<0.05; **P<0.005. P-values close to 0.05 are also shown.*

3.2.3 CKD Tfr2$^{-/-}$ and control mice have comparable renal damage and inflammation

Serum urea levels indicated that renal functionality was equally impaired in *Tfr2$^{-/-}$* mice and controls (**Figure 23A**). In agreement, histologic analysis showed comparable structural damage in the kidney of both groups (**Figure 23B**). The kidney expression levels of the pro-inflammatory cytokine *Il-6* (**Figure 23C**) and of the markers of proximal and distal tubular damage *Kim-1* and *Lcn-2* (**Figure 23D-E**) were comparable between the two groups, proving no differences in local inflammation. Also, fibrosis was similar, as indicated by *Pai-1* expression (**Figure 23F**). Exclusively *Cd45*, a marker of monocyte infiltration, was higher in the kidney of *Tfr2$^{-/-}$* mice compared to controls (**Figure 23G**).

The hepatic marker of systemic inflammation *Saa1* showed a trend toward an increase (**Figure 24A**), however circulating levels of IL-6 (**Figure 24B**) were similar. Also, *Il-6* mRNA levels were comparable between the two groups of mice both in the liver and in the spleen (**Figure 24C-D**). *Cd45* was increased also in the liver of *Tfr2$^{-/-}$* mice and showed a trend to be higher in the spleen (**Figure 24E-F**).

We hypothesize that the higher iron availability might be the cause of the increased expression of the monocyte marker *Cd45* in some tissues, since iron is known to activate macrophages (Recalcati *et al*, 2010; Cairo *et al*, 2011; Soares & Hamza, 2016). However, our data prove that renal damage is overall comparable between the 2 groups.

Taken together, our results prove that the total deletion of *Tfr2* is necessary and sufficient to ameliorate anemia in CKD mice, simultaneously increasing RBC production and iron supply, without augmenting EPO levels per se.

Figure 23

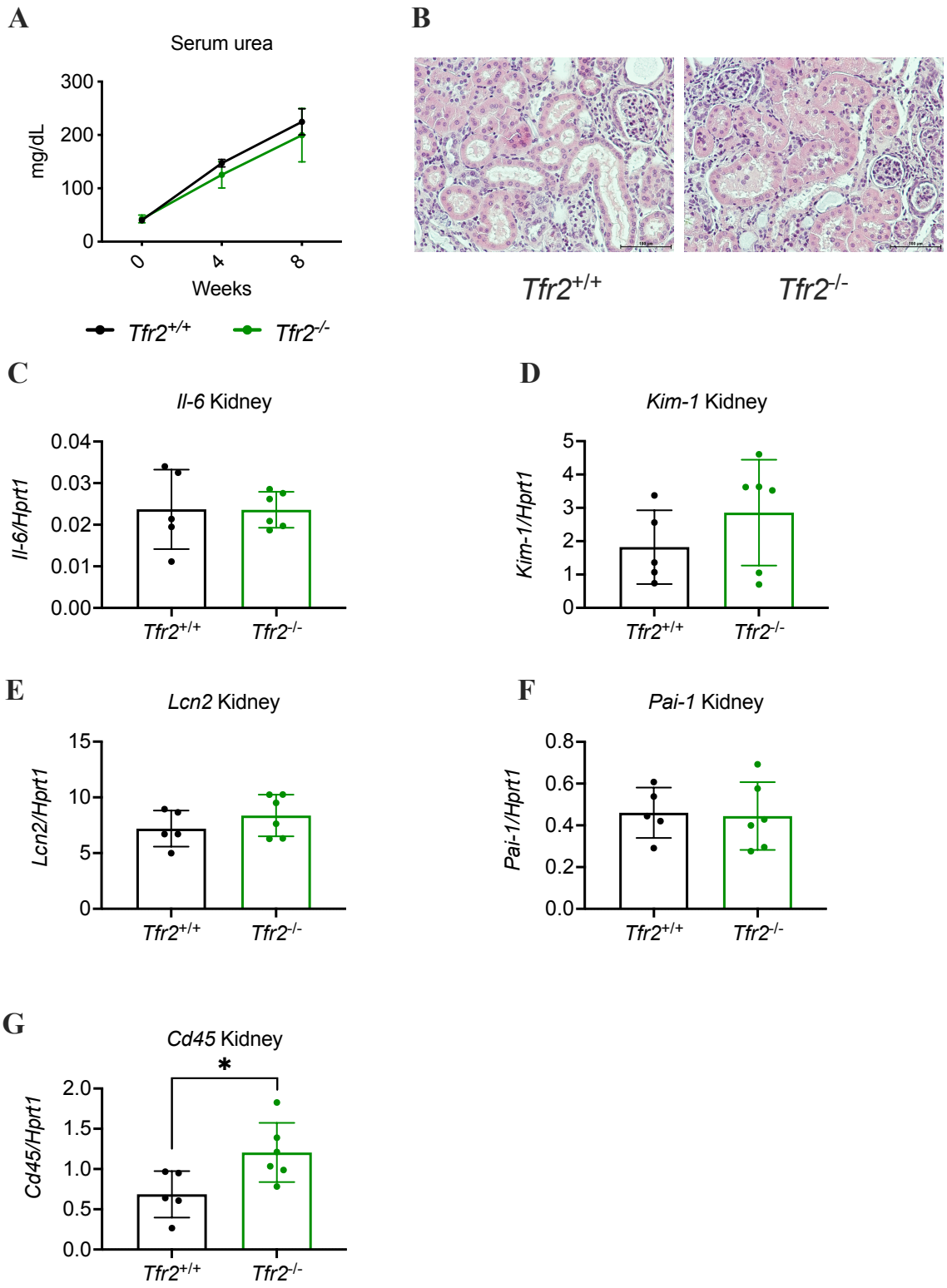
A
Serum urea
mg/dL
300
200
100
0
0
4
8
Weeks
Tfr2+/+
Tfr2-/-
B
Tfr2+/+
Tfr2-/-
C
Il-6 Kidney
Il-6/Hprt1
0.04
0.03
0.02
0.01
0.00
Tfr2+/+
Tfr2-/-
D
Kim-1 Kidney
Kim-1/Hprt1
5
4
3
2
1
0
Tfr2+/+
Tfr2-/-
E
Lcn2 Kidney
Lcn2/Hprt1
15
10
5
0
Tfr2+/+
Tfr2-/-
F
Pai-1 Kidney
Pai-1/Hprt1
0.8
0.6
0.4
0.2
0.0
Tfr2+/+
Tfr2-/-
G
Cd45 Kidney
*
Cd45/Hprt1
2.0
1.5
1.0
0.5
0.0
Tfr2+/+
Tfr2-/-

Figure 23. CKD Tfr2$^{-/-}$ and control mice have similar renal damage. *Eight-week-old Tfr2$^{+/+}$ and Tfr2$^{-/-}$ mice were fed the adenine-rich diet for 8 weeks. In the figure are represented: serum urea levels (**A**); representative images of hematoxylin-eosin staining of kidney sections (magnification 20x, **B**); mRNA levels of Inteleukin-6 (Il-6, **C**), Kidney injury molecule 1 (Kim-1, **D**), Lipocalin 2 (Lcn-2, **E**), Plasminogen activator inhibitor 1 (Pai-1, **F**) and Protein Tyrosine Phosphatase Receptor Type C (Cd45, **G**) relative to Hypoxanthine Phosphoribosyltransferase1 (Hprt1) in the kidney.*
*Mean values of 5-7 mice per group are represented. Two-way ANOVA for multiple comparisons (correction test Šídák, panel **A**) and unpaired 2-tailed Student's t-test (panels **C**-**G**) were used.*
*Bars indicate standard deviation (SD). Asterisks refer to statistically significant differences. *P<0.05.*

Figure 24

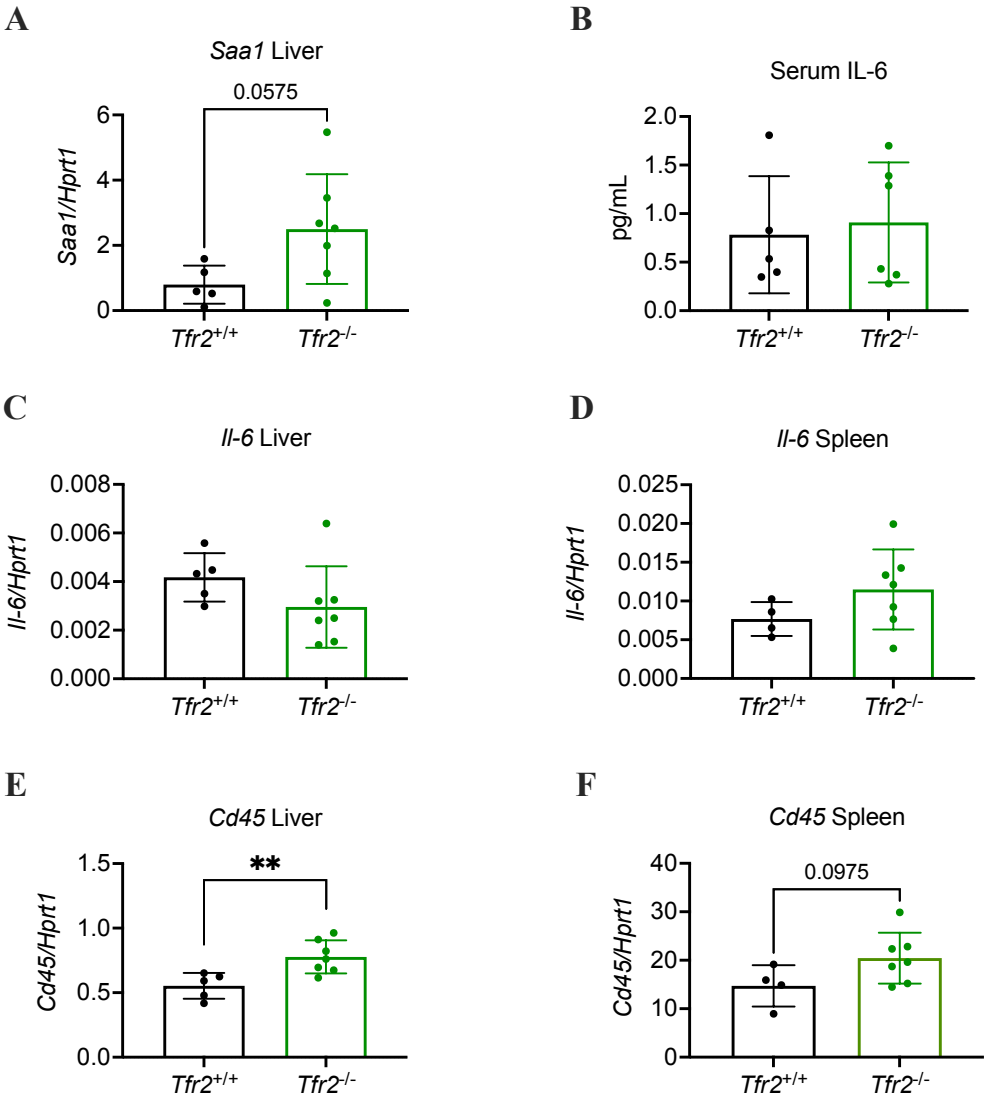

Figure 24. CKD Tfr2$^{-/-}$ and control mice have similar inflammation. *Eight-week-old Tfr2$^{+/+}$ and Tfr2$^{-/-}$ mice were fed the adenine-rich diet for 8 weeks. In the figure are represented: mRNA levels of Serum amyloid a-1 (Saa1) relative to Hypoxanthine Phosphoribosyltransferase1(Hprt1) in the liver (**A**); circulating levels of IL-6 (**B**); mRNA levels of Inteleukin-6 (Il-6) relative to Hprt1 in the liver (**C**) and in the spleen (**D**); mRNA levels of Protein Tyrosine Phosphatase Receptor Type C (Cd45) relative to (Hprt1) in the liver (**E**) and in the spleen (**F**).*
*Mean values of 5-7 mice per group are represented. Unpaired 2-tailed Student's t-test (panels **A-F**) was used. Bars indicate standard deviation (SD). Asterisks refer to statistically significant differences. **P<0.005. P-values close to 0.05 are also shown.*

3.3 Hepatic *Tfr2* targeting in a murine model of anemia of CKD

3.3.1 Validation of hepatic Tfr2 targeting through antisense oligonucleotides

Since *Tfr2*$^{-/-}$ mice are iron-loaded, we wanted to exclude that the beneficial effect obtained with total *Tfr2* deletion was exclusively due to the hepatic *Tfr2* role and the increased iron availability. To this aim, we treated wt mice with unfunctionalized anti-*Tfr2* antisense oligonucleotides (*Tfr2*-ASOs) and relative controls (Ctrl-ASOs) twice a week for 6 weeks, after renal damage induction (**Figure 25A**). At sacrifice, we proved that *Tfr2*-ASOs were able to downregulate both the α and β isoforms of *Tfr2* (Roetto *et al*, 2010) in the liver (**Figure 25B-C**), but not in the spleen (**Figure 25D-E**) and in the BM (**Figure 25F-G**). Interestingly, *Tfr2*-ASOs downregulated the α isoform also in the kidney of *Tfr2*-ASOs mice (**Figure 25H-I**), but a role for TFR2 in the kidney has never been described and no differences in kidney damage and/or morphology were observed (see below).

To exclude that erythroid *Tfr2* downregulation by the 6-week-long treatment with *Tfr2*-ASOs might be masked by erythroid expansion (see below), we performed a shorter experiment.

Eight-week-old wt mice were fed the adenine diet for 2 weeks to induce renal damage and then treated with 2 injections of *Tfr2*-ASOs or Ctrl-ASOs (**Figure 26A**). Also in this setting, *Tfr2*-ASOs successfully downregulated *Tfr2* in the liver (**Figure 26B**), but not in the BM (**Figure 26C**), proving that the treatment is unable to reduce erythroid *Tfr2* expression. This was likely due to a defective uptake of oligonucleotides by erythroid cells. Indeed, when murine erythroleukemia (MEL) cells were electroporated with *Tfr2*-ASOs, *Tfr2* mRNA levels were efficiently inhibited (**Figure 26D**).

Figure 25

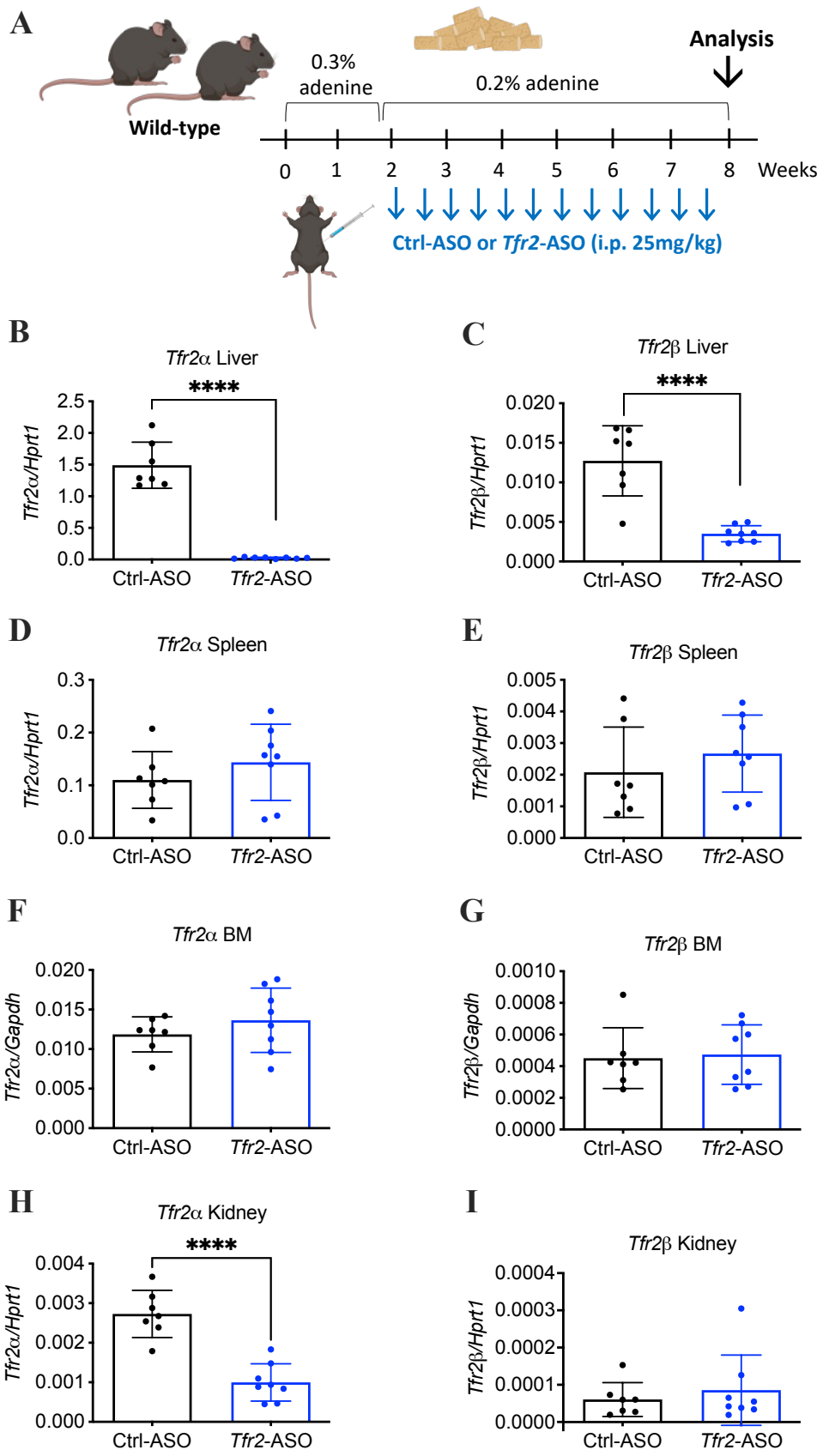
A
Wild-type
0.3% adenine
0.2% adenine
Analysis
0 1 2 3 4 5 6 7 8 Weeks
Ctrl-ASO or Tfr2-ASO (i.p. 25mg/kg)
B
Tfr2α Liver
****
Tfr2α/Hprt1
Ctrl-ASO
Tfr2-ASO
C
Tfr2β Liver
****
Tfr2β/Hprt1
D
Tfr2α Spleen
E
Tfr2β Spleen
F
Tfr2α BM
Tfr2α/Gapdh
G
Tfr2β BM
Tfr2β/Gapdh
H
Tfr2α Kidney
****
I
Tfr2β Kidney

Figure 25. Tfr2-ASOs downregulate hepatic, but not erythroid Tfr2. *Wt mice were fed the adenine diet and after 2 weeks were treated with Ctrl-ASOs and Tfr2-ASOs (25 mg/kg, i.p.) twice a week for 6 weeks. In the figure are represented: a scheme of the protocol (**A**); mRNA levels of Transferrin Receptor 2 α (Tfr2α, **B**) and β (Tfr2β, **C**) relative to Hypoxanthine Phosphoribosyltransferase1 (Hprt1) in the liver; mRNA levels of Tfr2α and Tfr2β relative to Hprt1 in the spleen (**D-E**), relative to Glyceraldehyde-3-phosphate dehydrogenase (Gapdh) in the BM (**F-G**) and relative to Hprt1 in the kidney (**H-I**).*
*Mean values of 7-8 mice per group are represented. Unpaired 2-tailed Student's t-test (panels **B-I**) were used.*
*Bars indicate standard deviation (SD). Asterisks refer to statistically significant differences. ****P<0.0001.*

Figure 26

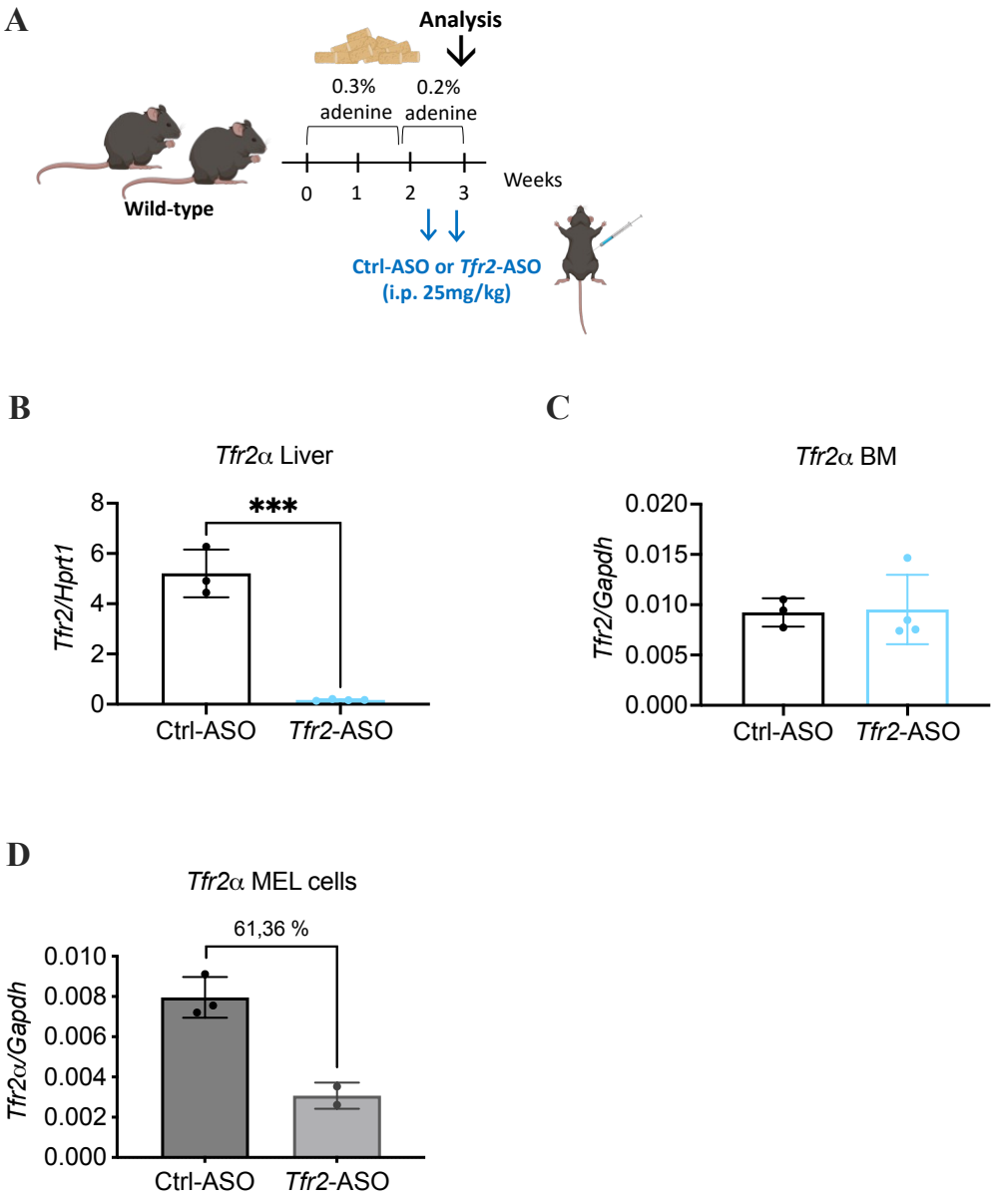

Figure 26. Tfr2-ASOs fail to downregulate erythroid Tfr2 in vivo.
A-C) *Wt mice were fed the adenine diet and after 2 weeks were treated twice with Ctrl-ASOs and Tfr2-ASOs (25 mg/kg, i.p.). In the figure are represented: a scheme of the protocol (**A**); mRNA levels of Transferrin Receptor 2 α (Tfr2α) in liver relative to Hypoxanthine Phosphoribosyltransferase1 (Hprt1) (**B**) and in BM (**C**) relative to Glyceraldehyde-3-phosphate dehydrogenase (Gapdh). Mean values of 3-4 mice per group are represented. Unpaired 2-tailed Student's t-test (panels **B**-**C**) was used. Bars indicate standard deviation (SD). Asterisks refer to statistically significant differences. ***P<0.001.*
D) *Murine erythro-leukemia (MEL) cells ($4x10^6$ cells) were electroporated with Ctrl-ASOs or Tfr2-ASOs (2μg). Forty-eight hours later cells were lysed and mRNA recovered. In the figure mRNA levels of Tfr2α relative to Gapdh and the relative percentage of decrease are shown. Bars indicate standard deviation (SD).*

3.3.2 Tfr2-ASOs correct iron-deficiency, but transiently increase RBC and Hb levels in CKD mice

At the end of the 6-week-long treatment, *Tfr2*-ASOs-mediated hepatic *Tfr2* downregulation inhibited hepcidin transcription (**Figure 27A**), as expected. This resulted in an increase in serum iron (**Figure 27B**) and transferrin saturation (**Figure 27C**) compared to controls, overcoming levels of wt healthy mice. Despite high circulating levels, tissue iron-overload was prevented. Indeed, LIC was comparable between the two groups (**Figure 27D**), while spleen and kidney iron content were even lower in *Tfr2*-ASOs mice (**Figure 27E-F**), likely reflecting an initial iron mobilization form stores due to hepcidin downmodulation.

The augmented iron availability transiently increased RBC count and Hb levels of *Tfr2*-ASOs mice (**Figure 28A-B**), preventing anemia development until week 4 of diet. However, both parameters reverted to control values before the end of the protocol, showing that iron per se is not sufficient to sustain anemia amelioration on a long-term. In line with circulating iron, both MCV and MCH (**Figure 28C-D**) were higher in *Tfr2*-ASOs mice.

Figure 27

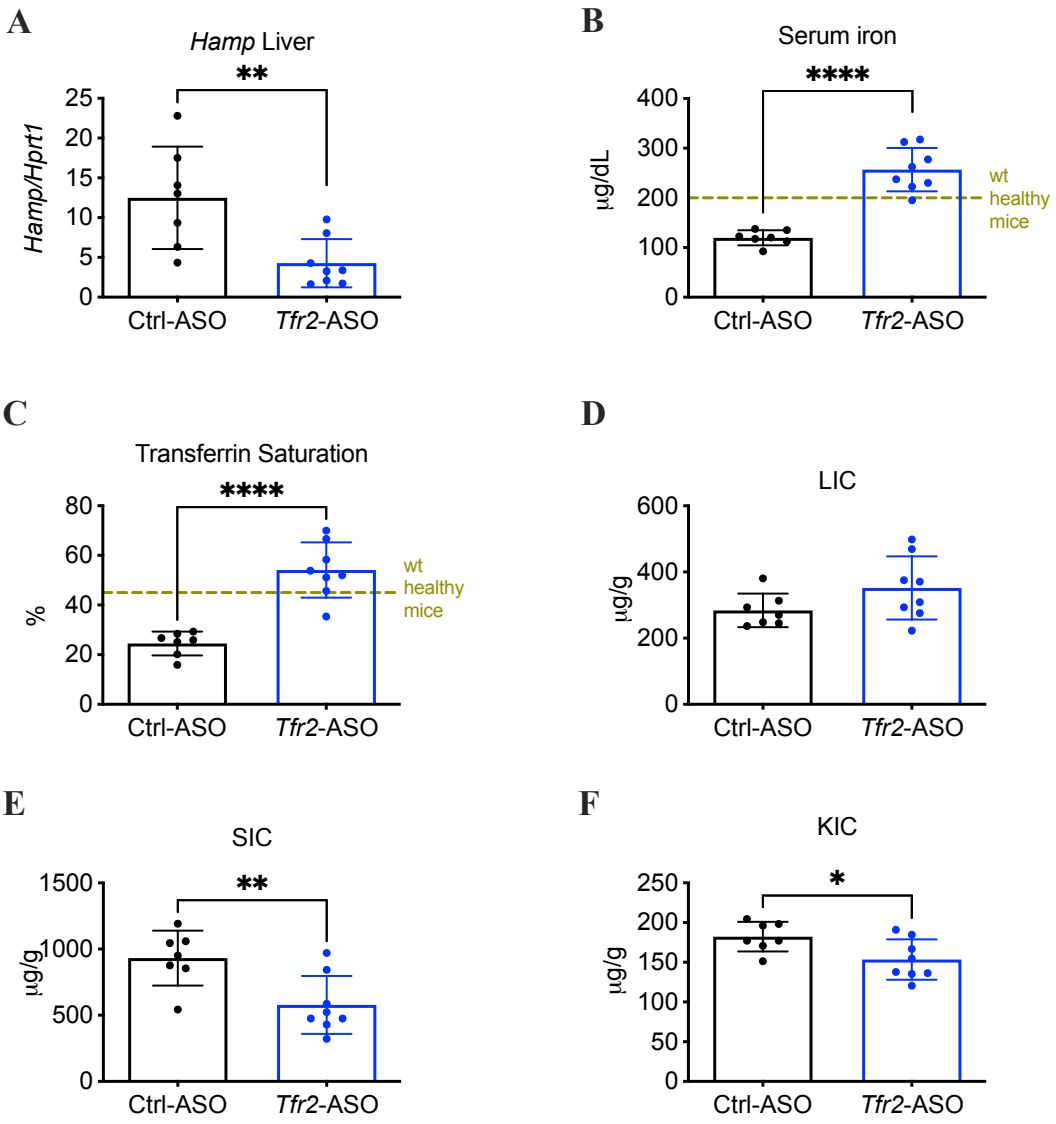

Figure 27. Tfr2-ASOs increase circulating iron levels in CKD. *Wt mice were fed the adenine diet and after 2 weeks were treated with Ctrl-ASOs and Tfr2-ASOs (25 mg/kg, i.p.) twice a week for 6 weeks. In the figure are represented: mRNA levels of hepcidin (Hamp) relative to Hypoxanthine Phosphoribosyltransferase1 (Hprt1) in the liver (**A**); serum iron levels (**B**); transferrin saturation (**C**); liver iron content (LIC, **D**); spleen iron content (SIC, **E**); kidney iron content (KIC, **F**).*
*Mean values of 7-8 mice per group are represented. Unpaired 2-tailed Student's t-test (panels **A-F**) was used. Bars indicate standard deviation (SD). Asterisks refer to statistically significant differences. *P<0.05; **P<0.005; ****P<0.0001.*

Figure 28

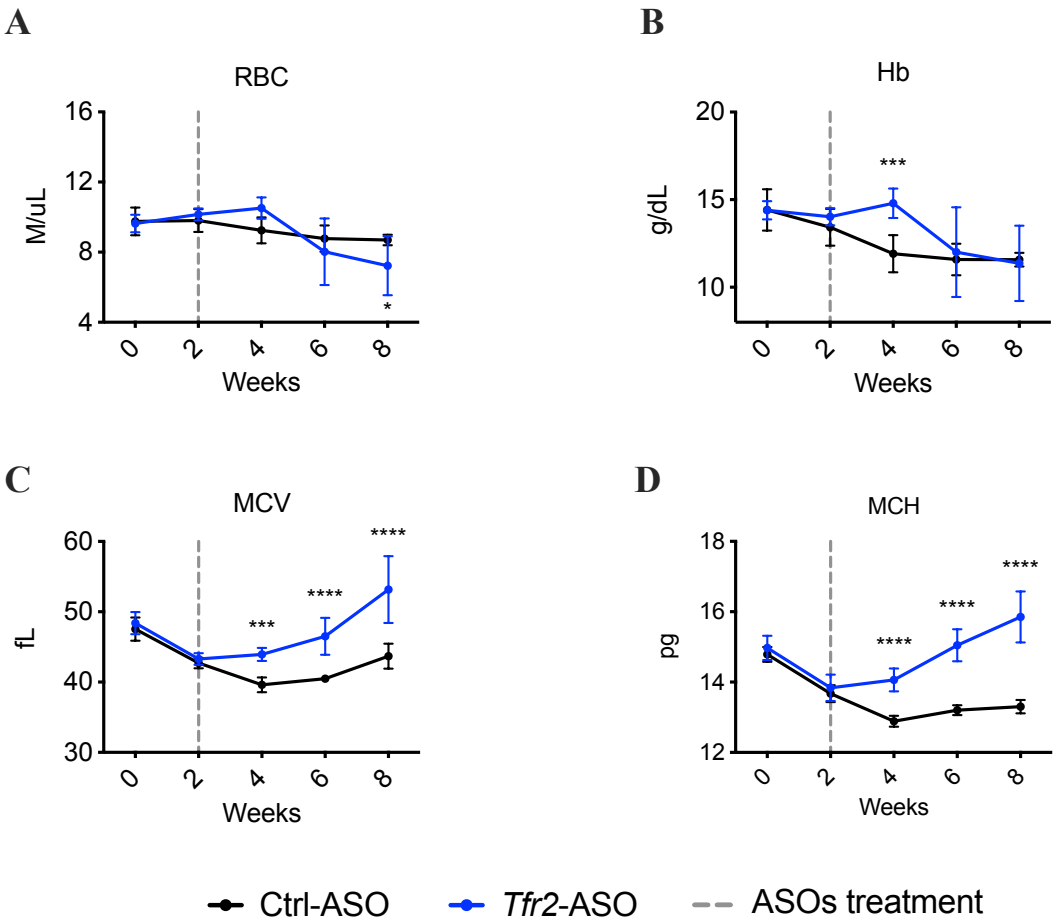

Figure 28. Tfr2-ASOs transiently ameliorate anemia of CKD. *Wt mice were fed the adenine diet and after 2 weeks were treated with Ctrl-ASOs and Tfr2-ASOs (25 mg/kg, i.p.) twice a week for 6 weeks. In the figure are represented: red blood cell count (RBC, **A**); hemoglobin levels (Hb, **B**); mean corpuscular volume (MCV, **C**) and mean corpuscular hemoglobin (MCH, **D**).*
*Mean values of 7-8 mice per group are represented. Two-way ANOVA for multiple comparisons (correction test Šídák, panels **A-D**) was used. Bars indicate standard deviation (SD). Asterisks refer to statistically significant differences. *P<0.05; ***P<0.001; ****P<0.0001.*

3.3.3 CKD mice treated with Tfr2-ASOs have enhanced ineffective erythropoiesis

The total percentage of Ter119^{+} cells in the BM was increased in *Tfr2*-ASOs mice mainly because of an expansion of basophilic and polychromatic erythroblasts (**Figure 29A**). A similar behavior was observed also in the spleen, reaching statistical significance exclusively for the basophilic erythroblasts (**Figure 29B**). This expansion of early erythroid precursors in the absence of an increase in more mature populations suggests the development of tentative erythropoiesis expansion to compensate the drop in RBC count, which failed effective differentiation likely because of insufficient EPO

stimulation. Iron-mediated toxicity might also contribute to ineffective erythropoiesis. However, the expression of markers of oxidative metabolism and ROS protection as NADPH oxidase 4 (*Nox4*), superoxide dismutase 1 (*Sod1*), Glutathione peroxidase 1 (*Gpx1*), Glutathione peroxidase 4 (*Gpx4*) (Pervaiz *et al*, 2009; Porto *et al*, 2015) and Aldehyde dehydrogenase 18 family member 1 (*Aldh18a1*, (Schwörer *et al*, 2020)) was not statistically significant different in the BM of *Tfr2*-ASOs and Ctrl-ASOs mice (**Figure 30A-E**), suggesting that the treatment caused no main erythroid toxicity.

In line with the degree of anemia, *Epo* expression in the kidney (**Figure 29C**) and circulating EPO levels (**Figure 29D**) were comparable between the two groups.

The expression levels of the EPO target genes *Bcl-xl* and *Epor* were higher in the BM of *Tfr2*-ASOs mice relative to controls (**Figure 29E** and **Figure 31A**), while comparable in the spleen (**Figure 29F** and **Figure 31B**). However, if mRNA levels were normalized on circulating EPO no differences were detected between the two groups (**Figure 29G-H** and **Figure 31C-D**), showing that hepatic *Tfr2* downregulation and iron-overload do not modulate erythroid EPO sensitivity.

Surprisingly, *Erfe* expression was higher in the BM and spleen of *Tfr2*-ASOs mice both as absolute levels and when normalized on circulating EPO (**Figure 31E-H**). Since *Erfe* is mainly produced by early erythroid precursors, we speculate that its increase is due to the massive expansion of these populations.

Figure 29

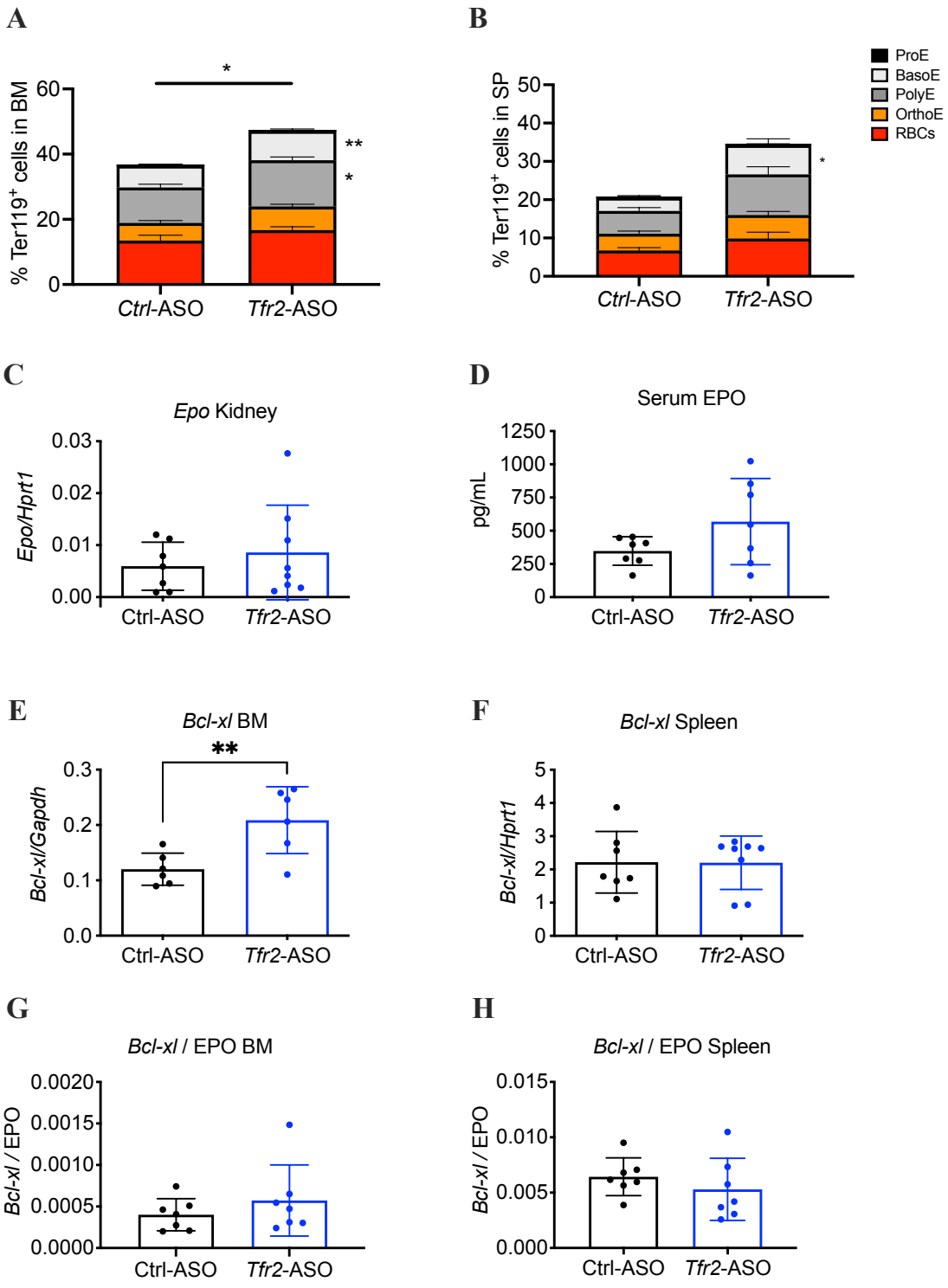
A
% Ter119+ cells in BM
60
40
20
0
*
**
*
Ctrl-ASO
Tfr2-ASO
B
% Ter119+ cells in SP
50
40
30
20
10
0
*
ProE
BasoE
PolyE
OrthoE
RBCs
Ctrl-ASO
Tfr2-ASO
C
Epo Kidney
Epo/Hprt1
0.03
0.02
0.01
0.00
Ctrl-ASO
Tfr2-ASO
D
Serum EPO
pg/mL
1250
1000
750
500
250
0
Ctrl-ASO
Tfr2-ASO
E
Bcl-xl BM
**
Bcl-xl/Gapdh
0.3
0.2
0.1
0.0
Ctrl-ASO
Tfr2-ASO
F
Bcl-xl Spleen
Bcl-xl/Hprt1
5
4
3
2
1
0
Ctrl-ASO
Tfr2-ASO
G
Bcl-xl / EPO BM
Bcl-xl / EPO
0.0020
0.0015
0.0010
0.0005
0.0000
Ctrl-ASO
Tfr2-ASO
H
Bcl-xl / EPO Spleen
Bcl-xl / EPO
0.015
0.010
0.005
0.000
Ctrl-ASO
Tfr2-ASO

Figure 29. CKD Tfr2-ASOs mice have enhanced ineffective erythropoiesis, but similar EPO responsiveness than controls. *Wt mice were fed the adenine diet and after 2 weeks were treated with Ctrl-ASOs and Tfr2-ASOs (25 mg/kg, i.p.) twice a week for 6 weeks. In the figure are represented: the percentage of total Ter119^{+} cells in the BM (**A**) and in the spleen (SP, **B**) and the contribution of the 5 erythroblasts populations [proerythroblasts (ProE), basophilic erythroblasts (BasoE), polychromatic erythroblasts (PolyE), orthochromatic erythroblasts and immature reticulocytes (OrthoE), and mature red cells (RBCs)], identified through the evaluation of cell size and Ter119/CD44 relative expression; mRNA levels of erythropoietin (Epo) relative to Hypoxanthine Phosphoribosyltransferase1 (Hprt1) in the kidney (**C**); serum EPO levels (**D**); mRNA levels of B-cell lymphoma-extra large (Bcl-xl) relative to Glyceraldehyde-3-phosphate dehydrogenase (Gapdh) in the BM (**E**) and relative to Hprt1 in the spleen (**F**); B-cell lymphoma-extra large (Bcl-xl) mRNA levels in the BM (**G**) and in the spleen (**H**) normalized on circulating EPO.*
*Mean values of 7-8 mice per group are represented. Unpaired 2-tailed Student's t-test (panels **A-H**) was used. Bars indicate standard deviation (SD). Asterisks refer to statistically significant differences. *P<0.05; **P<0.005.*

Figure 30

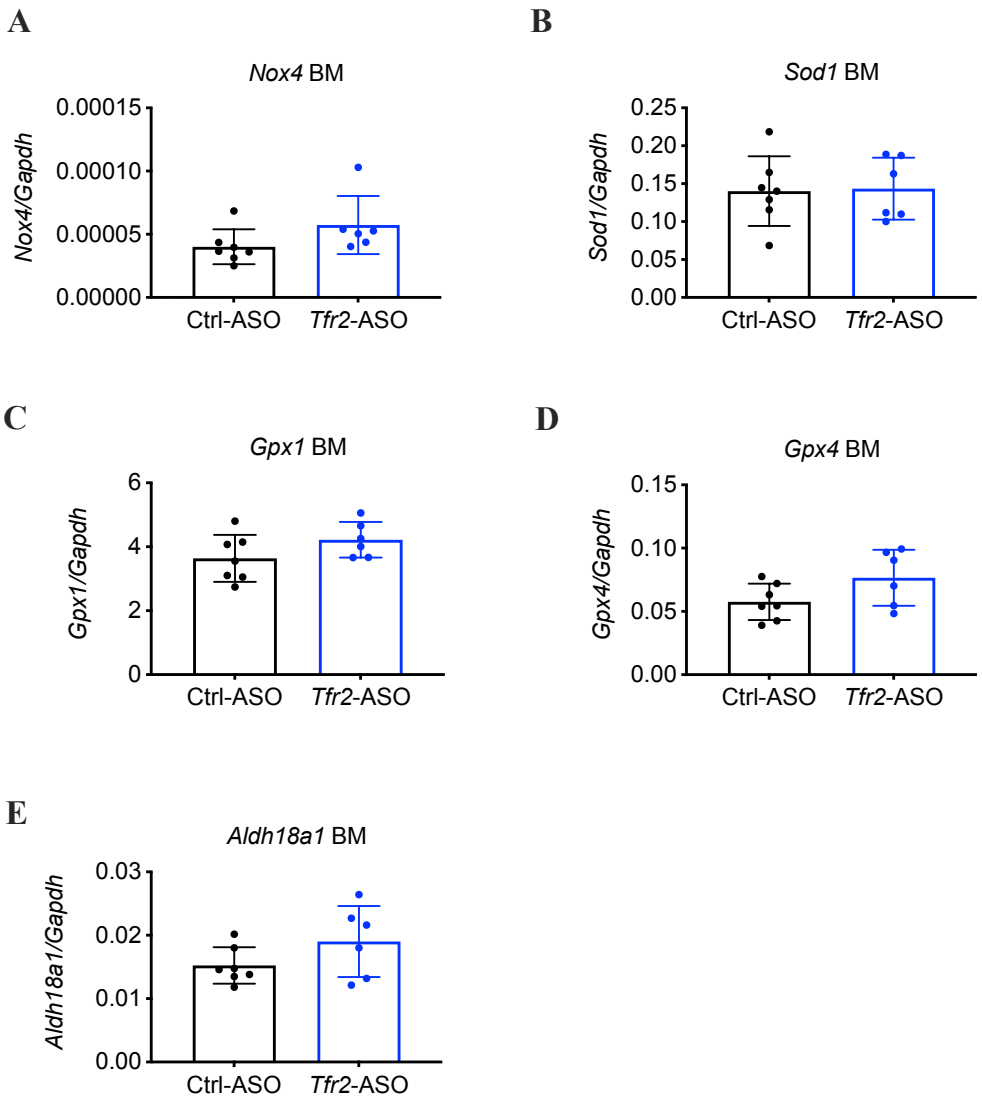

Figure 30. Tfr2-ASOs do not increase markers of oxidative metabolism and ROS protection in the bone marrow of CKD mice. *Wt mice were fed the adenine diet and after 2 weeks were treated with Ctrl-ASOs and Tfr2-ASOs (25 mg/kg, i.p.) twice a week for 6 weeks. In the figure are represented: mRNA levels of NADPH oxidase 4 (Nox4,* ***A****), superoxide dismutase 1 (Sod1,* ***B****), Glutathione peroxidase 1 (Gpx1,* ***C****), Glutathione peroxidase 4 (Gpx4,* ***D****), Aldehyde dehydrogenase 18 family member 1 (Aldh18a1,* ***E****) relative to Glyceraldehyde-3-phosphate dehydrogenase (Gapdh) in the BM.*
Mean values of 7 mice per group are represented. Unpaired 2-tailed Student's t-test (panels ***A-E****) was used. Bars indicate standard deviation (SD).*

Figure 31

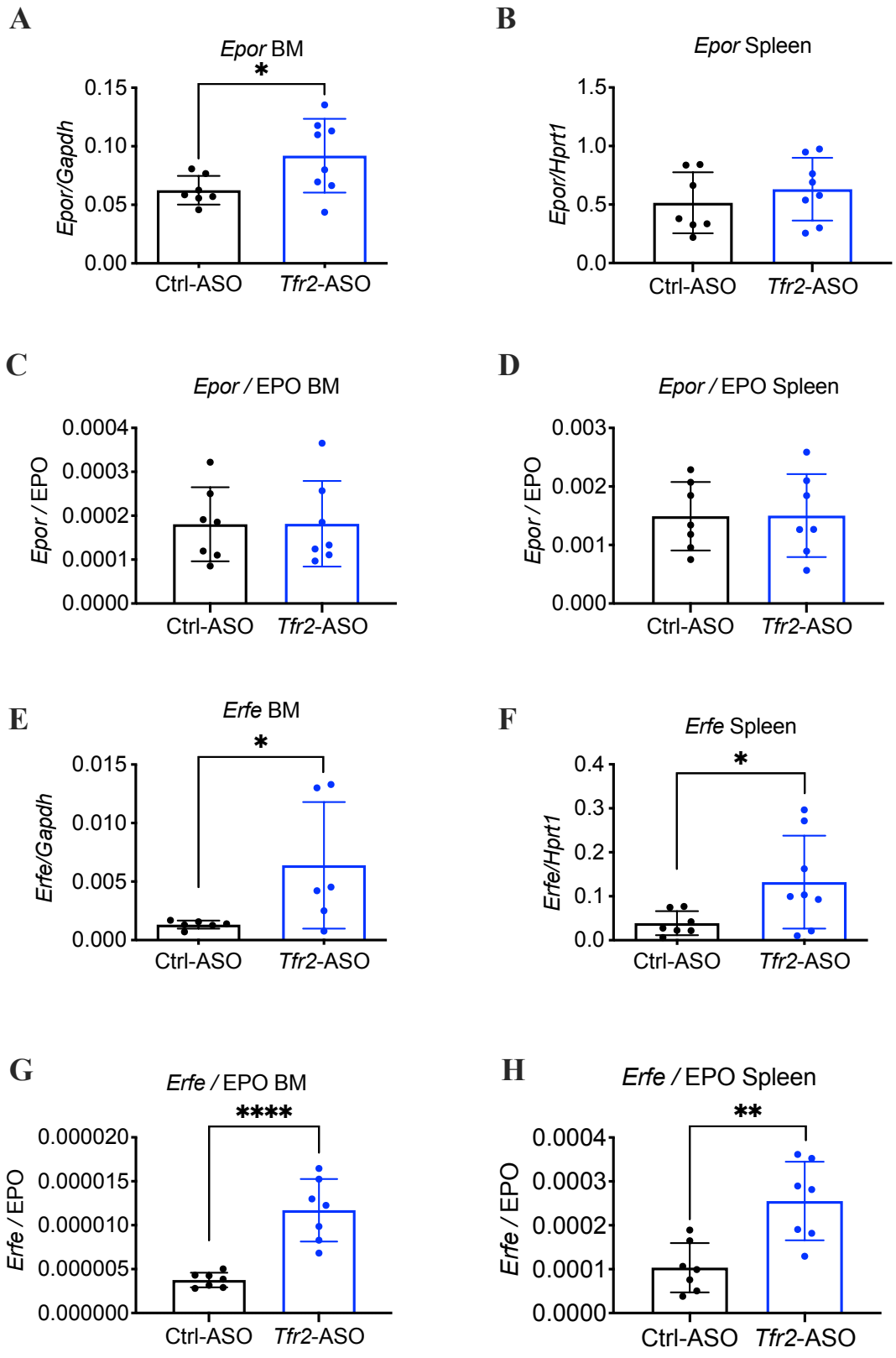
A
Epor BM
*
Epor/Gapdh
0.15
0.10
0.05
0.00
Ctrl-ASO
Tfr2-ASO
B
Epor Spleen
Epor/Hprt1
1.5
1.0
0.5
0.0
Ctrl-ASO
Tfr2-ASO
C
Epor / EPO BM
Epor / EPO
0.0004
0.0003
0.0002
0.0001
0.0000
Ctrl-ASO
Tfr2-ASO
D
Epor / EPO Spleen
Epor / EPO
0.003
0.002
0.001
0.000
Ctrl-ASO
Tfr2-ASO
E
Erfe BM
*
Erfe/Gapdh
0.015
0.010
0.005
0.000
Ctrl-ASO
Tfr2-ASO
F
Erfe Spleen
*
Erfe/Hprt1
0.4
0.3
0.2
0.1
0.0
Ctrl-ASO
Tfr2-ASO
G
Erfe / EPO BM
****
Erfe / EPO
0.000020
0.000015
0.000010
0.000005
0.000000
Ctrl-ASO
Tfr2-ASO
H
Erfe / EPO Spleen
**
Erfe / EPO
0.0004
0.0003
0.0002
0.0001
0.0000
Ctrl-ASO
Tfr2-ASO

Figure 31. CKD Tfr2-ASOs mice have EPO sensitivity comparable to controls, but higher Erythroferrone. *Wt mice were fed the adenine diet and after 2 weeks were treated with Ctrl-ASOs and Tfr2-ASOs (25 mg/kg, i.p.) twice a week for 6 weeks. In the figure are represented: mRNA levels of Erythropoietin receptor (Epor) relative to Glyceraldehyde-3-phosphate dehydrogenase (Gapdh) in the BM (**A**) and relative to Hypoxanthine Phosphoribosyltransferase1 (Hprt1) in the spleen (**B**); Epor mRNA levels in the BM (**C**) and in the spleen (**D**) normalized on circulating EPO; mRNA levels of Erythroferrone (Erfe) relative to Gapdh in the BM (**E**) and relative to Hprt1 in the spleen (**F**); Erfe mRNA levels in the BM (**G**) and in the spleen (**H**) normalized on circulating EPO.*
*Mean values of 7-8 mice per group are represented. Unpaired 2-tailed Student's t-test (panels **A-H**) was used. Bars indicate standard deviation (SD). Asterisks refer to statistically significant differences. *P<0.05; **P<0.005; ****P<0.0001.*

3.3.4 CKD Tfr2-ASOs and control mice have comparable renal damage and inflammation

Serum urea levels indicated that renal functionality was equally impaired by the diet in *Tfr2*-ASOs and Ctrl-ASOs mice (**Figure 32A**). In agreement, no differences in kidney damage were evident both at histologic (**Figure 32B**) and transcriptomic levels. Indeed, the expression of the markers of proximal and distal tubular damage *Kim-1* and *Lcn-2* was similar (**Figure 32C-D**). Also, the levels of the pro-inflammatory cytokine *Il-6* (**Figure 32E**), of the fibrosis marker *Pai-1* (**Figure 32F**) and of the monocyte infiltration marker *Cd45* (**Figure 32G**) in the kidney were comparable between the two groups.

In line with the kidney phenotype, no differences in systemic inflammation were observed between the 2 groups. Indeed, the expression of the hepatic marker of systemic inflammation *Saa1* (**Figure 33A**), IL-6 circulating levels (**Figure 33B**), and mRNA levels of *Il-6* (**Figure 33C**) and *Cd45* in the liver (**Figure 33D**) were comparable between *Tfr2*-ASOs and control mice.

Overall, our results show that hepatic *Tfr2* inhibition does not sensitize erythroid cells to EPO stimulation, and the consequent increased iron availability is not sufficient to sustain anemia amelioration on a long-term.

Figure 32

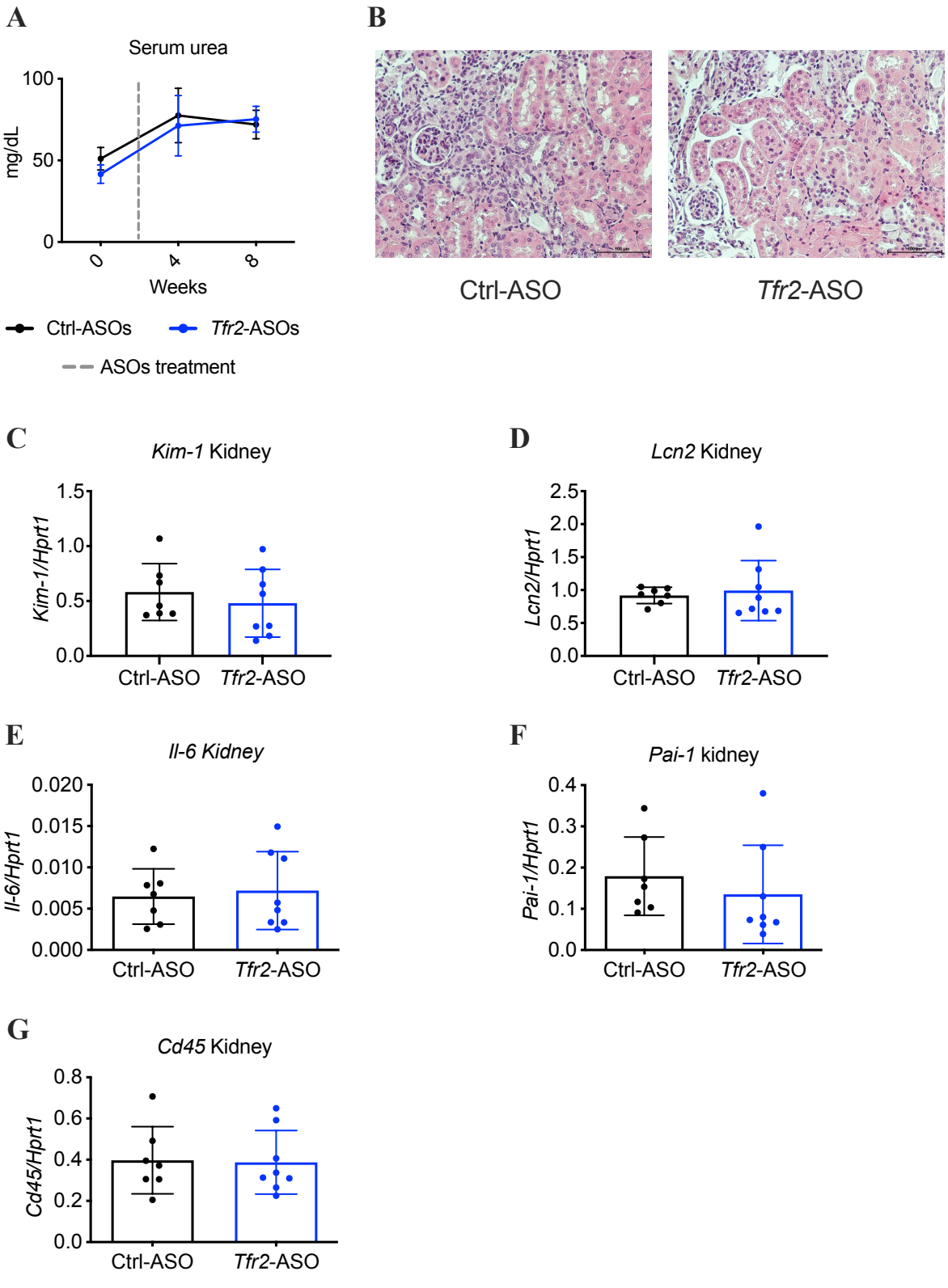
A
Serum urea
100
50
0
mg/dL
0
4
8
Weeks
Ctrl-ASOs
Tfr2-ASOs
ASOs treatment
B
Ctrl-ASO
Tfr2-ASO
C
Kim-1 Kidney
Kim-1/Hprt1
1.5
1.0
0.5
0.0
Ctrl-ASO
Tfr2-ASO
D
Lcn2 Kidney
Lcn2/Hprt1
2.5
2.0
1.5
1.0
0.5
0.0
Ctrl-ASO
Tfr2-ASO
E
Il-6 Kidney
Il-6/Hprt1
0.020
0.015
0.010
0.005
0.000
Ctrl-ASO
Tfr2-ASO
F
Pai-1 kidney
Pai-1/Hprt1
0.4
0.3
0.2
0.1
0.0
Ctrl-ASO
Tfr2-ASO
G
Cd45 Kidney
Cd45/Hprt1
0.8
0.6
0.4
0.2
0.0
Ctrl-ASO
Tfr2-ASO

Figure 32. CKD Tfr2-ASOs treated mice and controls have similar renal damage. *Wt mice were fed the adenine diet and after 2 weeks were treated with Ctrl-ASOs and Tfr2-ASOs (25 mg/kg, i.p.) twice a week for 6 weeks. In the figure are represented: serum urea levels (**A**); images of representative hematoxylin-eosin staining of kidney sections (magnification 20x, **B**); mRNA levels of Kidney injury molecule 1 (Kim-1, **C**), Lipocalin 2 (Lcn-2, **D**), Inteleukin-6 (Il-6, **E**) Plasminogen activator inhibitor 1 (Pai-1, **F**) and Protein Tyrosine Phosphatase Receptor Type C (Cd45, **G**) relative to Hypoxanthine Phosphoribosyltransferase1 (Hprt1) in the kidney.*
*Mean values of 7-8 mice per group are represented. Two-way ANOVA for multiple comparisons (correction test Šídák, panel **A**) and unpaired 2-tailed Student's t-test (panels **C**-**G**) were used. Bars indicate standard deviation (SD).*

Figure 33

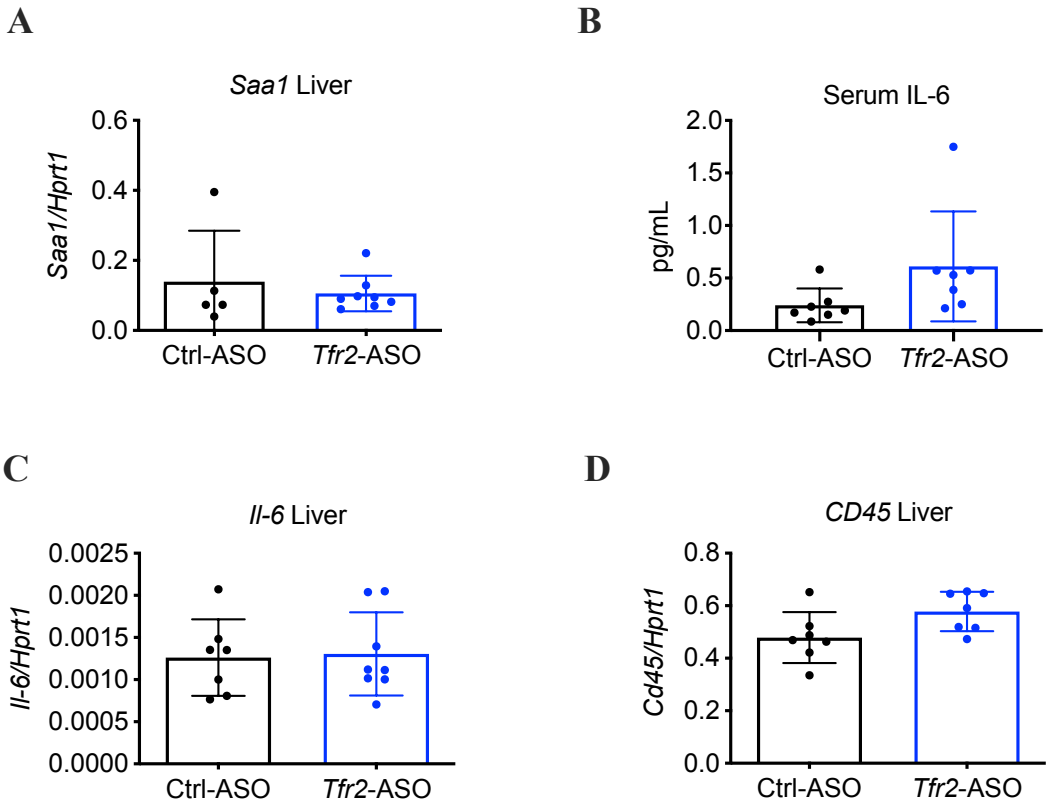

Figure 33. CKD Tfr2-ASOs treated mice and controls have similar inflammation. *Wt mice were fed the adenine diet and after 2 weeks were treated with Ctrl-ASOs and Tfr2-ASOs (25 mg/kg, i.p.) twice a week for 6 weeks. In the figure are represented: mRNA levels of Serum amyloid a-1 (Saa1, **A**) in the liver; circulating levels of IL-6 (**B**); mRNA levels of Inteleukin-6 (Il-6, **C**) and Protein Tyrosine Phosphatase Receptor Type C (Cd45, **D**) relative to Hypoxanthine Phosphoribosyltransferase1 (Hprt1) in the liver.*
*Mean values of 7-8 mice per group are represented. Unpaired 2-tailed Student's t-test (panels **A**-**D**) was used. Bars indicate standard deviation (SD).*

3.4 *Tfr2* role in bone homeostasis in a murine model of CKD

3.4.1 Total Tfr2 deletion increases bone mass in CKD mice spine

Tfr2 is mainly expressed in the liver and in the erythroid compartment, however a role for the protein in the regulation of bone homeostasis has been recently identified. Indeed, Rauner and colleagues demonstrated that healthy *Tfr2*$^{-/-}$ mice have higher bone mass and turnover, independently from the iron status (Rauner *et al*, 2019). Thus, we wondered whether *Tfr2* deletion might improve bone phenotype in CKD, a disorder characterized by bone defects. To this aim, 8-week-old *Tfr2*$^{+/+}$ and *Tfr2*$^{-/-}$ mice were fed the adenine diet as previously described and, at the end of the protocol, the bone structure of spine and femurs was analyzed using μ-Computed Tomography (μ-CT).

As expected, the adenine-rich diet induced bone defects in the spine of *Tfr2*$^{+/+}$ mice compared wt healthy mice (**Figure 34B-F**). CKD *Tfr2*$^{-/-}$ mice showed higher spine bone volume (**Figure 34A-B**) and trabeculae number (**Figure 34C**) than *Tfr2*$^{+/+}$ littermates, reaching levels comparable to healthy wt mice. Trabecular thickness was comparable in the two groups (**Figure 34D**), while the space between trabeculae was lower in *Tfr2*$^{-/-}$ mice (**Figure 34E**). Also, vertebral bone mineral density (**Figure 34F**) showed a trend toward an increase in *Tfr2*$^{-/-}$ mice.

Figure 34

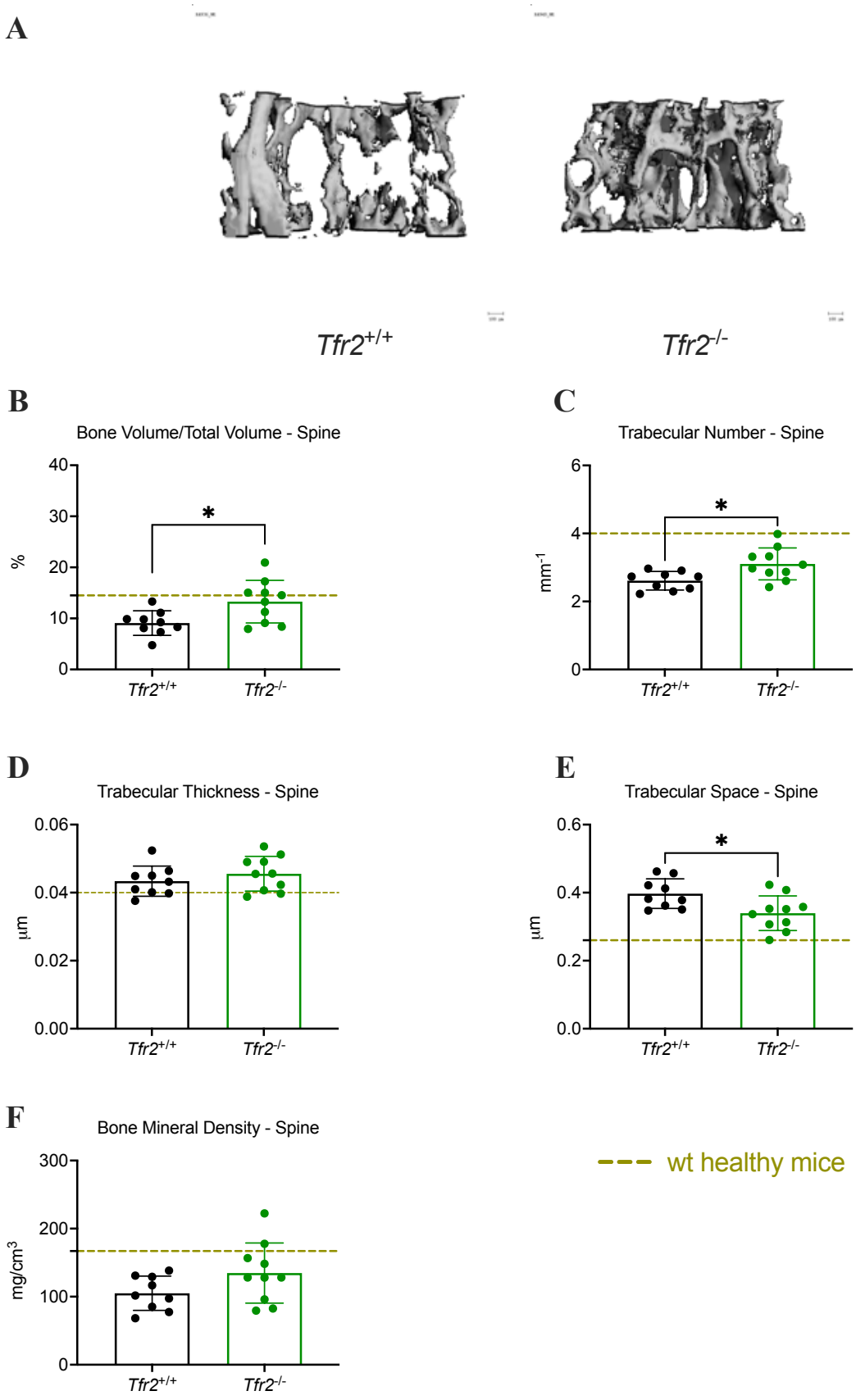
A
Tfr2+/+
Tfr2-/-
B
Bone Volume/Total Volume - Spine
%
40
30
20
10
0
*
Tfr2+/+
Tfr2-/-
C
Trabecular Number - Spine
mm-1
6
4
2
0
*
Tfr2+/+
Tfr2-/-
D
Trabecular Thickness - Spine
µm
0.06
0.04
0.02
0.00
Tfr2+/+
Tfr2-/-
E
Trabecular Space - Spine
µm
0.6
0.4
0.2
0.0
*
Tfr2+/+
Tfr2-/-
F
Bone Mineral Density - Spine
mg/cm3
300
200
100
0
Tfr2+/+
Tfr2-/-
wt healthy mice

Figure 34. CKD Tfr2$^{-/-}$ mice have higher trabecular bone mass in the spine than controls. *Eight-week-old Tfr2$^{+/+}$ and Tfr2$^{-/-}$ mice were fed the adenine-rich diet for 8 weeks. In the figure are represented bone parameters obtained through μ-Computed Tomography (μ-CT) analysis at the end of the protocol: representative 3D images of trabecular part of spine vertebrae of Tfr2$^{+/+}$ and Tfr2$^{-/-}$ animals (**A**); bone volume on total volume (**B**); trabecular number (**C**); trabecular thickness (**D**); trabecular space (**E**); bone mineral density (**F**).*
*Mean values of 9-10 mice per group are represented. Unpaired 2-tailed Student's t-test (panels **B-F**) was used. Bars indicate standard deviation (SD). Asterisks refer to statistically significant differences. *P<0.05.*

3.4.2 Total Tfr2 deletion increases bone mass in CKD mice femur

CKD-*Tfr2*$^{+/+}$ mice showed defects also in the trabecular part of femur as compared to wt healthy mice, which were almost fully corrected in *Tfr2*$^{-/-}$ mice (**Figure 35A-F**). Indeed, *Tfr2* deletion increased bone volume (**Figure 35A-B**) and trabecular number (**Figure 35C**) in the femur, without affecting trabecular thickness (**Figure 35D**). As a consequence, the space between trabeculae was lower in *Tfr2*$^{-/-}$ mice (**Figure 35E**). Moreover, bone mineral density of femur (**Figure 35F**) was higher in *Tfr2*$^{-/-}$ mice.
Bone parameters of the cortical part of femur were comparable between the two groups (**Figure 35G-H**).

Figure 35

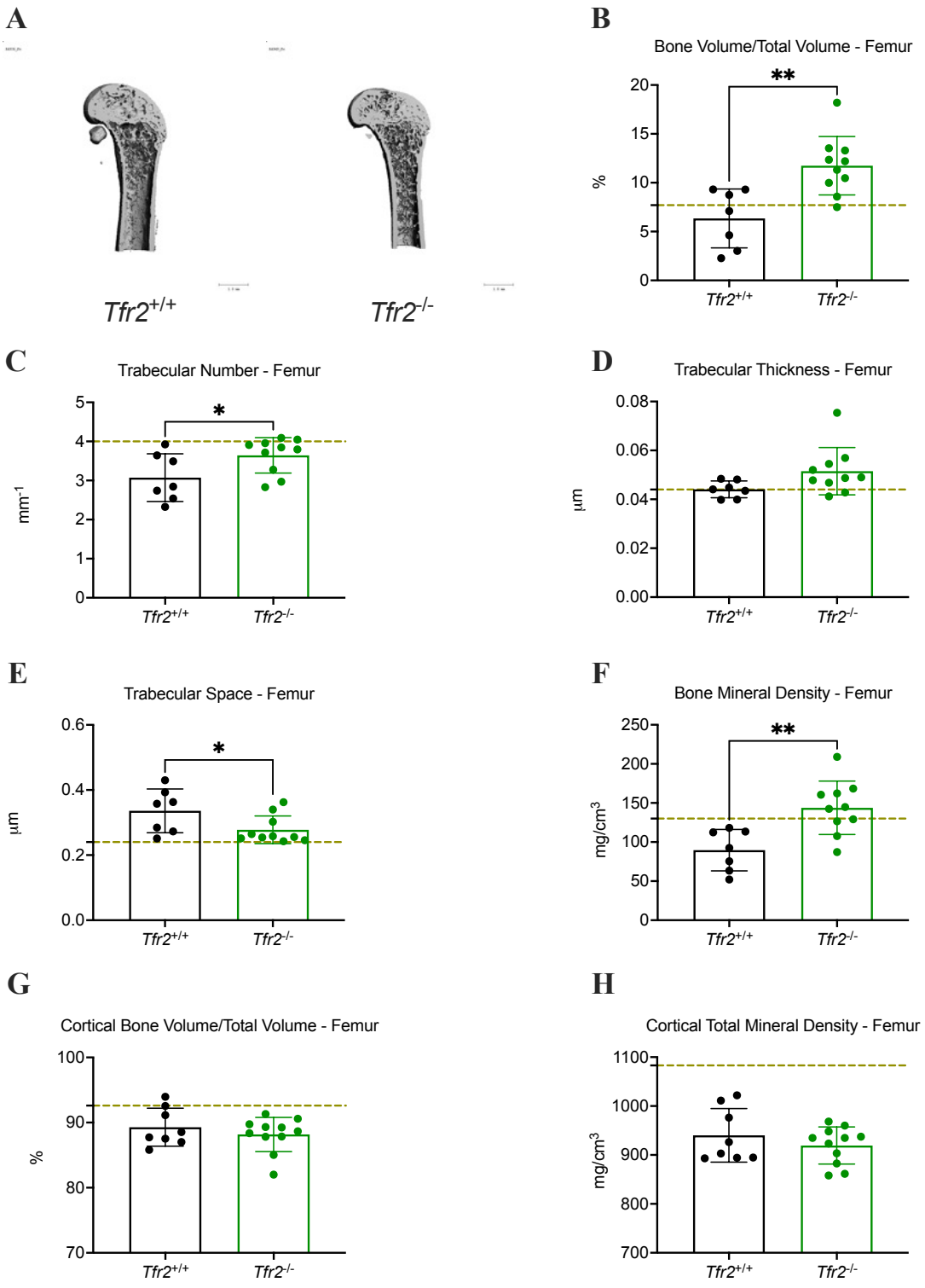
A
Tfr2+/+
Tfr2-/-
B
Bone Volume/Total Volume - Femur
%
**
C
Trabecular Number - Femur
mm-1
*
D
Trabecular Thickness - Femur
µm
E
Trabecular Space - Femur
µm
*
F
Bone Mineral Density - Femur
mg/cm3
**
G
Cortical Bone Volume/Total Volume - Femur
%
H
Cortical Total Mineral Density - Femur
mg/cm3
wt healthy mice

Figure 35. CKD Tfr2$^{-/-}$ mice have higher trabecular bone mass in femur than controls. *Eight-week-old Tfr2$^{+/+}$ and Tfr2$^{-/-}$ mice were fed the adenine-rich diet for 8 weeks. In the figure are represented bone parameters obtained through μ-Computed Tomography (μ-CT) analysis at the end of the protocol: representative 3D images of trabecular and cortical femur of Tfr2$^{+/+}$ and Tfr2$^{-/-}$ animals (**A**); bone volume on total volume (**B**); trabecular number (**C**); trabecular thickness (**D**); trabecular space (**E**); bone mineral density (**F**); cortical bone volume on total volume (**G**); cortical total mineral density (**H**).*
*Mean values of 9-10 mice per group are represented. Unpaired 2-tailed Student's t-test (panels **B-H**) was used. Bars indicate standard deviation (SD). Asterisks refer to statistically significant differences. *P<0.05; **P<0.005.*

3.4.3 Bone marrow Tfr2 deletion does not affect bone mass in CKD mice

To unravel whether *Tfr2* deletion in osteoblasts or in osteoclasts is responsible for the observed increase in bone mass, we analyzed bone parameters of *Tfr2*^{BMKO} mice. Indeed, in *Tfr2*^{BMKO} mice *Tfr2* lacks exclusively in the hematopoietic compartment. Thus, osteoclasts, that derive from myeloid lineage (Ash *et al*, 1980), are *Tfr2*-null, while osteoblasts (originating from mesenchymal cells, (Pittenger *et al*, 1999)) derive from wt recipient mice.

We proved that, at difference with *Tfr2*$^{-/-}$ mice, the spine of *Tfr2*^{BMKO} animals showed bone volume, trabecular number, thickness and space, and bone mineral density comparable to *Tfr2*^{BMWT} (**Figure 36A-F**).

Thus, the absence of *Tfr2* in osteoblasts, rather than in osteoclasts, is likely the cause of the increased bone mass in CKD-*Tfr2*$^{-/-}$ mice, in line with published results (Rauner *et al*, 2019).

Figure 36

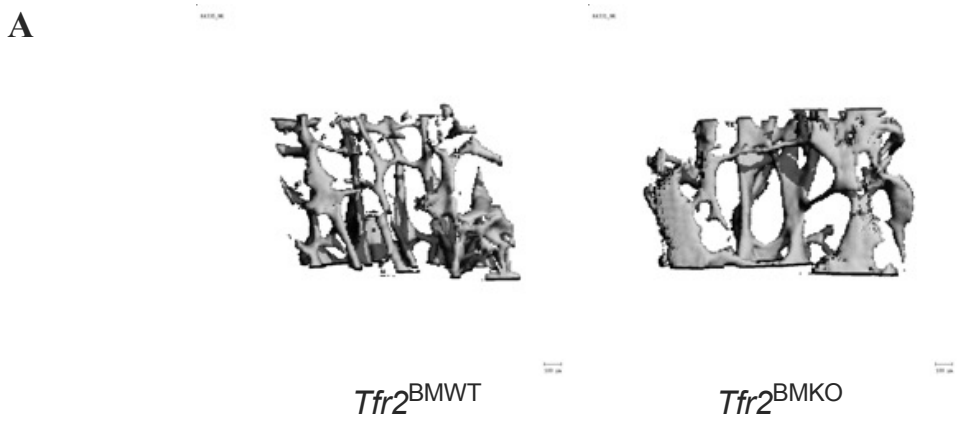
A
Tfr2BMWT
Tfr2BMKO
B
Bone Volume/Total Volume - Spine
%
40
30
20
10
0
Tfr2BMWT
Tfr2BMKO
C
Trabecular Number - Spine
mm-1
6
4
2
0
Tfr2BMWT
Tfr2BMKO
D
Trabecular Thickness - Spine
µm
0.06
0.04
0.02
0.00
Tfr2BMWT
Tfr2BMKO
E
Trabecular Space - Spine
µm
0.6
0.4
0.2
0.0
Tfr2BMWT
Tfr2BMKO
F
Bone Mineral Density - Spine
mg/cm3
300
200
100
0
Tfr2BMWT
Tfr2BMKO
wt healthy mice

Figure 36. CKD Tfr2^{BMKO} mice have trabecular bone mass comparable to controls. *Tfr2^{BMWT} and Tfr2^{BMKO} mice were generated through BM transplantation. Ten weeks later, mice were fed the adenine-rich diet for 8 weeks. In the figure are represented bone parameters obtained through μ-Computed Tomography (μ-CT) analysis at the end of the protocol: representative 3D images of trabecular part of spine vertebrae of Tfr2^{BMWT} and Tfr2^{BMKO} animals (**A**); bone volume on total volume (**B**); trabecular number (**C**); trabecular thickness (**D**); trabecular space (**E**); bone mineral density (**F**).*
*Mean values of 4 mice per group are represented. Unpaired 2-tailed Student's t-test (panels **B-F**) was used. Bars indicate standard deviation (SD).*

3.5 BM specific *Tfr2* targeting in a murine model of anemia of inflammation

3.5.1 Bone marrow Tfr2 deletion sustains RBC and Hb production in anemia of inflammation

Our results proved that BM *Tfr2* deletion was able to increase RBCs production in a CKD murine model, but iron levels were too low to sustain a long-lasting anemia amelioration. So, we tested whether this approach may instead be sufficient to improve anemia due to chronic inflammation, characterized by a functional, rather than absolute iron deficiency (Ganz, 2019). In this context, iron increase should be avoided since potentially detrimental for the inflammatory status.

To test this assumption, we generated mice lacking BM *Tfr2* and relative controls through BMT as above. Donor/host chimerism evaluated at the end of the experimental protocol was superior to 90% both in the BM and spleen in all animals. Ten weeks after transplantation, when erythropoiesis was fully recovered, mice were treated with oil of turpentine (5μl/g body weight, s.c.) once a week for 3 weeks to induce sterile inflammation. Then, one cohort of mice was sacrificed 2 days after the last injection, and the other 2 weeks after the last injection, to characterize mice both at maximum peak of anemia and at anemia recovery (**Figure 37A**).

Tfr2^{BMWT}, as expected, developed anemia that gradually restored during the two weeks of turpentine discontinuation. *Tfr2*^{BMKO} mice maintained higher RBCs and Hb levels (**Figure 37B-C**) for the entire protocol. MCV and MCH were similar between the 2 groups (**Figure 37D-E**), with only a mild non-statistically significant decrease of MCH in *Tfr2*^{BMKO} mice at maximum peak and at anemia recovery, proving that in this model iron levels were sufficient to sustain the enhanced RBCs production.

Figure 37

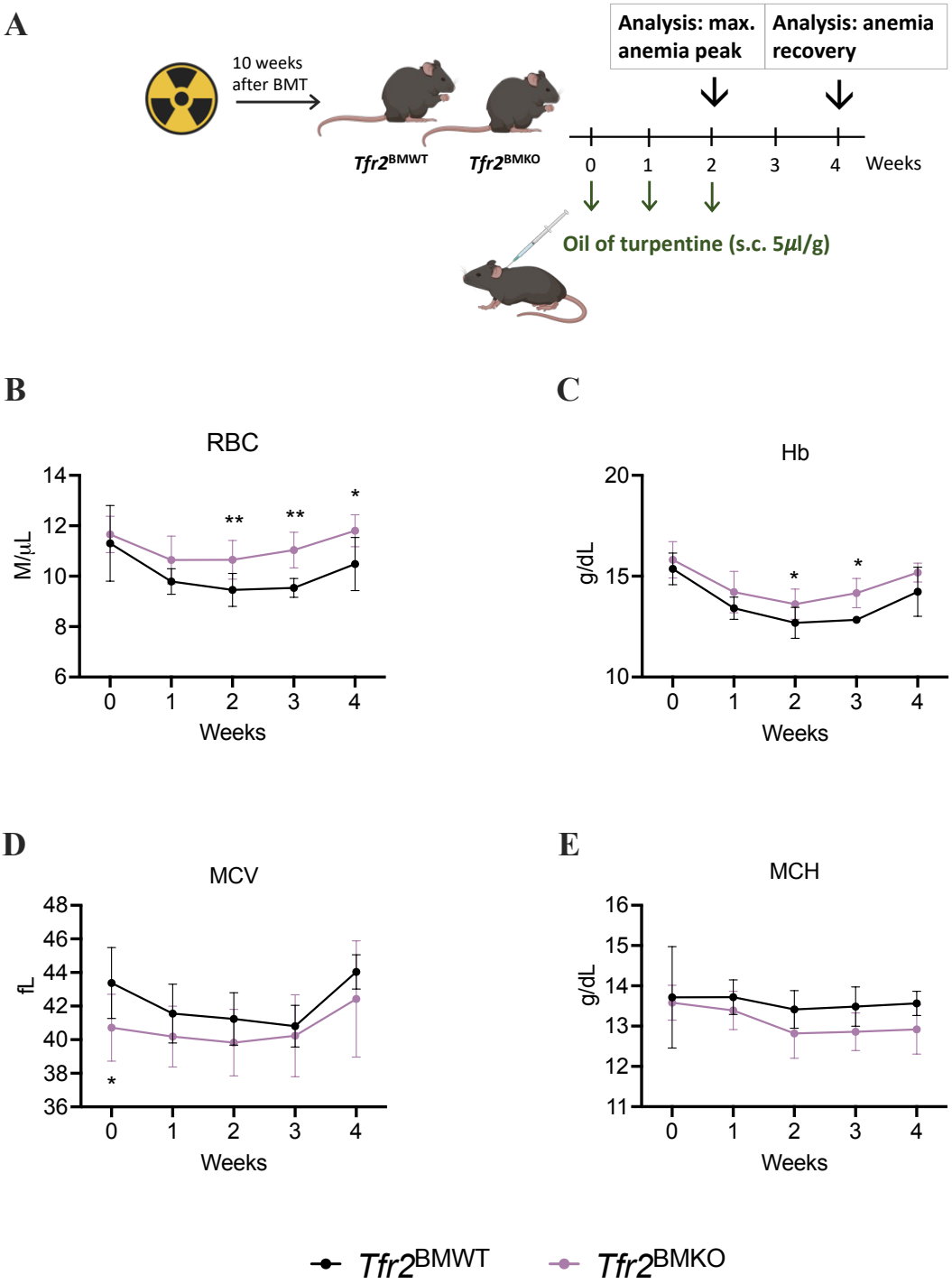
A
10 weeks
after BMT
Tfr2BMWT
Tfr2BMKO
Analysis: max. anemia peak
Analysis: anemia recovery
0
1
2
3
4
Weeks
Oil of turpentine (s.c. 5µl/g)
B
RBC
M/µL
Weeks
C
Hb
g/dL
Weeks
D
MCV
fL
Weeks
E
MCH
g/dL
Weeks
Tfr2BMWT
Tfr2BMKO

Figure 37. Turpentine-injected Tfr2^{BMKO} mice have improved anemia than controls. *Tfr2^{BMWT} and Tfr2^{BMKO} mice were generated through bone marrow (BM) transplantation. Ten weeks later, mice were treated with turpentine oil (5μl/g body weight, s.c.) once/week for 3 weeks and sacrificed 2 days (maximum anemia peak) or 2 weeks (anemia recovery) after the last injection. In the figure are represented: a scheme of the protocol (**A**); red blood cell count (RBC, **B**); hemoglobin levels (Hb, **C**); mean corpuscular volume (MCV, **D**) and mean corpuscular hemoglobin (MCH, **E**).*
*Mean values of 4-6 mice per group are represented. Two-way ANOVA for multiple comparisons (correction test Šídák, panels **B-E**) was used. Bars indicate standard deviation (SD). Asterisks refer to statistically significant differences. *P<0.05; **P<0.005.*

3.5.2 Turpentine-injected Tfr2^{BMKO} and control mice have comparable systemic inflammation and iron levels

We confirmed that systemic inflammation was comparable between *Tfr2*^{BMWT} and *Tfr2*^{BMKO} mice. Indeed, the expression levels of *Saa1* (**Figure 38A**), as expected higher after 3 turpentine injections than after 2 weeks of treatment discontinuation and circulating IL-6 levels (**Figure 38B**) were similar between the two groups at both time points, excluding a differential effect of the treatment in the two genotypes.

After 3 weeks of turpentine injections, *Tfr2*^{BMKO} mice showed lower serum iron levels than controls, likely because of the increased use of the metal for RBCs production. At the end of the protocol, serum iron was similar between *Tfr2*^{BMKO} mice and controls, but low as compared to wt healthy mice, as expected due to inflammation (**Figure38C**). Transferrin saturation showed an analogous trend, but no statistically significant differences between the genotypes were observed (**Figure 38D**).

Liver iron content was higher at maximum peak than at anemia recovery and comparable between the two groups (LIC, **Figure 38E**) and *Hamp* levels showed a similar behavior (**Figure 38F**). Spleen iron content was not affected by the genotype at the maximum peak of anemia but was higher in *Tfr2*^{BMKO} mice at anemia recovery (SIC, **Figure 38G**), likely as a tentative mechanism to preserve iron to sustain enhanced erythropoiesis. Finally, kidney iron content was overall comparable between the 2 groups at both time points (KIC, **Figure 38H**).

Figure 38

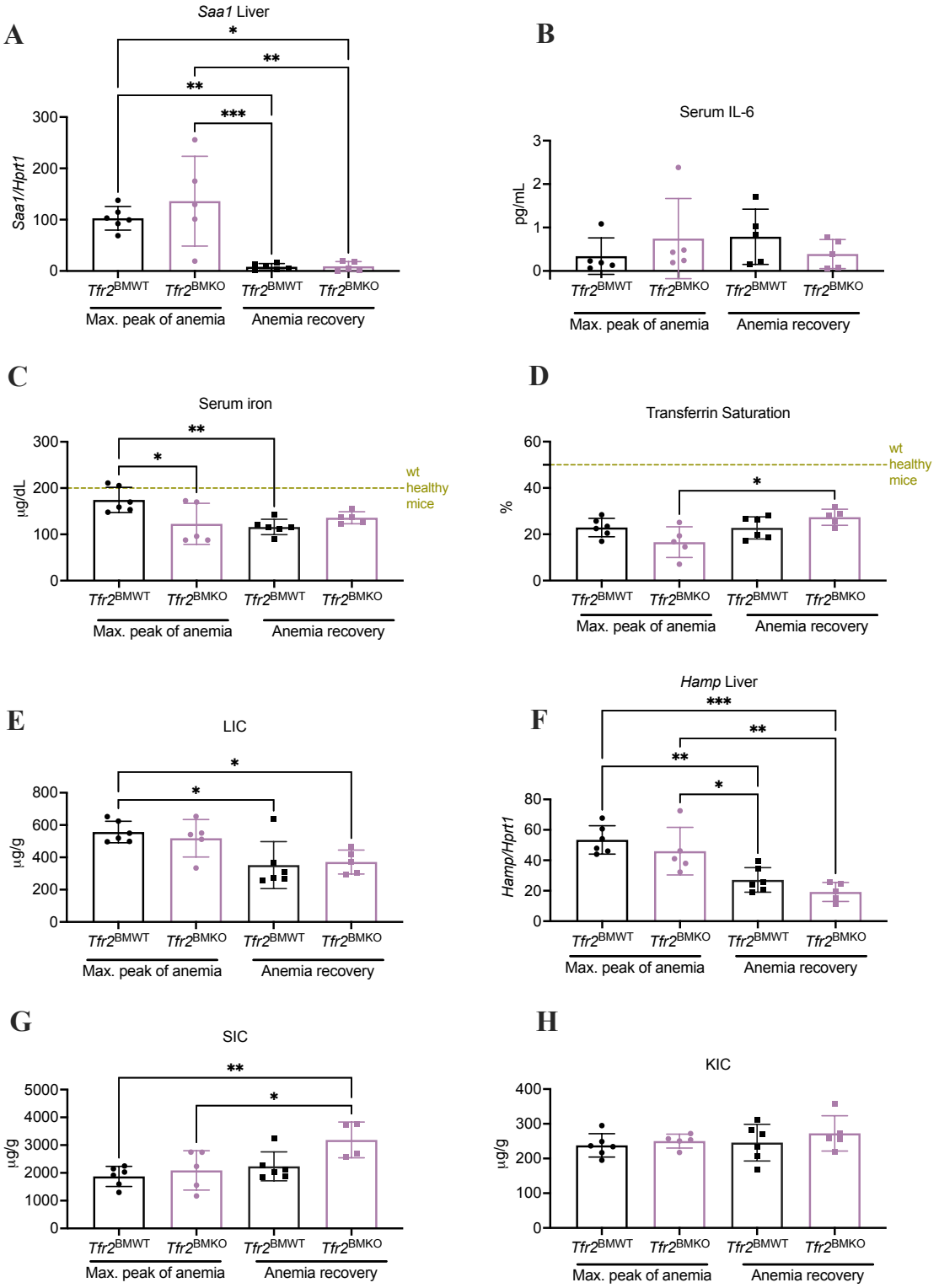
A
Saa1 Liver
Saa1/Hprt1
300
200
100
0
*
**
**
***
Tfr2BMWT
Tfr2BMKO
Tfr2BMWT
Tfr2BMKO
Max. peak of anemia
Anemia recovery
B
Serum IL-6
pg/mL
3
2
1
0
Tfr2BMWT
Tfr2BMKO
Tfr2BMWT
Tfr2BMKO
Max. peak of anemia
Anemia recovery
C
Serum iron
µg/dL
300
200
100
0
**
*
wt
healthy
mice
Tfr2BMWT
Tfr2BMKO
Tfr2BMWT
Tfr2BMKO
Max. peak of anemia
Anemia recovery
D
Transferrin Saturation
%
60
40
20
0
wt
healthy
mice
*
Tfr2BMWT
Tfr2BMKO
Tfr2BMWT
Tfr2BMKO
Max. peak of anemia
Anemia recovery
E
LIC
µg/g
800
600
400
200
0
*
*
Tfr2BMWT
Tfr2BMKO
Tfr2BMWT
Tfr2BMKO
Max. peak of anemia
Anemia recovery
F
Hamp Liver
Hamp/Hprt1
80
60
40
20
0
***
**
**
*
Tfr2BMWT
Tfr2BMKO
Tfr2BMWT
Tfr2BMKO
Max. peak of anemia
Anemia recovery
G
SIC
µg/g
5000
4000
3000
2000
1000
0
**
*
Tfr2BMWT
Tfr2BMKO
Tfr2BMWT
Tfr2BMKO
Max. peak of anemia
Anemia recovery
H
KIC
µg/g
400
300
200
100
0
Tfr2BMWT
Tfr2BMKO
Tfr2BMWT
Tfr2BMKO
Max. peak of anemia
Anemia recovery

Figure 38. Turpentine-injected Tfr2^{BMKO} and control mice have similar inflammation and iron levels. *Tfr2^{BMWT} and Tfr2^{BMKO} mice were generated through bone marrow (BM) transplantation. Ten weeks later, mice were treated with turpentine oil (5µl/g body weight, s.c.) once/week for 3 weeks and sacrificed 2 days (maximum anemia peak) or 2 weeks (anemia recovery) after the last injection. In the figure are represented: mRNA levels of Serum amyloid a-1 (Saa1, **A)** relative to Hypoxanthine Phosphoribosyltransferase1(Hprt1) in the liver; circulating levels of IL-6 (**B**); serum iron levels (**C**); transferrin saturation (**D**); liver iron content (LIC, **E**); mRNA levels of hepcidin (Hamp, **F**) relative to Hprt1 in the liver; spleen (SIC, **G**) and kidney (KIC, **H**) iron content.*
*Mean values of 5-6 mice per group are represented. One-way ANOVA (correction test Tukey, panels **A-H**) was used. Bars indicate standard deviation (SD). Asterisks refer to statistically significant differences. *P<0.05; **P<0.005; ***P<0.001.*

3.5.3 Bone marrow Tfr2 deletion increases erythroid EPO responsiveness in inflamed mice

At the maximum peak of anemia, *Tfr2*^{BMKO} mice showed a trend toward an increased percentage of Ter119^{+} cells in the BM, that became statistically significant at anemia recovery, mainly due to an expansion of mature RBCs (**Figure 39A**). In the spleen there was an increase in the proportion of basophilic and polychromatic erythroblasts in *Tfr2*^{BMKO} mice after 3 turpentine injections, but no differences at recovery (**Figure 39B**). The increased erythropoiesis of *Tfr2*^{BMKO} mice was due to higher erythroblasts sensitivity to EPO rather than to an enhanced EPO production, as previously shown (Nai *et al*, 2015; Artuso *et al*, 2018; Di Modica *et al*, 2022). Indeed, in line with anemia improvement, serum EPO levels were lower in *Tfr2*^{BMKO} than in controls at both time points (**Figure 39C**), and *Epo* expression in the kidney was lower in *Tfr2*^{BMKO} mice at recovery (**Figure 39D**). However, the expression of the EPO target genes *Bcl-xl*, *Epor* and *Erfe* was comparable between the 2 genotypes at absolute level (**Figure 39E-F**, **40A-B** and **40E-F**), but higher in *Tfr2*^{BMKO} mice when normalized on circulating EPO (**Figure 39G-H**, **40C-D** and **40G-H**), confirming the overactivation of the EPO-EPOR pathway in the absence of *Tfr2*.

Overall, we showed that in a model of sterile inflammation the specific deletion of *Tfr2* in the BM induced a sustained increase in RBCs and Hb production, supported by the sufficient iron availability, without increasing EPO levels and affecting inflammation.

Figure 39

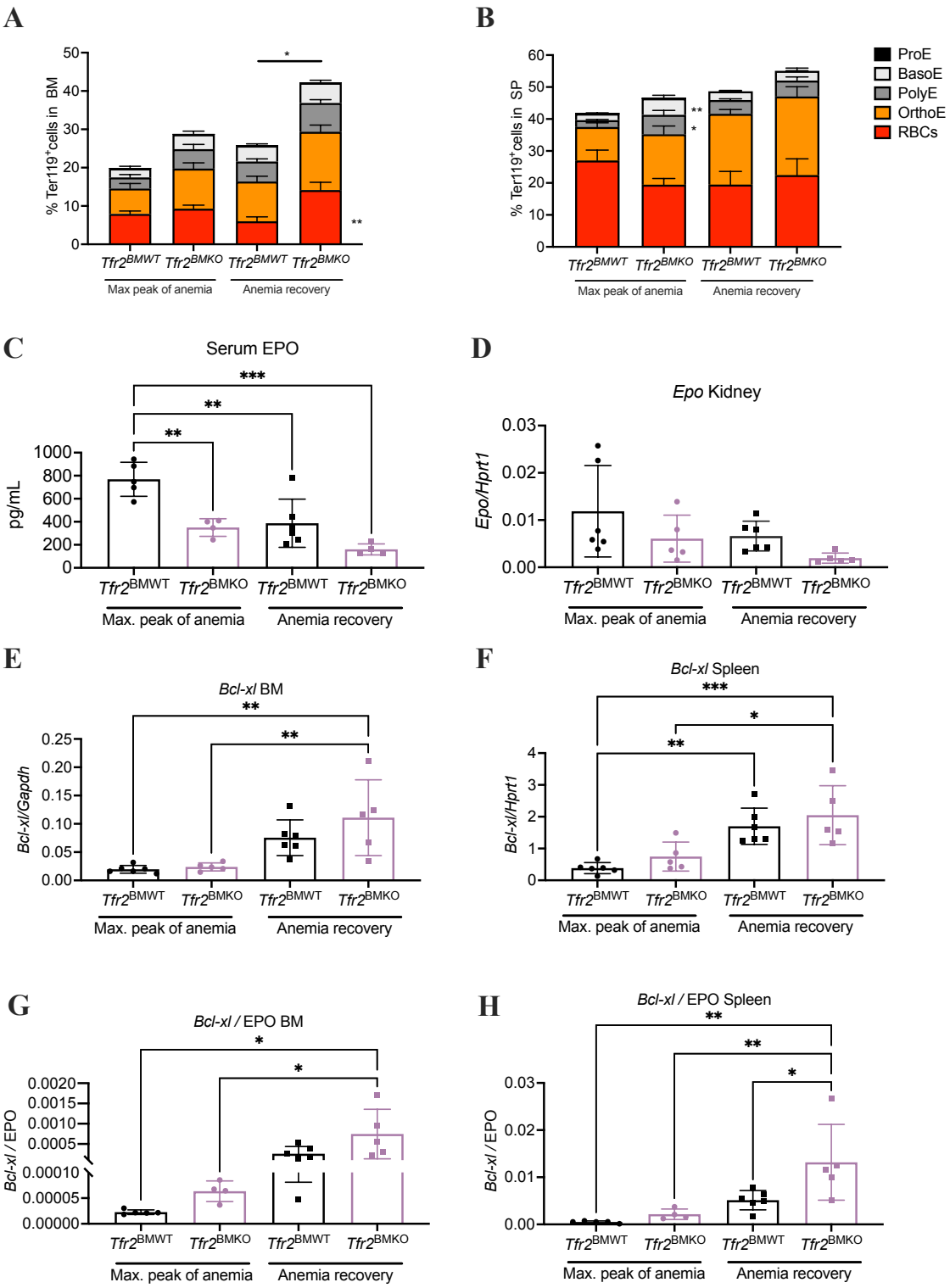
A
% Ter119+cells in BM
Tfr2BMWT Tfr2BMKO Tfr2BMWT Tfr2BMKO
Max peak of anemia
Anemia recovery
B
% Ter119+cells in SP
ProE
BasoE
PolyE
OrthoE
RBCs
C
Serum EPO
pg/mL
D
Epo Kidney
Epo/Hprt1
E
Bcl-xl BM
Bcl-xl/Gapdh
F
Bcl-xl Spleen
Bcl-xl/Hprt1
G
Bcl-xl / EPO BM
Bcl-xl / EPO
H
Bcl-xl / EPO Spleen
Bcl-xl / EPO

Figure 39. Turpentine-injected $Tfr2^{BMKO}$ mice have increased EPO responsiveness and activation of EPO-EPOR pathway. *$Tfr2^{BMWT}$ and $Tfr2^{BMKO}$ mice were generated through BM transplantation. Ten weeks later, mice were treated with turpentine oil (5µl/g body weight, s.c.) once/week for 3 weeks and sacrificed 2 days (maximum anemia peak) or 2 weeks (anemia recovery) after the last injection. In the figure are represented: the percentage of total $Ter119^+$ cells in the BM (**A**) and in the spleen (SP, **B**) and the contribution of the 5 erythroblasts populations [proerythroblasts (ProE), basophilic erythroblasts (BasoE), polychromatic erythroblasts (PolyE), orthochromatic erythroblasts and immature reticulocytes (OrthoE), and mature red cells (RBCs)], identified through the evaluation of cell size and Ter119/CD44 relative expression; serum erythropoietin levels (EPO, **C**); mRNA levels of Epo relative to Hypoxanthine Phosphoribosyltransferase1 (Hprt1) in the kidney (**D**); mRNA levels of B-cell lymphoma-extra large (Bcl-xl) relative to Glyceraldehyde-3-phosphate dehydrogenase (Gapdh) in the BM (**E**) and relative to Hprt1 in the spleen (**F**); B-cell lymphoma-extra large (Bcl-xl) mRNA levels normalized on circulating EPO in the BM (**G**) and in the spleen (**H**).*
*Mean values of 4-6 mice per group are represented. One-way ANOVA (correction test Tukey, panels **A-H**) was used. Bars indicate standard deviation (SD). Asterisks refer to statistically significant differences. *P<0.05; **P<0.005; ***P<0.001.*

Figure 40

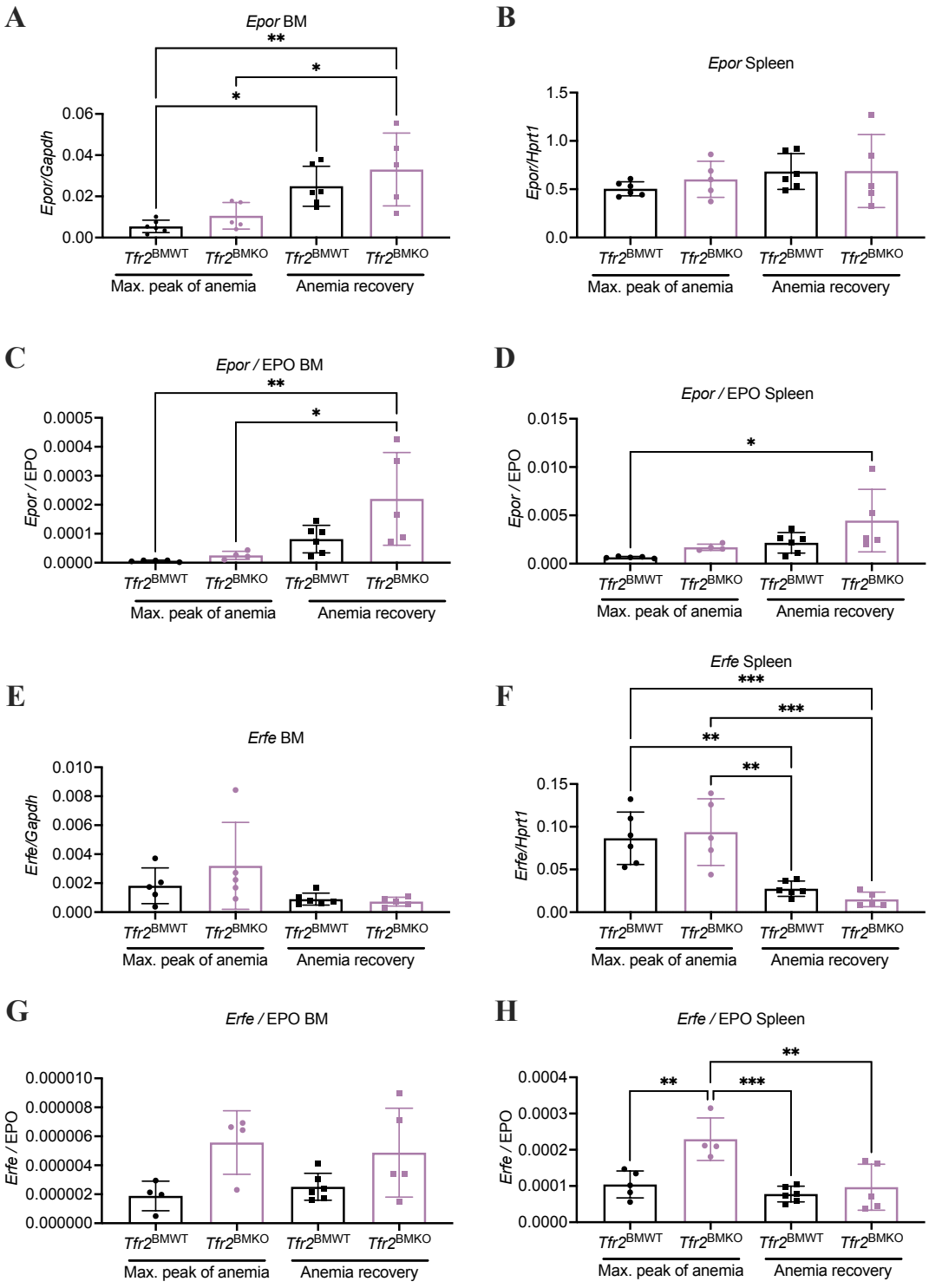
A
Epor BM
Epor/Gapdh
0.06
0.04
0.02
0.00
Tfr2BMWT
Tfr2BMKO
Tfr2BMWT
Tfr2BMKO
Max. peak of anemia
Anemia recovery
B
Epor Spleen
Epor/Hprt1
1.5
1.0
0.5
0.0
C
Epor / EPO BM
Epor / EPO
0.0005
0.0004
0.0003
0.0002
0.0001
0.0000
D
Epor / EPO Spleen
0.015
0.010
0.005
0.000
E
Erfe BM
Erfe/Gapdh
0.010
0.008
0.006
0.004
0.002
0.000
F
Erfe Spleen
Erfe/Hprt1
0.15
0.10
0.05
0.00
G
Erfe / EPO BM
Erfe / EPO
0.000010
0.000008
0.000006
0.000004
0.000002
0.000000
H
Erfe / EPO Spleen
0.0004
0.0003
0.0002
0.0001
0.0000

Figure 40. Turpentine-injected Tfr2^{BMKO} mice have increased activation of EPO-EPOR pathway. *Tfr2^{BMWT} and Tfr2^{BMKO} mice were generated through BM transplantation. Ten weeks later, mice were treated with turpentine oil (5μl/g body weight, s.c.) once/week for 3 weeks and sacrificed 2 days (maximum anemia peak) or 2 weeks (anemia recovery) after the last injection. In the figure are represented: mRNA levels of Erythropoietin receptor (Epor) relative to Glyceraldehyde-3-phosphate dehydrogenase (Gapdh) in the bone marrow (BM, **A**) and relative to Hypoxanthine Phosphoribosyltransferase1 (Hprt1)in the spleen (**B**); Epor mRNA levels normalized on circulating EPO in the BM (**C**) and in the spleen (**D**); mRNA levels of Erythroferrone (Erfe) relative to Gapdh in the BM (**E**) and relative to Hprt1 in the spleen (**F**); Erfe mRNA levels normalized on circulating EPO in the BM (**G**) and in the spleen (**H**).*
*Mean values of 4-6 mice per group are represented. One-way ANOVA (correction test Tukey, panels **A-H**) was used. Bars indicate standard deviation (SD). Asterisks refer to statistically significant differences. *P<0.05; **P<0.005; ***P<0.001.*

3.6 *Tfr2* targeting in a murine model of malaria anemia

3.6.1 Bone marrow Tfr2 deletion maintains higher RBCs and Hb levels and lower parasitemia in malaria anemia

Finally, we moved to test whether BM specific *Tfr2* deletion may ameliorate also malaria anemia, a peculiar form of anemia of inflammation due to parasite infection in which inflammation and RBCs hemolysis coexist. Also in this case, we avoided total *Tfr2* deletion to prevent iron-loading.

We induced malaria infecting *Tfr2^{BMKO}* mice and relative controls with *Plasmodium chabaudi chabaudi* (*Pcc*), a commonly used murine specific malaria strain. This model shows similarities with human *Plasmodium falciparum* infection, especially in the erythroid cycle, while it lacks the liver stage, being thus easy to be exploited in an experimental setting. Moreover, it induces chronic infection but has low mortality rate (Lamikanra *et al*, 2007; Spence *et al*, 2011, 2013).

Donor/host chimerism of transplanted mice evaluated at the end of the experimental protocol was superior to 90% both in the BM and spleen in all animals. *Pcc*-infected RBCs were injected in *Tfr2*^{BMWT} and *Tfr2*^{BMKO} mice 10 weeks after BMT and hematological parameters and parasitemia were analyzed every 2-4 days (**Figure 41A**). *Tfr2*^{BMWT} mice developed anemia 8 days after parasite infection, reached maximum peak at day 12 and gradually recovered starting from day 16 (**Figure 41B-E**). Also *Tfr2*^{BMKO} mice showed a decrease in RBCs and Hb levels starting from day 8, but reached a lower degree of anemia as compared to *Tfr2*^{BMWT} animals, and rapidly recovered starting from

day 12 (**Figure 41B-C**). MCV and MCH strongly increased over time in *Tfr2*^{BMWT} mice (**Figure 41D-E**), likely indicating an augment in the release of erythroid progenitors to compensate for anemia development. In agreement, the percentage of circulating reticulocytes became higher (**Figure 41F**). All these parameters were maintained low in *Tfr2*^{BMKO}, suggesting the preservation of a more effective and iron-restricted erythropoiesis.

Parasitemia, the percentage of infected RBCs, increased starting from day 6 in *Tfr2*^{BMWT} animals, was maintained high until day 16 and then came back to 0 on day 20. Intriguingly, *Tfr2*^{BMKO} mice showed exclusively a very mild RBCs infection at day 10, which rapidly disappeared (**Figure 42A**). In agreement, no signs of damaged RBCs and hemolysis were evident in blood smears from *Tfr2*-null mice (**Figure 42B**).
These findings suggest that plasmodium growth is hampered in *Tfr2*-deficient erythroblasts, likely because of the limited iron availability.

Figure 41

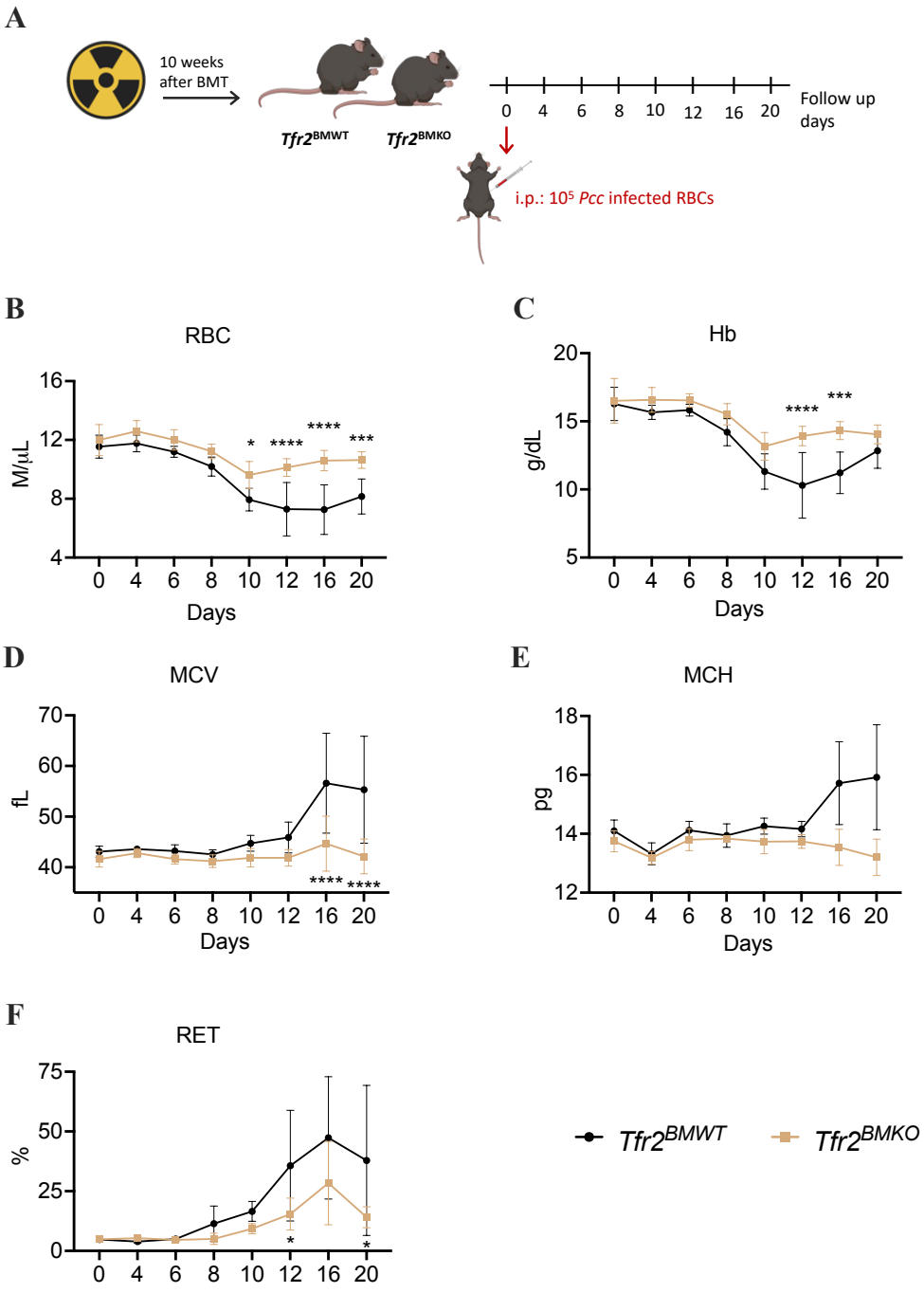

Figure 41. Pcc-infected $Tfr2^{BMKO}$ mice have higher RBCs and Hb levels than controls and signs of iron-restricted erythropoiesis. *$Tfr2^{BMWT}$ and $Tfr2^{BMKO}$ mice were generated through bone marrow transplantation. Ten weeks later, mice were i.p. injected with Pcc infected blood. In the figure are represented: a scheme of the protocol (**A**); red blood cell count (RBC, **B**); hemoglobin levels (Hb, **C**); mean corpuscular volume (MCV, **D**); mean corpuscular hemoglobin (MCH, **E**) and reticulocytes percentage (RET, **F**).*
*Mean values of 6-12 mice per group are represented. Two-way ANOVA for multiple comparisons (correction test Šídák, panels **B-F**) was used. Bars indicate standard deviation (SD). Asterisks refer to statistically significant differences. *P<0.05; ***P<0.001; ****P<0.0001*

Figure 42

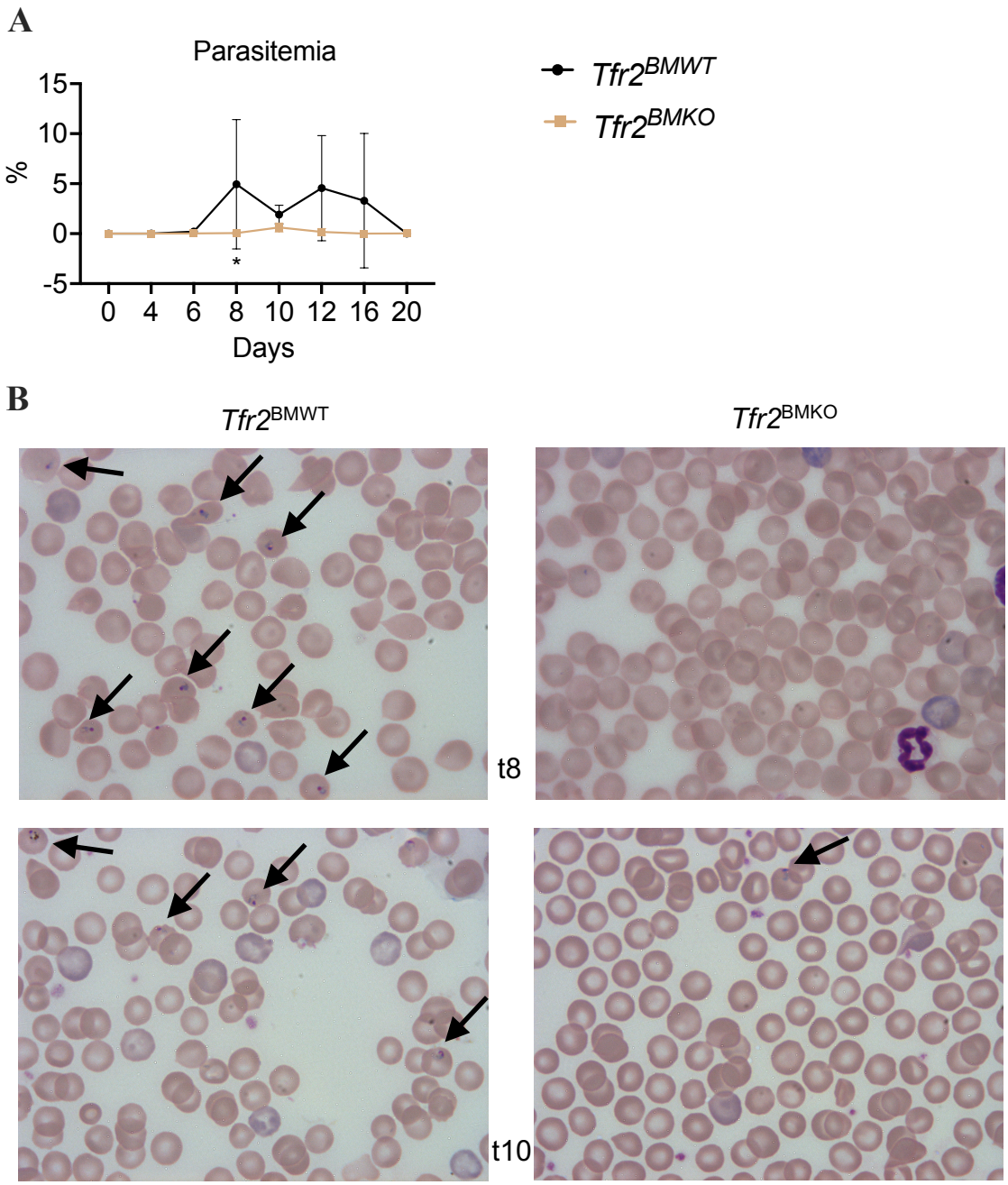

Figure 42. Pcc-infected Tfr2^{BMKO} mice have lower parasitemia than controls. *Tfr2^{BMWT} and Tfr2^{BMKO} mice were generated through bone marrow transplantation. Ten weeks later, mice were i.p. injected with Pcc infected blood. In the figure are represented: percentage of infected red blood cells (iRBCs, **A**); representative images of blood smears (Giemsa's Staining) from Tfr2^{BMWT} and Tfr2^{BMKO} mice 8 and 10 days after infection. Black arrows indicate iRBCs (magnification 100x, **B**).*

*Mean values of 6-12 mice per group are represented. Two-way ANOVA for multiple comparisons (correction test Šídák, panel **A**) was used. Bars indicate standard deviation (SD). *P<0.05*

3.6.2 Iron-overload hampers the beneficial effect of bone marrow Tfr2 deletion in malaria anemia

To test whether low iron availability is the driver of reduced plasmodium growth in *Tfr2*^{BMKO} mice, we induced malaria in mice with total *Tfr2* deletion. *Pcc*-infected RBCs were injected in *Tfr2*$^{-/-}$ and controls mice and parasitemia was analyzed every 3 days (**Figure 43A**). *Tfr2*$^{+/+}$ and *Tfr2*$^{-/-}$ mice developed anemia in a similar manner as indicated by RBC and Hb levels (**Figure 42B-C**). MCV and MCH were higher in *Tfr2*$^{-/-}$ mice (**Figure 42D-E**), as expected due to higher iron availability, reaching levels comparable to *Tfr2*$^{+/+}$ after drop in RBC and Hb levels between day 12 and 15, likely because of the development of reticulocytosis. In agreement, reticulocyte percentage increased at the same timepoints and in a comparable manner between the 2 genotypes (**Figure 42F**).

Tfr2$^{-/-}$ mice reached the peak of parasitemia with a modest delay as compared to controls, but the magnitude of RBCs infection was comparable between the 2 groups (**Figure 42G**).

Thus, increased iron availability leads to the loss of the beneficial effect of BM *Tfr2* deletion on anemia and parasitemia, supporting the hypothesis that limited iron availability in erythroblasts protects against *Pcc* infections.

Figure 43

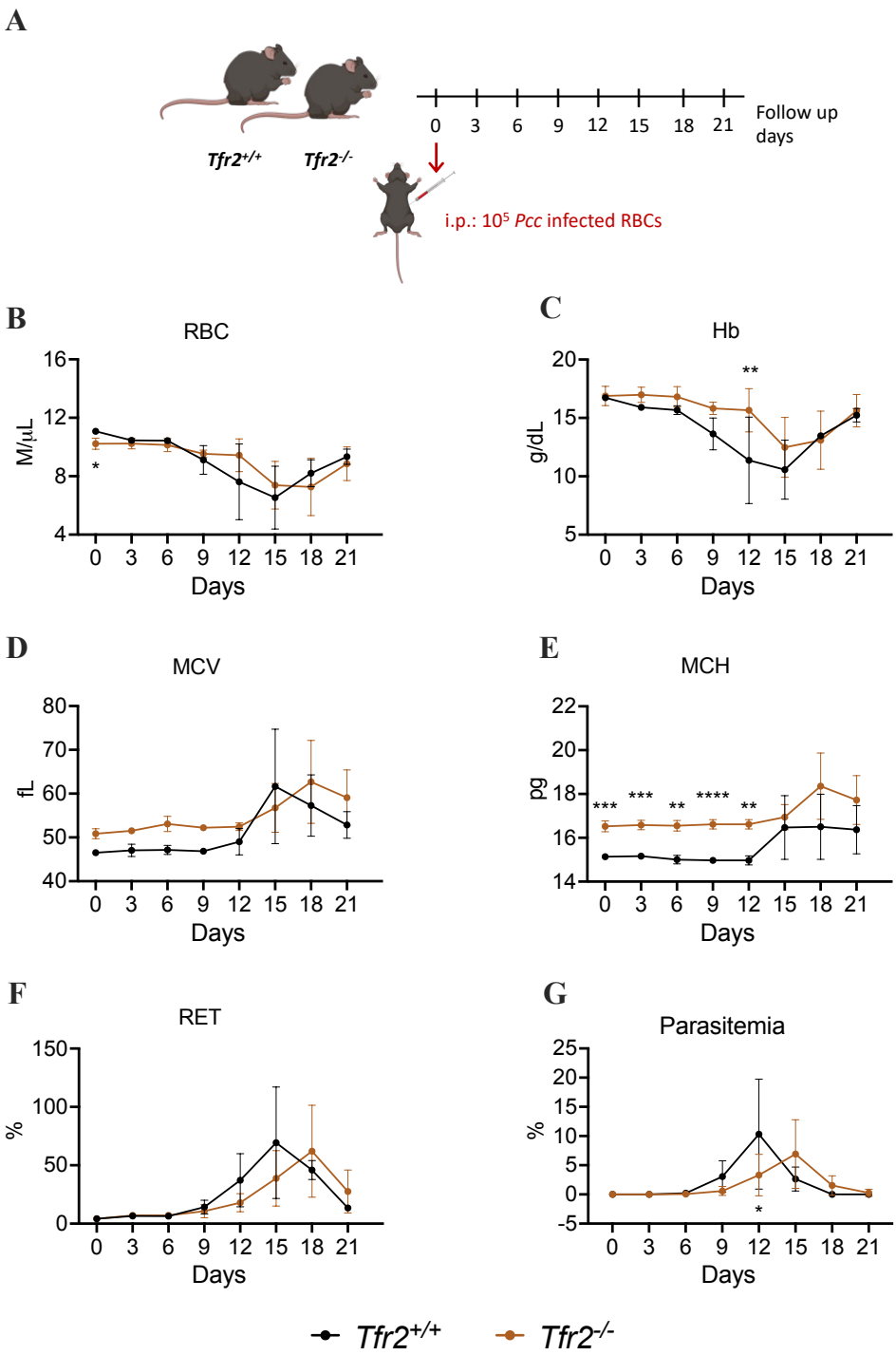

Figure 43. Pcc-infected Tfr2$^{-/-}$ mice have hematological analysis and parasitemia similar to controls. *Eight-week-old Tfr2$^{+/+}$ and Tfr2$^{-/-}$ mice were i.p. injected with Pcc infected blood. In the figure are represented a scheme of the protocol (**A**); red blood cell count (RBC, **B**); hemoglobin levels (Hb, **C**); mean corpuscular volume (MCV, **D**); mean corpuscular hemoglobin (MCH, **E**) and reticulocytes (RET, **F**); percentage of infected RBCs (iRBCs, **G**).*
*Mean values of 3-5 mice per group are represented. Two-way ANOVA for multiple comparisons (correction test Šídák, panels **B-G**) was used. Bars indicate standard deviation (SD). Asterisks refer to statistically significant differences. *P<0.05; **P<0.005; ***P<0.001; ****P<0.0001*

4. DISCUSSION

Anemia is a disorder of heterogeneous etiology affecting about 42% of children below 5-year-old and 40% pregnant women worldwide (WHO). Beside nutritional deficiencies, chronic inflammation, due to pathogens infections, as malaria, several forms of cancer, autoimmune diseases and chronic diseases, as CKD, is the second contributor to the burden of anemia. Anemia of inflammation is caused by increased pro-inflammatory cytokines production that leads to reduced erythroid EPO sensitivity, BM reprograming, shortened erythrocyte lifespan and iron-restriction (Ganz, 2019). Anemia caused by malaria infection is worsened by hemolysis, while in anemia of CKD inappropriately low EPO levels and iron-deficiency strongly contribute to the pathogenesis. The treatment of anemia of inflammation with EPO mimetics is unsatisfactory, because of hyporesponsiveness to EPO (Gluba-Brzózka *et al*, 2020; Bikbov *et al*, 2020) and adverse events, mainly cardiovascular, due to EPO activity in non-erythroid organs and tissues (Unger *et al*, 2010). In anemia of CKD iron supplementation is often needed, increasing the occurrence of side effects (Feldman *et al*, 2002; Besarab & Coyne, 2010).
Here, we demonstrated that targeting the iron sensor TFR2 might represent a promising novel therapeutic opportunity for the correction of anemia caused by CKD, sterile inflammation and malaria infection. However, *Tfr2* manipulation has to be tuned based on the pathophysiology of the disease.

Anemia of CKD

As a CKD model we exploited the adenine-rich diet, that induces kidney failure through tubules obstruction and toxic metabolites production (Yokozawa *et al*, 1982; Jia *et al*, 2013). Even if it presents some limitations, such as gender differences in renal impairment (Diwan *et al*, 2014; Metzger *et al*, 2021) and the induction of a selective tubulointerstitial disease (Jia *et al*, 2013), it recapitulates the main features of human CKD. Moreover, it has reduced mortality rate and variability as compared to other available surgical (i.e. 5/6th nephrectomy (Shimamura & Morrison, 1975) and unilateral ureteral obstruction (Manucha *et al*, 2004)) and non-surgical (i.e. nephrotoxic drugs (Yang *et al*, 2010), radiations (Yang *et al*, 2010) and oxalate diet (Mulay *et al*, 2016)) approaches. Even if the adenine diet represents a widely used system to induce CKD in

experimental models, some variability on the degree of renal damage induction exists, mainly due to differences in raw materials and diet-producing processes between different providers. For this reason, before starting the experimental protocol we confirmed that our diet was effective in recapitulating all the features of human CKD, i.e., renal damage, anemia, systemic inflammation and iron-deficiency.

We started investigating the effect on anemia development of specific *Tfr2* deletion in BM-derived cells, with the aim of increasing erythroid EPO responsiveness. With this approach the entire hematopoietic compartment is replaced, not only in the BM but also in the spleen, an important hematopoietic organ in mice (Iseki *et al*, 2008). We proved that the diet induced gradual impairment of renal functionality and progressive anemia in *Tfr2*^{BMWT} mice, as expected. Notwithstanding comparable renal damage and functionality, systemic and local inflammation, and iron availability, *Tfr2*^{BMKO} mice showed lower anemia severity. Only at 8 weeks, Hb dropped to control values, while RBCs remained higher for the entire timespan. This was accompanied by lower MCV and MCH, signs of iron-restricted erythropoiesis, suggesting that iron levels were not sufficient to sustain on a long-term proper Hb production for the enhanced erythropoiesis of *Tfr2*-deficient animals. Importantly, EPO levels were not increased, and the expression of EPO target genes was upregulated in *Tfr2*^{BMKO} mice, further confirming that BM *Tfr2* deletion promotes erythropoiesis increasing erythroid responsiveness to EPO.

Since we proved that BM-specific *Tfr2* deletion increased RBC production without affecting EPO levels, but iron availability was not adequate for the higher demand, we moved to *Tfr2* germline deletion, to simultaneously increase erythropoiesis and iron availability. *Tfr2*$^{-/-}$ mice maintained higher RBCs and Hb levels relative to wild-type littermates for the entire timespan. MCV and MCH were comparable between the two groups, indicating iron-sufficient erythropoiesis, and, in agreement, circulating iron levels were higher in *Tfr2*$^{-/-}$ animals than in controls, reaching levels of wt healthy mice. In line with the improved anemia, EPO levels were lower in *Tfr2*$^{-/-}$ animals than in controls and the expression of EPO target genes in erythroid tissues normalized on circulating EPO levels was higher, as observed in mice with BM-specific *Tfr2* deletion. So, we propose that in *Tfr2*$^{-/-}$ mice the simultaneous absence of TFR2 in hepatocytes and in the erythroid

compartment is necessary and sufficient to induce a balanced increment of iron availability and erythropoietic output, respectively, leading to a sustained amelioration of anemia of CKD.

We excluded that iron alone plays a major role in the improvement of anemia mediated by total *Tfr2* deletion. Indeed, wild-type mice fed the adenine diet and treated with *Tfr2*-ASOs that inhibit hepatic, but not erythroid *Tfr2,* showed a modest anemia amelioration, in accordance with the evidence that the iron-loaded hepcidin KO mice are partially protected from adenine-induced anemia (Akchurin *et al*, 2016). However, the beneficial effect was transient and RBCs and Hb reached levels of Ctrl-ASOs treated mice before the end of the protocol. As expected, MCV and MCH were increased in *Tfr2*-ASOs mice and were maintained higher until the end of the protocol, indicating increased iron availability. In agreement, circulating iron levels were high in *Tfr2*-ASOs mice, overcoming values of wt healthy animals. However, the EPO sensitivity of erythroid cells was not enhanced, as shown by comparable activation of EPO target genes relative to circulating EPO levels in both Ctrl-ASOs and *Tfr2*-ASOs mice. This resulted in an iron-mediated induction of erythropoiesis, which became ineffective because of insufficient EPO stimulation, finally resulting in a transient anemia amelioration. We excluded a possible detrimental role for iron toxicity on erythroid differentiation, since the expression of genes involved in radical detoxification and lipid peroxidation was comparable in the BM of the two groups.

Interestingly, even if markers of systemic inflammation were comparable between *Tfr2*$^{-/-}$ and control mice, the expression of *Cd45* was higher in the kidney and liver of *Tfr2*$^{-/-}$ mice, indicating an increased infiltration by monocytes. Since macrophages polarization is modulated by iron content (Recalcati *et al*, 2010; Cairo *et al*, 2011; Soares & Hamza, 2016), higher iron levels in *Tfr2*$^{-/-}$ mice might trigger some degree of macrophages activation. However, this was not evident in *Tfr2*-ASOs mice. This difference could be due to the milder systemic iron overload, as evident by lower tissue iron levels in *Tfr2*-ASOs than in *Tfr2*$^{-/-}$ mice, or to a direct effect of *Tfr2* deletion on macrophages activation. Indeed, even if systemic iron homeostasis is not affected by *Tfr2* deletion in the myeloid lineage (Rishi *et al*, 2016), the TFR2 role in macrophages'

function has not been deeply investigated. Further analyses are currently ongoing in the lab to unravel this point.

Of note, CKD *Tfr2*$^{-/-}$ mice had higher trabecular bone mass and density compared to controls both in femur and spine, reaching levels of wt healthy mice, showing that the recently identified negative regulatory function of TFR2 in bone homeostasis (Rauner *et al*, 2019) is conserved also in pathologic conditions. Indeed, bone fragility is a common complication of CKD (Fried *et al*, 2007; Pimentel *et al*, 2021) and the adenine diet recapitulates this phenotype in mice (Jia *et al*, 2013; Metzger *et al*, 2021). The beneficial effect on bone was not present in *Tfr2*^{BMKO} mice, suggesting that *Tfr2* deficiency in osteoblasts, rather than in osteoclasts, is responsible for bone protection in CKD mice, as previously shown by Rauner and colleagues in healthy mice (Rauner *et al*, 2019). Indeed, while osteoblasts derive from mesenchymal stem cells, osteoclasts are of hematopoietic origin and are replaced with donor cells in mice undergoing BM transplantation. Of course, this is an indirect observation, and further studies (e.g., using cell-specific conditional models) are required to investigate this aspect more in deep.

Anemia of inflammation

While anemia of CKD benefits from erythropoiesis induction accompanied by increased iron availability, iron administration can be detrimental in anemia of inflammation, eventually promoting pathogens growth and worsening inflammation (Ganz, 2019). For this reason, in this model we focused exclusively on BM *Tfr2* deletion, to promote erythropoiesis without increasing iron absorption and release.

We modeled pathogen-free inflammation administering turpentine oil to mice. This is a widely used resin distillate (Nicolas *et al*, 2002; Sukumaran *et al*, 2012; Prince *et al*, 2012; Langdon *et al*, 2014; Wang *et al*, 2017) obtained from various trees (Rivera & Ganz, 2009), that induces inflammation avoiding the use of infectious pathogens, through a mechanism not completely understood.

At difference with results obtained in the CKD model, inflamed *Tfr2*^{BMKO} mice maintained higher RBCs and Hb levels than controls for the entire time-span, suggesting

that when iron is present, even if restricted in stores, the sole induction of erythropoiesis is sufficient to sustain anemia amelioration. In agreement, MCV and MCH were comparable between the 2 groups, indicating iron sufficient erythropoiesis.

Of note, circulating iron levels at maximum peak of anemia were lower in *Tfr2*^{BMKO} mice, likely because of the increased erythropoietic demand. However, at anemia recovery serum iron was comparable between the 2 genotypes, probably following a compensatory iron release from stores. In agreement, liver iron content was lower at anemia recovery than at the maximum peak of anemia in both groups of mice, without inducing a significant increase in circulating iron levels. These findings suggest that, during anemia of inflammation, iron can be released from the stores in a controlled manner based on the erythroid demand, to sustain erythropoiesis without increasing circulating iron. As expected, this regulation likely involves hepcidin, whose levels were comparable between *Tfr2*^{BMKO} and *Tfr2*^{BMWT} mice, but lower at anemia recovery than during the acute inflammatory phase, in line with hepatic iron content and the degree of systemic inflammation.

Also in this model, BM *Tfr2* deletion promoted erythropoiesis without increasing EPO levels, which were even lower in *Tfr2*^{BMKO} mice at both time points compared to controls, but increasing the EPO sensitivity of erythroid cells, as confirmed by the higher expression of EPO target genes normalized on circulating EPO. Interestingly, while the transcript levels of both *Bcl-xl* and *Epor* were lower at maximum peak of anemia than at recovery, likely reflecting the degree of erythropoiesis induction, *Erfe* showed an opposite behavior. This is coherent with previous findings proving that *Erfe* production is enhanced during acute inflammation to promote iron release from stores, thus sustaining erythropoiesis (Kautz *et al*, 2014), and further support our hypothesis that, in inflammation, erythropoiesis induction is sufficient to improve anemia because of an efficient ERFE-mediated iron mobilization.

Malaria anemia

To add another layer of complexity, we decided to test whether BM *Tfr2* deletion ameliorates anemia of inflammation during the infection from a pathogen, such as malaria

Plasmodium. Indeed, malaria anemia is one of the principal causes of morbidity and mortality worldwide (WHO, 2021), whose treatment, despite the recent development of a new promising malaria vaccine (Datoo *et al*, 2022), is still unsatisfactory (White, 2018).

Several murine models for malaria infection are available. We used the non-lethal *Plasmodium chabaudi chabaudi* that, despite skipping the hepatic phase, invades erythroid cells at all stages of differentiation, similarly to the human *Plasmodium falciparum*, and is widely characterized in literature (Lamikanra *et al*, 2007; Seixas *et al*, 2009; Gozzelino *et al*, 2012; Spence *et al*, 2011, 2013).

In line with results obtained with turpentine injection, *Tfr2*^{BMKO} mice maintained RBCs and Hb levels higher than *Tfr2*^{BMWT} mice for the entire time-span, and their recover was faster. MCV and MCH were drastically lower in *Tfr2*^{BMKO} between day 10-20, indicating iron-restricted and more effective erythropoiesis.

Surprisingly, anemia improvement in *Tfr2*^{BMKO} mice was accompanied by almost absent RBCs infection throughout the entire protocol. This might be due to a direct role for TFR2 in RBCs invasion by the parasite, in line with the identification of TFR1 as a reticulocyte-specific receptor for *Plasmodium vivax* (Gruszczyk *et al*, 2018), or to the iron-restricted erythropoiesis induced by *Tfr2* deficiency, since it is well known that low erythroid iron availability hampers *Plasmodium* infections (Gwamaka *et al*, 2012; Latour *et al*, 2017). However, when germline *Tfr2*$^{-/-}$ mice were infected with *Pcc*, no overt anemia amelioration or infection prevention were observed, but only a possible mild delay. These results likely rule-out a direct role for TFR2 in RBCs invasion by *Pcc* and suggest that, following malaria infection, BM *Tfr2* inactivation not only promotes erythropoiesis, but also limits *Plasmodium* growth reducing erythroid iron content.

<u>*Concluding remarks*</u>

Overall, this study confirmed that hematopoietic *Tfr2* deletion, here obtained through BM transplantation, is an effective tool to increase erythroid EPO responsiveness in different types of anemia without affecting EPO levels per se, thus increasing RBCs and

Hb production according to iron availability. When iron in the body is sufficient, as in the models of sterile and malaria inflammation, this is enough to improve anemia. On the contrary, when iron is lacking, as in CKD, additional iron is necessary to sustain the augmented erythropoietic effort, in analogy with the current clinical practice of administering iron in combination with ESAs, and a simultaneous inactivation of hepatic *Tfr2* is required to ameliorate anemia on a long term.

The erythroid response induced by BM *Tfr2* deletion is comparable in all the models analyzed. However, the magnitude of the effect is different in terms of EPO levels, erythropoiesis and EPO target genes expression between CKD and inflammation, because of the impaired renal functionality of CKD mice, which strongly reduces EPO production and the ability to properly respond to changes in the system.

Our results provide the proof of principle for the development of a TFR2-targeted therapy for the treatment of different forms of anemia. Ideally, a compound able to target specifically erythroid cells and hepatocytes in a tunable manner (e.g., based on RBCs and iron levels) would be the best option. Moreover, since *Tfr2* targeting promotes erythropoiesis without increasing endogenous EPO, this therapeutic approach is expected to be free from the off-target effects of the current treatments.

In this setting, technologies able to disrupt RNA as ASOs or small-interfering RNAs represent a promising opportunity, easily transferable to the clinics. However, obtaining effective downregulation of the target of interest within erythroid cells remains a challenging task. Indeed, the unfunctionalized ASOs we used in our experimental protocol efficiently downregulated hepatic *Tfr2*, while failed both in the spleen and in the BM, likely because of a poor uptake from erythroid cells. In agreement, when murine erythroleukemia cells were electroporated with *Tfr2*-ASOs, *Tfr2* mRNA was efficiently downregulated. In the future, this limitation might be overcome by the use of conjugated groups for organ-specific delivery (eg., cholesteryl group (Halloy *et al*, 2020), in analogy with the well-established *N*-acetylgalactosamine (GalNAc) modification used for hepatic targeting (Debacker *et al*, 2020)). However, the most appropriate strategy for erythroid delivery of oligonucleotides remains to be identified.

Of note, BM transplantation replaces not only erythroid cells, but the entire hematopoietic compartment (lymphoid and myeloid lineages). A better characterization of the possible role for TFR2 in other hematopoietic cell types, especially macrophages, is a future perspective and will be taken into account for translatable approaches.

Overall, this study proved that when TFR2 is absent in the erythroid compartment and in the liver, RBCs production and iron levels are increased and balanced, leading to anemia of CKD amelioration. During inflammation and malaria, on the other hand, BM *Tfr2* deletion alone is sufficient to ameliorate anemia, exploiting body iron stores. Thus, we propose *Tfr2* targeting as a promising tunable erythropoiesis-stimulating approach for different types of anemia.

5. MATERIALS AND METHODS

5.1 Murine models

Wild-type 8-week-old C57BL/6N and C57BL/6-Ly5.1 mice were purchased from Charles River. *Tfr2*$^{-/-}$ male mice and control littermates (both on a pure 129S2 strain and on a mixed 129S-C57BL/6N background) were as previously described (Roetto *et al*, 2010). Animals were housed under a standard 12-hour light/dark cycle in a pathogen-free animal facility of San Raffaele Scientific Institute in accordance with the EU guidelines. The animal studies were approved by the Institutional Animal Care and Use Committee of the San Raffaele Scientific Institute and by the Italian Ministry of Health.

5.2 Bone marrow transplantation

Mice with specific BM *Tfr2* deletion were obtained through bone marrow transplantation (BMT) as previously described (Nai *et al*, 2015). Bone marrow (BM) cells were harvested from 12-week-old male *Tfr2*$^{-/-}$ mice or control WT littermates (on a pure 129S2 strain, expressing the CD45.2 B-cell surface antigen). Five x 10^6 cells/mouse were i.v. injected into lethally irradiated (950 cGy in 2 doses) 8-week-old C57BL/6-Ly-5.1 male mice (expressing the CD45.1 B-cell surface antigen), obtaining animals with (*Tfr2*^{BMWT}) or without *Tfr2* (*Tfr2*^{BMKO}) in BM-derived cells. At sacrifice, donor/host chimerism was evaluated in the BM and in the spleen.

5.3 Adenine diet model of CKD

CKD was induced using a casein-based adenine-rich diet (supplied by Charles River Italia, Calco, LC) in *Tfr2*$^{-/-}$ mice and control littermates (10-week-old, on a mixed 129S-C57BL/6N background), in *Tfr2*^{BMKO} and *Tfr2*^{BMWT} (10 weeks after BMT) and in C57Bl/6N wild-type mice (10-week-old). Animals were allowed acclimatization feeding them the same, but adenine-free, diet for 1 week before starting the protocol. Then, mice were fed a diet containing 0.30% adenine for 10 days (induction phase, day 0-9), followed by a maintenance phase with 0.20% adenine until sacrifice (at day 56), as previously described (Jia *et al*, 2013).

Mice were weighted once a week, while blood was collected by tail vein puncture every 14 days for CBC and urea measurement starting from day 0. At the end of the protocol, mice were anesthetized and sacrificed by cervical dislocation. Blood was collected for hematological analysis and serum biochemistry. Kidneys, liver, spleen and BM were dissected, weighted and immediately snap-frozen for RNA and/or protein analysis, dried for tissue iron quantification or processed for histological or flow-cytometry analysis.

5.4 Antisense oligonucleotides (ASOs) treatment

ASOs were provided by Ionis Pharmaceuticals. All oligonucleotides used in these studies were 16 nucleotides in length and chemically modified with phosphorothioate in the backbone, 3 constrained ethyl residues at each terminus, and a central deoxynucleotide region of 10 residues (3-10-3 gapmer). The Applied Biosystems 380B automated DNA synthesizer (PerkinElmer Life and Analytical Sciences–Applied Biosystems) was utilized to synthesize oligonucleotides, then purified as previously described (Bennett & Swayze, 2010). ASOs were dissolved in PBS (Ca-Mg; Invitrogen) for *in vivo* experiments. Starting 2 weeks after renal damage induction, wild-type C57BL/6N mice were intraperitoneally injected with *Tfr2*-ASO or Ctrl-ASO (25mg/kg) twice a week for 1 week, for the short-term experiment, or 6 weeks, for the full 8-week-long adenine protocol. Two days after the last injection mice were sacrificed and analyzed as described above.

5.5 Murine Erythro-Leukemia cell line electroporation

Murine Erythro-Leukemia cells ($4x10^6$) were electroporated with 2 μg of Ctrl-ASOs or *Tfr2*-ASOs using Amaxa Nucleofector™ 2b (Lonza Bioscience, Morrisville, NC, USA) program Y-013 and Mirus Transfection kit (Thermo Fisher Scientific, Waltham, MA, US). Cells were then cultured in classic RPMI enriched with 10% Fetal Bovine Serum and 1% penicillin/streptomycin. Forty-eight hours after electroporation, cells were harvested for RNA extraction, using ReliaPrep™ RNA MiniPrep System (Promega Italia S.r.l., Milan, Italy), following manufacturer's recommendations.

5.6 Turpentine oil treatment

To induce anemia of inflammation, *Tfr2*^{BMKO} and *Tfr2*^{BMWT} mice were treated weekly with a sub-cutaneous injection of turpentine oil (SIGMA Aldrich, 5µl/g body weight) into the intrascapular fat pad (Nicolas *et al*, 2002) for 3 weeks, starting 10 weeks after BMT. Blood for complete blood count (CBC) was collected by tail vein puncture before starting the treatment and then every week. Two days or 2 weeks after the last injection mice were sacrificed and analyzed as described above.

5.7 Malaria infection

Eight-10 week-old C57BL6/N wild-type mice were intraperitoneally injected with frozen *Pcc*-infected RBCs, to allow accrual of the pathogen. When parasitemia reached 0.1-0-2%, mice were euthanized and blood was collected via cardiac puncture and processed as described (Spence *et al*, 2011). Then, *Tfr2*^{BMKO} and *Tfr2*^{BMWT} mice were i.p. injected with 10^5 *Pcc*-infected RBCs 10 weeks after BMT.

Blood for CBC and parasitemia evaluation was collected by tail vein puncture before starting the treatment and then every 2-4 days.

5.8 Hematological and biochemical analysis

Complete blood count was determined using the IDEXX ProCyte Dx hemocytometer (IDEXX Laboratories, Inc., Westbrook, Maine, US).

Serum iron and total iron binding capacity were determined using Fe Kit and Total Iron Binding Capacity Kit (Randox Laboratories Ltd., Crumlin, UK), according to the manufacturer's recommendations. Transferrin saturation was calculated as the ratio between serum iron and total iron binding capacity.

IL-6 and EPO levels were measured using the IL-6 Mouse Pro Quantum Immunoassay Kit (Thermo Fisher Scientific, Waltham, MA, US) and the mouse EPO Quantikine set (R&D Systems, Minneapolis, MN, US) respectively, following the manufacturer's instructions.

Urea in serum samples was quantified through a colorimetric assay using the ILab Aries analyzer and kits and controls provided by Ilab Aries (Instrumentation Laboratory, Werfen Group, Milan, Italy) at the Ospedale San Raffaele Mouse Clinic. Before each

determination, experiment precision was determined running the standard controls and the values obtained for controls were always within the expected ranges.
Parasitemia was evaluated by counting the percentage of infected over total RBCs in Giemsa-stained blood smears. Images were captured using a Leica DM5000 microscope furnished with a Leica DFC480 digital camera.

5.9 Micro-CT testing

Spine and femur were formalin-fixed for 24 hours and then conserved in 70% ethanol. Bones were cleaned from flash and then bone microarchitecture analyses were performed using VivaCT40 (Scanco Medical, Switzerland) as previously described (Rauner *et al*, 2019). The femur and the fourth lumbar vertebra were imaged at a resolution of 10.5 μm with X-ray energy of 70 kVp, 114 mA, and an integration time of 200 ms. Femur trabecular bone was assessed in the metaphysis 20 slices below the growth plate using 150 slices. In the vertebral bone, 150 slices were measured between both growth plates. The cortical bone was determined in the femoral midshaft (150 slices).

5.10 Flow cytometry analysis

BM and spleen cells were isolated, re-suspended in MACS Buffer (Miltenyi Biotec, Bergisch Gladbach, Germany) and pre-treated with Rat-anti Mouse CD16/CD32 (BD Biosciences, Franklin Lakes, NJ, US) to block unspecific Ig binding.
Cells were stained with FITC Rat Anti-Mouse TER-119 and APC rat anti-mouse CD44 (BD Biosciences, Franklin Lakes, NJ, US) for 30 min in the dark at 4°C for phenotypic analysis of erythropoiesis.
Donor/host chimerism was evaluated on BM and spleen cells from transplanted mice by using FITC-conjugated anti-mouse CD45.1 and APC–conjugated anti-mouse CD45.2 anti- bodies (BD Biosciences, Franklin Lakes, NJ, US).
Samples were acquired at FACS Canto^{TM}II (BD Biosciences, Franklin Lakes, NJ, US) and analyzed with FCS express software (De Novo Software, Pasadena, CA, US), as previously described (Nai *et al*, 2015).

5.11 Tissue iron content

Ten-20mg of dried tissue samples (65°C for 1 week) were incubated in 1 mL of acid solution (3M HCl, 0.6M trichloroacetic acid) for 20 hours at 65°C. Twenty microliters of the acid extract were added to 1 mL of working chromogen reagent (1 volume of 0.1% bathophenanthroline sulfate and 1% thioglycolic acid solution, 5 volumes of water, and 5 volumes of saturated sodium acetate) and incubated for 30 minutes at room temperature. Increasing amounts of iron ammonium sulfate were added to acid solution to generate a standard curve. The absorbance of the solutions was measured at 535 nm using a classic spectrophotometer (Bio-Rad Laboratories, Hercules, CA, US) as previously described (Nai *et al*, 2020).

5.12 Quantitative RT-PCR

RNA was extracted from kidneys, livers and spleens using the guanidinium thiocyanate–phenol–chloroform method (TriFast, Euroclone S.p.A., Pero, Italy), while from BM using a hybrid extraction method (Pedersen *et al*, 2019) which combines TriFast and ReliaPrep^{TM} RNA MiniPrep System (Promega Italia S.r.l., Milan, Italy), following manufacturer's recommendations.

RNA (1-2 μg) was retro-transcribed using the High-Capacity cDNA Reverse Transcription kit (Applied Biosystems, Thermo Fisher Scientific, Waltham, MA, US), according to the standard protocol. For quantitative RT-PCR analysis we used specific murine Assays-on-Demand products (20x) and TaqMan Master Mix (2x) (Applied Biosystems, Thermo Fisher Scientific, Waltham, MA, US) or specific murine oligos (designed using the Universal ProbeLibrary Assay Design Center by Roche and generated by MilliporeSigma, Merck group, St. Louis, MO, US) and SYBRgreen Master Mix (2x) (Applied Biosystems, Thermo Fisher Scientific, Waltham, MA, US). The reactions were run on a 7900HT Fast Real-Time PCR System (Applied Biosystems, Thermo Fisher Scientific, Waltham, MA, US). Each cDNA sample was amplified in duplicate, and the RNA level was normalized to the corresponding level of *Hprt1* or *Gapdh* mRNA. Primers used for qRT-PCR are indicated in Table 1 and Table 2.

Table 1. *Oligonucleotide primers used for qRT-PCR by TaqMan*

Transcript	**Assay Id**
Hprt1	Mm01318743_m1
Epo	Mm01202755_m1
Cd45	Mm01293575_m1
Saa1	Mm00656927_g1

Table 2. *Oligonucleotide primers used for qRT-PCR by Sybr Green*

Transcript	**Forward primer**	**Reverse primer**
Hprt1	5'- tcctcctcagaccgctttt -3'	5'- aacctggttcatcatcgctaa -3'
Gapdh	5'-tccactcacggcaaattcaa-3'	5'-tttgatgttagtggggtctcg-3'
Hamp	5'- aagcagggcagacattgcgat -3'	5'- caggatgtggctctaggctatgt -3'
Tfr2-α	5'- gccatgtttctcccggttcct -3'	5'- tggcgcgagagcttatcg -3'
Tfr2-β	5'- cctggcccctagtgtgatttc -3'	5'- tggcgcgagagcttatcg -3'
Epor	5'-gtcctcatctcgctgttgct-3	5'-atgccaggccagatcttct-3'
Erfe	5'-atggggctggagaacagc-3'	5'-tggcattgtccaagaagaca-3'
Bcl-xl	5'-tgaccacctagagccttgga-3'	5'-gctgcattgttcccgtaga-3'
Il-6	5'-cgtggaaatgagaaaagagttgtg-3'	5'-ccagtttggtagcatccatcatttct-3'
Pai-1	5'-aggatcgaggtaaacgagagc-3'	5'-gcgggctgagatgacaaa-3'
Kim-1	5'-ttggcatctgcatcgcagccc-3'	5'-gggaatgcacaaccgctgcgt-3'
Lcn2	5'-tccccctgcagccagacttcc-3'	5'-agtagcgacagccctggtcctg-3'
Nox4	5'-tcatttggctgtccctaaacg-3'	5'-aaggatgaggctgcagttgag-3'
Sod1	5'-gagacctgggcaatgtgact-3'	5'-gtttactgcgcaatcccaat-3'
Gpx1	5'-cacagtccaccgtgtatgccttc-3'	5'-accgagcaccaccagtccac-3'
Gpx4	5'-ccgtctgagccgcttactt-3'	5'-atgcacacgaaacccctgta-3'
Aldh18a1	5'-cccttcaggcaacgtcttct-3'	5'-gagggctggacacgatttga-3'

5.13 Histological analysis

Kidneys were formalin-fixed for 24 hours and paraffin-embedded. Deparaffinized tissue sections (3-4 μm) were stained with Hematoxylin/Eosin and Sirius Red solutions at the Ospedale San Raffaele Mouse Clinic for morphological analysis.

Pictures were captured using a Nikon Eclipse Ni Microscope with a Nikon DS-Fi2 Camera equipped with a Nikon DS-U3 Controller and analyzed with the Nikon NiS-Elements (version F.4.00.00) software (Nikon Corporation, Minato City, Japan) or using Leica Biosystem software (Leica Camera AG, Wetzlar, Germany).

5.14 Statistical analysis

Data are presented as mean±standard deviation (SD). Unpaired 2-tailed Student's t-test, one-way ANOVA (correction test Tukey) or two-way ANOVA for multiple comparisons (correction test Šídák) were performed using GraphPad Prism 9.0 (GraphPad). $P<0.05$ was considered statistically significant.

6. REFERENCES

Akchurin O, Sureshbabu A, Doty SB, Zhu Y-S, Patino E, Cunningham-Rundles S, Choi ME, Boskey A & Rivella S (2016) Lack of hepcidin ameliorates anemia and improves growth in an adenine-induced mouse model of chronic kidney disease. *Am J Physiol Physiol* 311: F877–F889

Akizawa T, Iwasaki M, Yamaguchi Y, Majikawa Y & Reusch M (2020) Phase 3, Randomized, Double-Blind, Active-Comparator (Darbepoetin Alfa) Study of Oral Roxadustat in CKD Patients with Anemia on Hemodialysis in Japan. *J Am Soc Nephrol* 31: 1628–1639

An X, Schulz VP, Li J, Wu K, Liu J, Xue F, Hu J, Mohandas N & Gallagher PG (2014) Global transcriptome analyses of human and murine terminal erythroid differentiation. *Blood* 123: 3466–3477

An X, Schulz VP, Mohandas N & Gallagher PG (2015) Human and murine erythropoiesis. *Curr Opin Hematol* 22: 206–211

Anderson HL, Brodsky IE & Mangalmurti NS (2018) The Evolving Erythrocyte: Red Blood Cells as Modulators of Innate Immunity. *J Immunol* 201: 1343–1351

Arezes J, Foy N, McHugh K, Sawant A, Quinkert D, Terraube V, Brinth A, Tam M, LaVallie ER, Taylor S, *et al* (2018) Erythroferrone inhibits the induction of hepcidin by BMP6. *Blood* 132: 1473–1477

Arezes J, Jung G, Gabayan V, Valore E, Ruchala P, Gulig PA, Ganz T, Nemeth E & Bulut Y (2015) Hepcidin-Induced Hypoferremia Is a Critical Host Defense Mechanism against the Siderophilic Bacterium Vibrio vulnificus. *Cell Host Microbe* 17: 47–57

Armitage AE, Eddowes LA, Gileadi U, Cole S, Spottiswoode N, Selvakumar TA, Ho L-P, Townsend ARM & Drakesmith H (2011) Hepcidin regulation by innate immune and infectious stimuli. *Blood* 118: 4129–4139

Artuso I, Lidonnici MR, Altamura S, Mandelli G, Pettinato M, Muckenthaler MU, Silvestri L, Ferrari G, Camaschella C & Nai A (2018) Transferrin receptor 2 is a potential novel therapeutic target for β-thalassemia: evidence from a murine model. *Blood* 132: 2286–2297

Aschemeyer S, Qiao B, Stefanova D, Valore E V., Sek AC, Ruwe TA, Vieth KR, Jung G, Casu C, Rivella S, *et al* (2018) Structure-function analysis of ferroportin defines the binding site and an alternative mechanism of action of hepcidin. *Blood* 131: 899–

910

Ash P, Loutit JF & Townsend KMS (1980) Osteoclasts derived from haematopoietic stem cells. *Nature* 283: 669–670

Ashby DR, Gale DP, Busbridge M, Murphy KG, Duncan ND, Cairns TD, Taube DH, Bloom SR, Tam FWK, Chapman RS, *et al* (2009) Plasma hepcidin levels are elevated but responsive to erythropoietin therapy in renal disease. *Kidney Int* 75: 976–981

Astrazeneca Press Releases (2021) Status on FDA Advisory Committee vote on roxadustat in anaemia of chronic kidney disease. *https://www.astrazeneca.com/media-centre/press-releases/2021/status-on-us-fda-advisory-committee-for-roxadustat.html*

Auer PL, Teumer A, Schick U, O'Shaughnessy A, Lo KS, Chami N, Carlson C, de Denus S, Dubé M-P, Haessler J, *et al* (2014) Rare and low-frequency coding variants in CXCR2 and other genes are associated with hematological traits. *Nat Genet* 46: 629–634

Babitt JL & Lin HY (2010) Molecular Mechanisms of Hepcidin Regulation: Implications for the Anemia of CKD. *Am J Kidney Dis* 55: 726–741

Babitt JL & Lin HY (2012) Mechanisms of anemia in CKD. *J Am Soc Nephrol* 23: 1631–1634

Barrett TD, Palomino HL, Brondstetter TI, Kanelakis KC, Wu X, Yan W, Merton KP, Schoetens F, Ma JY, Skaptason J, *et al* (2015) Prolyl hydroxylase inhibition corrects functional iron deficiency and inflammation-induced anaemia in rats. *Br J Pharmacol* 172: 4078–4088

Bennett CF & Swayze EE (2010) RNA Targeting Therapeutics: Molecular Mechanisms of Antisense Oligonucleotides as a Therapeutic Platform. *Annu Rev Pharmacol Toxicol* 50: 259–293

Besarab A, Bolton WK, Browne JK, Egrie JC, Nissenson AR, Okamoto DM, Schwab SJ & Goodkin DA (1998) The Effects of Normal as Compared with Low Hematocrit Values in Patients with Cardiac Disease Who Are Receiving Hemodialysis and Epoetin. *N Engl J Med* 339: 584–590

Besarab A & Coyne DW (2010) Iron supplementation to treat anemia in patients with chronic kidney disease. *Nat Rev Nephrol* 6: 699–710

Bhoopalan SV, Huang LJ & Weiss MJ (2020) Erythropoietin regulation of red blood cell production: from bench to bedside and back. *F1000Research* 9: 1153

Bikbov B, Purcell CA, Levey AS, Smith M, Abdoli A, Abebe M, Adebayo OM, Afarideh M, Agarwal SK, Agudelo-Botero M, *et al* (2020) Global, regional, and national burden of chronic kidney disease, 1990–2017: a systematic analysis for the Global Burden of Disease Study 2017. *Lancet* 395: 709–733

Bondurant MC & Koury MJ (1986) Anemia induces accumulation of erythropoietin mRNA in the kidney and liver. *Mol Cell Biol* 6: 2731–2733

Bunn HF (2013) Erythropoietin. *Cold Spring Harb Perspect Med* 3: a011619–a011619

Burwick N & Aktas BH (2017) The eIF2-alpha kinase HRI: a potential target beyond the red blood cell. *Expert Opin Ther Targets* 21: 1171–1177

Cairo G, Recalcati S, Mantovani A & Locati M (2011) Iron trafficking and metabolism in macrophages: contribution to the polarized phenotype. *Trends Immunol* 32: 241–247

Camaschella C, Roetto A, Calì A, De Gobbi M, Garozzo G, Carella M, Majorano N, Totaro A & Gasparini P (2000) The gene TFR2 is mutated in a new type of haemochromatosis mapping to 7q22. *Nat Genet* 25: 14–15

Canali S, Zumbrennen-Bullough KB, Core AB, Wang C-Y, Nairz M, Bouley R, Swirski FK & Babitt JL (2017) Endothelial cells produce bone morphogenetic protein 6 required for iron homeostasis in mice. *Blood* 129: 405–414

Casals-Pascual C, Kai O, Cheung JOP, Williams S, Lowe B, Nyanoti M, Williams TN, Maitland K, Molyneux M, Newton CRJC, *et al* (2006) Suppression of erythropoiesis in malarial anemia is associated with hemozoin in vitro and in vivo. *Blood* 108: 2569–2577

Cazzola M (2022) Ineffective erythropoiesis and its treatment. *Blood* 139: 2460–2470

Chen JJ (2007) Regulation of protein synthesis by the heme-regulated eIF2α kinase: Relevance to anemias. *Blood* 109: 2693–2699

Chen N, Hao C, Liu B-C, Lin H, Wang C, Xing C, Liang X, Jiang G, Liu Z, Li X, *et al* (2019) Roxadustat Treatment for Anemia in Patients Undergoing Long-Term Dialysis. *N Engl J Med* 381: 1011–1022

Chiabrando D, Marro S, Mercurio S, Giorgi C, Petrillo S, Vinchi F, Fiorito V, Fagoonee S, Camporeale A, Turco E, *et al* (2012) The mitochondrial heme exporter FLVCR1b

mediates erythroid differentiation. *J Clin Invest* 122: 4569–4579

Chiabrando D, Vinchi F, Fiorito V, Mercurio S & Tolosano E (2014) Heme in pathophysiology: a matter of scavenging, metabolism and trafficking across cell membranes. *Front Pharmacol* 5: 1–24

Clarke B (2008) Normal Bone Anatomy and Physiology. *Clin J Am Soc Nephrol* 3: S131–S139

Coffey R, Jung G, Olivera JD, Karin G, Pereira RC, Nemeth E & Ganz T (2022) Erythroid overproduction of erythroferrone causes iron overload and developmental abnormalities in mice. *Blood* 139: 439–451

Cui Y, Riedlinger G, Miyoshi K, Tang W, Li C, Deng C-X, Robinson GW & Hennighausen L (2004) Inactivation of Stat5 in Mouse Mammary Epithelium during Pregnancy Reveals Distinct Functions in Cell Proliferation, Survival, and Differentiation. *Mol Cell Biol* 24: 8037–8047

Datoo MS, Natama HM, Somé A, Bellamy D, Traoré O, Rouamba T, Tahita MC, Ido NFA, Yameogo P, Valia D, *et al* (2022) Efficacy and immunogenicity of R21/Matrix-M vaccine against clinical malaria after 2 years' follow-up in children in Burkina Faso: a phase 1/2b randomised controlled trial. *Lancet Infect Dis*

Datta HK, Ng WF, Walker JA, Tuck SP & Varanasi SS (2008) The cell biology of bone metabolism. *J Clin Pathol* 61: 577–587

Deaglio S, Capobianco A, Calì A, Bellora F, Alberti F, Righi L, Sapino A, Camaschella C & Malavasi F (2002) Structural, functional, and tissue distribution analysis of human transferrin receptor-2 by murine monoclonal antibodies and a polyclonal antiserum. *Blood* 100: 3782–3789

Debacker AJ, Voutila J, Catley M, Blakey D & Habib N (2020) Delivery of Oligonucleotides to the Liver with GalNAc: From Research to Registered Therapeutic Drug. *Mol Ther* 28: 1759–1771

Deshet-Unger N, Hiram-Bab S, Haim-Ohana Y, Mittelman M, Gabet Y & Neumann D (2016) Erythropoietin treatment in murine multiple myeloma: immune gain and bone loss. *Sci Rep* 6: 30998

Dhaliwal G, Cornett PA & Jr LMT (2004) Hemolytic Anemia. In *Am Fam Physician.* p Jun 1;69(11):2599-606. PMID: 15202694. Elsevier

Dhillon S (2019) Roxadustat: First Global Approval. *Drugs* 79: 563–572

Digicaylioglu M & Lipton SA (2001) Erythropoietin-mediated neuroprotection involves cross-talk between Jak2 and NF-κB signalling cascades. *Nature* 412: 641–647

Diwan V, Small D, Kauter K, Gobe GC & Brown L (2014) Gender differences in adenine-induced chronic kidney disease and cardiovascular complications in rats. *Am J Physiol Physiol* 307: F1169–F1178

Donovan A, Brownlie A, Zhou Y, Shepard J, Pratt SJ, Moynihan J, Paw BH, Drejer A, Barut B, Zapata A, *et al* (2000) Positional cloning of zebrafish ferroportin1 identifies a conserved vertebrate iron exporter. *Nature* 403: 776–781

Eddy AA & Fogo AB (2006) Plasminogen Activator Inhibitor-1 in Chronic Kidney Disease: Evidence and Mechanisms of Action. *J Am Soc Nephrol* 17: 2999–3012

Eggold JT & Rankin EB (2019) Erythropoiesis, EPO, macrophages, and bone. *Bone* 119: 36–41

Fathman JW, Bhattacharya D, Inlay MA, Seita J, Karsunky H & Weissman IL (2011) Identification of the earliest natural killer cell–committed progenitor in murine bone marrow. *Blood* 118: 5439–5447

Del Fattore A, Capannolo M & Rucci N (2010) Bone and bone marrow: The same organ. *Arch Biochem Biophys* 503: 28–34

Feder JN, Gnirke A, Thomas W, Tsuchihashi Z, Ruddy DA, Basava A, Dormishian F, Domingo R, Ellis MC, Fullan A, *et al* (1996) A novel MHC class I–like gene is mutated in patients with hereditary haemochromatosis. *Nat Genet* 13: 399–408

Feldman HI, Santanna J, Guo W, Furst H, Franklin E, Joffe M, Marcus S & Faich G (2002) Iron Administration and Clinical Outcomes in Hemodialysis Patients. *J Am Soc Nephrol* 13: 734–744

Ferreira A, Balla J, Jeney V, Balla G & Soares MP (2008) A central role for free heme in the pathogenesis of severe malaria: the missing link? *J Mol Med* 86: 1097–1111

Finberg KE, Heeney MM, Campagna DR, Aydınok Y, Pearson HA, Hartman KR, Mayo MM, Samuel SM, Strouse JJ, Markianos K, *et al* (2008) Mutations in TMPRSS6 cause iron-refractory iron deficiency anemia (IRIDA). *Nat Genet* 40: 569–571

Finberg KE, Whittlesey RL, Fleming MD & Andrews NC (2010) Down-regulation of Bmp/Smad signaling by Tmprss6 is required for maintenance of systemic iron homeostasis. *Blood* 115: 3817–3826

Finch C (1994) Regulators of iron balance in humans. *Blood* 84: 1697–1702

Florencio-Silva R, Sasso GRDS, Sasso-Cerri E, Simões MJ & Cerri PS (2015) Biology of Bone Tissue: Structure, Function, and Factors That Influence Bone Cells. *Biomed Res Int* 2015: 1–17

Forejtnikovà H, Vieillevoye M, Zermati Y, Lambert M, Pellegrino RM, Guihard S, Gaudry M, Camaschella C, Lacombe C, Roetto A, *et al* (2010) Transferrin receptor 2 is a component of the erythropoietin receptor complex and is required for efficient erythropoiesis. *Blood* 116: 5357–5367

Francis SE, Sullivan DJ & Goldberg and DE (1997) HEMOGLOBIN METABOLISM IN THE MALARIA PARASITE PLASMODIUM FALCIPARUM. *Annu Rev Microbiol* 51: 97–123

Fried LF, Biggs ML, Shlipak MG, Seliger S, Kestenbaum B, Stehman-Breen C, Sarnak M, Siscovick D, Harris T, Cauley J, *et al* (2007) Association of Kidney Function with Incident Hip Fracture in Older Adults. *J Am Soc Nephrol* 18: 282–286

Ganesh SK, Zakai NA, van Rooij FJA, Soranzo N, Smith A V, Nalls MA, Chen M-H, Kottgen A, Glazer NL, Dehghan A, *et al* (2009) Multiple loci influence erythrocyte phenotypes in the CHARGE Consortium. *Nat Genet* 41: 1191–1198

Ganz T (2019) Anemia of Inflammation. *N Engl J Med* 381: 1148–1157

Gluba-Brzózka A, Franczyk B, Olszewski R & Rysz J (2020) The Influence of Inflammation on Anemia in CKD Patients. *Int J Mol Sci* 21: 725

Goodnough LT, Skikne B & Brugnara C (2000) Erythropoietin, iron, and erythropoiesis. *Blood* 96: 823–833

Gozzelino R, Andrade BB, Larsen R, Luz NF, Vanoaica L, Seixas E, Coutinho A, Cardoso S, Rebelo S, Poli M, *et al* (2012) Metabolic Adaptation to Tissue Iron Overload Confers Tolerance to Malaria. *Cell Host Microbe* 12: 693–704

Gruszczyk J, Kanjee U, Chan L-J, Menant S, Malleret B, Lim NTY, Schmidt CQ, Mok Y-F, Lin K-M, Pearson RD, *et al* (2018) Transferrin receptor 1 is a reticulocyte-specific receptor for Plasmodium vivax. *Science (80-)* 359: 48–55

Gudbjartsson DF, Holm H, Indridason OS, Thorleifsson G, Edvardsson V, Sulem P, de Vegt F, D'Ancona FCH, den Heijer M, Franzson L, *et al* (2010) Association of Variants at UMOD with Chronic Kidney Disease and Kidney Stones—Role of Age and Comorbid Diseases. *PLoS Genet* 6: e1001039

Gurkan UA & Akkus O (2008) The Mechanical Environment of Bone Marrow: A

Review. *Ann Biomed Eng* 36: 1978–1991

Gwamaka M, Kurtis JD, Sorensen BE, Holte S, Morrison R, Mutabingwa TK, Fried M & Duffy PE (2012) Iron Deficiency Protects Against Severe Plasmodium falciparum Malaria and Death in Young Children. *Clin Infect Dis* 54: 1137–1144

Haase VH (2010) Hypoxic regulation of erythropoiesis and iron metabolism. *Am J Physiol Physiol* 299: F1–F13

Haase VH (2021) Hypoxia-inducible factor–prolyl hydroxylase inhibitors in the treatment of anemia of chronic kidney disease. *Kidney Int Suppl* 11: 8–25

Halloy F, Iyer PS, Ćwiek P, Ghidini A, Barman-Aksözen J, Wildner-Verhey van Wijk N, Theocharides APA, Minder EI, Schneider-Yin X, Schümperli D, *et al* (2020) Delivery of oligonucleotides to bone marrow to modulate ferrochelatase splicing in a mouse model of erythropoietic protoporphyria. *Nucleic Acids Res* 48: 4658–4671

Han A-P, Yu C, Lu L, Fujiwara Y, Browne C, Chin G, Fleming M, Leboulch P, H.Orkin S & Chen J-J (2001) Heme-regulated eIF2alpha kinase (HRI) is required for translational regulation and survival of erythroid precursors in iron deficiency. *EMBO J* 20: 6909–6918

van der Harst P, Zhang W, Mateo Leach I, Rendon A, Verweij N, Sehmi J, Paul DS, Elling U, Allayee H, Li X, *et al* (2012) Seventy-five genetic loci influencing the human red blood cell. *Nature* 492: 369–375

Hassan AMA El, Saeed AM, Fandrey J & Jelkmann W (2009) Decreased erythropoietin response in Plasmodium falciparum malaria-associated anaemia. *Eur J Haematol* 59: 299–304

Hattangadi SM, Wong P, Zhang L, Flygare J & Lodish HF (2011) From stem cell to red cell: regulation of erythropoiesis at multiple levels by multiple proteins, RNAs, and chromatin modifications. *Blood* 118: 6258–6268

Hentze MW, Muckenthaler MU, Galy B & Camaschella C (2010) Two to Tango: Regulation of Mammalian Iron Metabolism. *Cell* 142: 24–38

Higgins JM (2015) Red Blood Cell Population Dynamics. *Clin Lab Med* 35: 43–57

Hirakawa Y, Tanaka T & Nangaku M (2017) Renal Hypoxia in CKD; Pathophysiology and Detecting Methods. *Front Physiol* 8: 1–10

Hiram-Bab S, Liron T, Deshet-Unger N, Mittelman M, Gassmann M, Rauner M, Franke K, Wielockx B, Neumann D & Gabet Y (2015) Erythropoietin directly stimulates

osteoclast precursors and induces bone loss. *FASEB J* 29: 1890–1900

Holstein JH, Orth M, Scheuer C, Tami A, Becker SC, Garcia P, Histing T, Mörsdorf P, Klein M, Pohlemann T, *et al* (2011) Erythropoietin stimulates bone formation, cell proliferation, and angiogenesis in a femoral segmental defect model in mice. *Bone* 49: 1037–1045

Howard CT, McKakpo US, Quakyi IA, Bosompem KM, Addison EA, Sun K, Sullivan D & Semba RD (2007) Relationship of Hepcidin with Parasitemia and Anemia among Patients with Uncomplicated Plasmodium falciparum Malaria in Ghana. *Am J Trop Med Hyg* 77: 623–626

Iseki A, Morita Y, Nakauchi H & Ema H (2008) Hematopoietic Stem Cells in the Mouse Spleen. *Blood* 112: 2421–2421

Jia T, Olauson H, Lindberg K, Amin R, Edvardsson K, Lindholm B, Andersson G, Wernerson A, Sabbagh Y, Schiavi S, *et al* (2013) A novel model of adenine-induced tubulointerstitial nephropathy in mice. *BMC Nephrol* 14: 116

Johnson MB, Chen J, Murchison N, Green FA & Enns CA (2007) Transferrin Receptor 2: Evidence for Ligand-induced Stabilization and Redirection to a Recycling Pathway. *Mol Biol Cell* 18: 743–754

Johnson MB & Enns CA (2004) Diferric transferrin regulates transferrin receptor 2 protein stability. *Blood* 104: 4287–4293

Kanamori Y, Murakami M, Matsui T & Funaba M (2014) The regulation of hepcidin expression by serum treatment: Requirements of the BMP response element and STAT- and AP-1-binding sites. *Gene* 551: 119–126

Katsarou A & Pantopoulos K (2020) Basics and principles of cellular and systemic iron homeostasis. *Mol Aspects Med* 75: 100866

Kautz L, Jung G, Du X, Gabayan V, Chapman J, Nasoff M, Nemeth E & Ganz T (2015) Erythroferrone contributes to hepcidin suppression and iron overload in a mouse model of β-thalassemia. *Blood* 126: 2031–2037

Kautz L, Jung G, Valore E V, Rivella S, Nemeth E & Ganz T (2014) Identification of erythroferrone as an erythroid regulator of iron metabolism. *Nat Genet* 46: 678–684

Kautz L, Meynard D, Monnier A, Darnaud V, Bouvet R, Wang R-H, Deng C, Vaulont S, Mosser J, Coppin H, *et al* (2008) Iron regulates phosphorylation of Smad1/5/8 and gene expression of Bmp6, Smad7, Id1, and Atoh8 in the mouse liver. *Blood* 112:

1503–1509

Kawabata H, Fleming RE, Gui D, Moon SY, Saitoh T, O'Kelly J, Umehara Y, Wano Y, Said JW & Koeffler HP (2005) Expression of hepcidin is down-regulated in TfR2 mutant mice manifesting a phenotype of hereditary hemochromatosis. *Blood* 105: 376–381

Kawabata H, Germain RS, Ikezoe T, Tong X, Green EM, Gombart AF & Koeffler HP (2001) Regulation of expression of murine transferrin receptor 2. *Blood* 98: 1949–1954

Kawabata H, Germain RS, Vuong PT, Nakamaki T, Said JW & Koeffler HP (2000) Transferrin Receptor 2-α Supports Cell Growth Both in Iron-chelated Cultured Cells and in Vivo. *J Biol Chem* 275: 16618–16625

Kawabata H, Yang R, Hirama T, Vuong PT, Kawano S, Gombart AF & Koeffler HP (1999) Molecular Cloning of Transferrin Receptor 2. *J Biol Chem* 274: 20826–20832

Kertesz N, Wu J, Chen THP, Sucov HM & Wu H (2004) The role of erythropoietin in regulating angiogenesis. *Dev Biol* 276: 101–110

Kim A, Fung E, Parikh SG, Valore E V., Gabayan V, Nemeth E & Ganz T (2014) A mouse model of anemia of inflammation: Complex pathogenesis with partial dependence on hepcidin. *Blood* 123: 1129–1136

Kimachi M, Fukuma S, Yamazaki S, Yamamoto Y, Akizawa T, Akiba T, Saito A & Fukuhara S (2015) Minor Elevation in C-Reactive Protein Levels Predicts Incidence of Erythropoiesis-Stimulating Agent Hyporesponsiveness among Hemodialysis Patients. *Nephron* 131: 123–130

Koch PS, Olsavszky V, Ulbrich F, Sticht C, Demory A, Leibing T, Henzler T, Meyer M, Zierow J, Schneider S, *et al* (2017) Angiocrine Bmp2 signaling in murine liver controls normal iron homeostasis. *Blood* 129: 415–419

Korolnek T & Hamza I (2015) Macrophages and iron trafficking at the birth and death of red cells. *Blood* 125: 2893–2897

Köttgen A, Cornec-Le Gall E, Halbritter J, Kiryluk K, Mallett AJ, Parekh RS, Rasouly HM, Sampson MG, Tin A, Antignac C, *et al* (2022) Genetics in chronic kidney disease: conclusions from a Kidney Disease: Improving Global Outcomes (KDIGO) Controversies Conference. *Kidney Int* 101: 1126–1141

Koury S, Bondurant M & Koury M (1988) Localization of erythropoietin synthesizing cells in murine kidneys by in situ hybridization. *Blood* 71: 524–527

Koury S, Koury M, Bondurant M, Caro J & Graber S (1989) Quantitation of erythropoietin-producing cells in kidneys of mice by in situ hybridization: correlation with hematocrit, renal erythropoietin mRNA, and serum erythropoietin concentration. *Blood* 74: 645–651

Kovesdy CP, Trivedi BK, Kalantar-Zadeh K & Anderson JE (2006) Association of anemia with outcomes in men with moderate and severe chronic kidney disease. *Kidney Int* 69: 560–564

Kuhn V, Diederich L, Keller TCS, Kramer CM, Lückstädt W, Panknin C, Suvorava T, Isakson BE, Kelm M & Cortese-Krott MM (2017) Red Blood Cell Function and Dysfunction: Redox Regulation, Nitric Oxide Metabolism, Anemia. *Antioxidants Redox Signal* 26: 718–742

Laishram DD, Sutton PL, Nanda N, Sharma VL, Sobti RC, Carlton JM & Joshi H (2012) The complexities of malaria disease manifestations with a focus on asymptomatic malaria. *Malar J* 11: 29

Lam LKM, Murphy S, Kokkinaki D, Venosa A, Sherrill-Mix S, Casu C, Rivella S, Weiner A, Park J, Shin S, *et al* (2021) DNA binding to TLR9 expressed by red blood cells promotes innate immune activation and anemia. *Sci Transl Med* 13

Lamikanra AA, Brown D, Potocnik A, Casals-Pascual C, Langhorne J & Roberts DJ (2007) Malarial anemia: of mice and men. *Blood* 110: 18–28

Langdon JM, Yates SC, Femnou LK, McCranor BJ, Cheadle C, Xue Q, Vaulont S, Civin CI, Walston JD & Roy CN (2014) Hepcidin-dependent and hepcidin-independent regulation of erythropoiesis in a mouse model of anemia of chronic inflammation. *Am J Hematol* 89: 470–479

Latour C, Wlodarczyk MF, Jung G, Gineste A, Blanchard N, Ganz T, Roth M-P, Coppin H & Kautz L (2017) Erythroferrone contributes to hepcidin repression in a mouse model of malarial anemia. *Haematologica* 102: 60–68

Layoun A, Samba-Mondonga M, Fragoso G, Calvé A & Santos MM (2018) MyD88 Adaptor Protein Is Required for Appropriate Hepcidin Induction in Response to Dietary Iron Overload in Mice. *Front Physiol* 9

Lee P, Peng H, Gelbart T, Wang L & Beutler E (2005) Regulation of hepcidin

transcription by interleukin-1 and interleukin-6. *Proc Natl Acad Sci* 102: 1906–1910

Levin D, Ranu RS, Ernst V & London IM (1976) Regulation of protein synthesis in reticulocyte lysates: phosphorylation of methionyl-tRNAf binding factor by protein kinase activity of translational inhibitor isolated from hemedeficient lysates. *Proc Natl Acad Sci* 73: 3112–3116

Libregts SF, Gutiérrez L, de Bruin AM, Wensveen FM, Papadopoulos P, van Ijcken W, Özgür Z, Philipsen S & Nolte MA (2011) Chronic IFN-γ production in mice induces anemia by reducing erythrocyte life span and inhibiting erythropoiesis through an IRF-1/PU.1 axis. *Blood* 118: 2578–2588

Lin L, Valore E V., Nemeth E, Goodnough JB, Gabayan V & Ganz T (2007) Iron transferrin regulates hepcidin synthesis in primary hepatocyte culture through hemojuvelin and BMP2/4. *Blood* 110: 2182–2189

Lo KS, Wilson JG, Lange LA, Folsom AR, Galarneau G, Ganesh SK, Grant SFA, Keating BJ, McCarroll SA, Mohler III ER, *et al* (2011) Genetic association analysis highlights new loci that modulate hematological trait variation in Caucasians and African Americans. *Hum Genet* 129: 307–317

Macdougall IC & Cooper A (2002) The inflammatory response and epoetin sensitivity. *Nephrol Dial Transplant* 17: 48–52

Mancias JD, Pontano Vaites L, Nissim S, Biancur DE, Kim AJ, Wang X, Liu Y, Goessling W, Kimmelman AC & Harper JW (2015) Ferritinophagy via NCOA4 is required for erythropoiesis and is regulated by iron dependent HERC2-mediated proteolysis. *Elife* 4: 1–19

Mancias JD, Wang X, Gygi SP, Harper JW & Kimmelman AC (2014) Quantitative proteomics identifies NCOA4 as the cargo receptor mediating ferritinophagy. *Nature* 509: 105–109

Manucha W, Oliveros L, Carrizo L, Seltzer A & Vallés P (2004) Losartan modulation on NOS isoforms and COX-2 expression in early renal fibrogenesis in unilateral obstruction. *Kidney Int* 65: 2091–2107

de Mast Q, Nadjm B, Reyburn H, Kemna EHJM, Amos B, Laarakkers CMM, Silalye S, Verhoef H, Sauerwein RW, Swinkels DW, *et al* (2009) Assessment of Urinary Concentrations of Hepcidin Provides Novel Insight into Disturbances in Iron Homeostasis during Malarial Infection. *J Infect Dis* 199: 253–262

de Mast Q, Syafruddin D, Keijmel S, Riekerink TO, Deky O, Asih PB, Swinkels DW & van der Ven AJ (2010) Increased serum hepcidin and alterations in blood iron parameters associated with asymptomatic P. falciparum and P. vivax malaria. *Haematologica* 95: 1068–1074

Mastrogiannaki M, Matak P, Keith B, Simon MC, Vaulont S & Peyssonnaux C (2009) HIF-2α, but not HIF-1α, promotes iron absorption in mice. *J Clin Invest* 119: 1159–1166

Matsuo S, Ogawa M, Muckenthaler MU, Mizui Y, Sasaki S, Fujimura T, Takizawa M, Ariga N, Ozaki H, Sakaguchi M, *et al* (2015) Hepatocyte Nuclear Factor 4α Controls Iron Metabolism and Regulates Transferrin Receptor 2 in Mouse Liver. *J Biol Chem* 290: 30855–30865

Maxwell PH, Osmond MK, Pugh CW, Heryet A, Nicholls LG, Tan CC, Doe BG, Ferguson DJP, Johnson MH & Ratcliffe PJ (1993) Identification of the renal erythropoietin-producing cells using transgenic mice. *Kidney Int* 44: 1149–1162

McGonigle RJS, Wallin JD, Shadduck RK & Fisher JW (1984) Erythropoietin deficiency and inhibition of erythropoiesis in renal insufficiency. *Kidney Int* 25: 437–444

McKie AT, Marciani P, Rolfs A, Brennan K, Wehr K, Barrow D, Miret S, Bomford A, Peters TJ, Farzaneh F, *et al* (2000) A Novel Duodenal Iron-Regulated Transporter, IREG1, Implicated in the Basolateral Transfer of Iron to the Circulation. *Mol Cell* 5: 299–309

Means RJ & Krantz S (1991) Inhibition of human erythroid colony-forming units by gamma interferon can be corrected by recombinant human erythropoietin [see comments]. *Blood* 78: 2564–2567

Means RT, Dessypris EN & Krantz SB (1992) Inhibition of human erythroid colony-forming units by interleukin-1 is mediated by gamma interferon. *J Cell Physiol* 150: 59–64

Metzger CE, Swallow EA, Stacy AJ & Allen MR (2021) Adenine-induced chronic kidney disease induces a similar skeletal phenotype in male and female C57BL/6 mice with more severe deficits in cortical bone properties of male mice. *PLoS One* 16: e0250438

Di Modica SM, Tanzi E, Olivari V, Lidonnici MR, Pettinato M, Pagani A, Tiboni F, Furiosi V, Silvestri L, Ferrari G, *et al* (2022) Transferrin receptor 2 (Tfr2) genetic

deletion makes transfusion-independent a murine model of transfusion-dependent β-thalassemia. *Am J Hematol* 97: 1324–1336

Morceau F, Dicato M & Diederich M (2009) Pro-Inflammatory Cytokine-Mediated Anemia: Regarding Molecular Mechanisms of Erythropoiesis. *Mediators Inflamm* 2009: 1–11

Morgan MJ & Liu Z (2011) Crosstalk of reactive oxygen species and NF-κB signaling. *Cell Res* 21: 103–115

Muckenthaler MU, Rivella S, Hentze MW & Galy B (2017) A Red Carpet for Iron Metabolism. *Cell* 168: 344–361

Mujais SK, Story K, Brouillette J, Takano T, Soroka S, Franek C, Mendelssohn D & Finkelstein FO (2009) Health-related Quality of Life in CKD Patients: Correlates and Evolution over Time. *Clin J Am Soc Nephrol* 4: 1293–1301

Mulay SR, Eberhard JN, Pfann V, Marschner JA, Darisipudi MN, Daniel C, Romoli S, Desai J, Grigorescu M, Kumar S V., *et al* (2016) Oxalate-induced chronic kidney disease with its uremic and cardiovascular complications in C57BL/6 mice. *Am J Physiol Physiol* 310: F785–F795

Nai A, Lidonnici MR, Rausa M, Mandelli G, Pagani A, Silvestri L, Ferrari G & Camaschella C (2015) The second transferrin receptor regulates red blood cell production in mice. *Blood* 125: 1170–1179

Nai A, Pellegrino RM, Rausa M, Pagani A, Boero M, Silvestri L, Saglio G, Roetto A & Camaschella C (2014) The erythroid function of transferrin receptor 2 revealed by Tmprss6 inactivation in different models of transferrin receptor 2 knockout mice. *Haematologica* 99: 1016–1021

Nai A, Rubio A, Campanella A, Gourbeyre O, Artuso I, Bordini J, Gineste A, Latour C, Besson-Fournier C, Lin HY, *et al* (2016) Limiting hepatic Bmp-Smad signaling by matriptase-2 is required for erythropoietin-mediated hepcidin suppression in mice. *Blood* 127: 2327–2336

Nai, Lidonnici, Federico, Pettinato, Olivari, Carrillo, Geninatti Crich, Ferrari, Camaschella, Silvestri, *et al* (2020) NCOA4-mediated ferritinophagy in macrophages is crucial to sustain erythropoiesis in mice. *Haematologica* 106: 795–805

Nakagawa S, Nishihara K, Miyata H, Shinke H, Tomita E, Kajiwara M, Matsubara T,

Iehara N, Igarashi Y, Yamada H, *et al* (2015) Molecular Markers of Tubulointerstitial Fibrosis and Tubular Cell Damage in Patients with Chronic Kidney Disease. *PLoS One* 10: e0136994

Nakamura H (2007) Morphology, Function, and Differentiation of Bone Cells. *J Hard Tissue Biol* 16: 15–22

Nakatani S, Nakatani A, Ishimura E, Toi N, Tsuda A, Mori K, Emoto M, Hirayama Y, Saito A & Inaba M (2018) Urinary Iron Excretion is Associated with Urinary Full-Length Megalin and Renal Oxidative Stress in Chronic Kidney Disease. *Kidney Blood Press Res* 43: 458–470

National Kidney Foundation (2002) K/DOQI clinical practice guidelines for chronic kidney disease: evaluation, classification, and stratification

Nemeth E, Rivera S, Gabayan V, Keller C, Taudorf S, Pedersen BK & Ganz T (2004a) IL-6 mediates hypoferremia of inflammation by inducing the synthesis of the iron regulatory hormone hepcidin. *J Clin Invest* 113: 1271–1276

Nemeth E, Roetto A, Garozzo G, Ganz T & Camaschella C (2005) Hepcidin is decreased in TFR2 hemochromatosis. *Blood* 105: 1803–1806

Nemeth E, Tuttle MS, Powelson J, Vaughn MB, Donovan A, Ward DM, Ganz T & Kaplan J (2004b) Hepcidin Regulates Cellular Iron Efflux by Binding to Ferroportin and Inducing Its Internalization. *Science (80-)* 306: 2090–2093

Nicolas G, Chauvet C, Viatte L, Danan JL, Bigard X, Devaux I, Beaumont C, Kahn A & Vaulont S (2002) The gene encoding the iron regulatory peptide hepcidin is regulated by anemia, hypoxia, and inflammation. *J Clin Invest* 110: 1037–1044

Pagani A, Vieillevoye M, Nai A, Rausa M, Ladli M, Lacombe C, Mayeux P, Verdier F, Camaschella C & Silvestri L (2015) Regulation of cell surface transferrin receptor-2 by iron-dependent cleavage and release of a soluble form. *Haematologica* 100: 458–465

Palaka E, Grandy S, van Haalen H, McEwan P & Darlington O (2020) The Impact of CKD Anaemia on Patients: Incidence, Risk Factors, and Clinical Outcomes—A Systematic Literature Review. *Int J Nephrol* 2020: 1–21

Palis J (2014) Primitive and definitive erythropoiesis in mammals. *Front Physiol* 5: 1–9

Papanikolaou G, Samuels ME, Ludwig EH, MacDonald MLE, Franchini PL, Dubé M-P, Andres L, MacFarlane J, Sakellaropoulos N, Politou M, *et al* (2004) Mutations in

HFE2 cause iron overload in chromosome 1q–linked juvenile hemochromatosis. *Nat Genet* 36: 77–82

Pedersen KB, Williams A, Watt J & Ronis MJ (2019) Improved method for isolating high-quality RNA from mouse bone with RNAlater at room temperature. *Bone Reports* 11: 100211

Pervaiz S, Taneja R & Ghaffari S (2009) Oxidative Stress Regulation of Stem and Progenitor Cells. *Antioxid Redox Signal* 11: 2777–2789

Pigeon C, Ilyin G, Courselaud B, Leroyer P, Turlin B, Brissot P & Loréal O (2001) A New Mouse Liver-specific Gene, Encoding a Protein Homologous to Human Antimicrobial Peptide Hepcidin, Is Overexpressed during Iron Overload. *J Biol Chem* 276: 7811–7819

Pimentel A, Ureña-Torres P, Bover J, Luis Fernandez-Martín J & Cohen-Solal M (2021) Bone Fragility Fractures in CKD Patients. *Calcif Tissue Int* 108: 539–550

Pittenger MF, Mackay AM, Beck SC, Jaiswal RK, Douglas R, Mosca JD, Moorman MA, Simonetti DW, Craig S & Marshak DR (1999) Multilineage Potential of Adult Human Mesenchymal Stem Cells. *Science (80-)* 284: 143–147

Porto ML, Rodrigues BP, Menezes TN, Ceschim SL, Casarini DE, Gava AL, Pereira TMC, Vasquez EC, Campagnaro BP & Meyrelles SS (2015) Reactive oxygen species contribute to dysfunction of bone marrow hematopoietic stem cells in aged C57BL/6 J mice. *J Biomed Sci* 22: 97

Prince OD, Langdon JM, Layman AJ, Prince IC, Sabogal M, Mak HH, Berger AE, Cheadle C, Chrest FJ, Yu Q, *et al* (2012) Late stage erythroid precursor production is impaired in mice with chronic inflammation. *Haematologica* 97: 1648–1656

Rankin EB, Biju MP, Liu Q, Unger TL, Rha J, Johnson RS, Simon MC, Keith B & Haase VH (2007) Hypoxia-inducible factor–2 (HIF-2) regulates hepatic erythropoietin in vivo. *J Clin Invest* 117: 1068–1077

Rauner M, Baschant U, Roetto A, Pellegrino RM, Rother S, Salbach-Hirsch J, Weidner H, Hintze V, Campbell G, Petzold A, *et al* (2019) Transferrin receptor 2 controls bone mass and pathological bone formation via BMP and Wnt signalling. *Nat Metab* 1: 111–124

Recalcati S, Locati M, Marini A, Santambrogio P, Zaninotto F, De Pizzol M, Zammataro L, Girelli D & Cairo G (2010) Differential regulation of iron homeostasis during

human macrophage polarized activation. *Eur J Immunol* 40: 824–835

Regidor DL, Kopple JD, Kovesdy CP, Kilpatrick RD, McAllister CJ, Aronovitz J, Greenland S & Kalantar-Zadeh K (2006) Associations between Changes in Hemoglobin and Administered Erythropoiesis-Stimulating Agent and Survival in Hemodialysis Patients. *J Am Soc Nephrol* 17: 1181–1191

Rishi G, Secondes ES, Wallace DF & Subramaniam VN (2016) Normal systemic iron homeostasis in mice with macrophage-specific deletion of transferrin receptor 2. *Am J Physiol Liver Physiol* 310: G171–G180

Rivera S & Ganz T (2009) Animal Models of Anemia of Inflammation. *Semin Hematol* 46: 351–357

Robb A & Wessling-Resnick M (2004) Regulation of transferrin receptor 2 protein levels by transferrin. *Blood* 104: 4294–4299

Robling AG, Castillo AB & Turner CH (2006) BIOMECHANICAL AND MOLECULAR REGULATION OF BONE REMODELING. *Annu Rev Biomed Eng* 8: 455–498

Roetto A, Di Cunto F, Pellegrino RM, Hirsch E, Azzolino O, Bondi A, Defilippi I, Carturan S, Miniscalco B, Riondato F, *et al* (2010) Comparison of 3 Tfr2-deficient murine models suggests distinct functions for Tfr2-α and Tfr2-β isoforms in different tissues. *Blood* 115: 3382–3389

Roetto A, Papanikolaou G, Politou M, Alberti F, Girelli D, Christakis J, Loukopoulos D & Camaschella C (2003) Mutant antimicrobial peptide hepcidin is associated with severe juvenile hemochromatosis. *Nat Genet* 33: 21–22

Sazawal S, Black RE, Ramsan M, Chwaya HM, Stoltzfus RJ, Dutta A, Dhingra U, Kabole I, Deb S, Othman MK, *et al* (2006) Effects of routine prophylactic supplementation with iron and folic acid on admission to hospital and mortality in preschool children in a high malaria transmission setting: community-based, randomised, placebo-controlled trial. *Lancet* 367: 133–143

Schwartz AJ, Das NK, Ramakrishnan SK, Jain C, Jurkovic MT, Wu J, Nemeth E, Lakhal-Littleton S, Colacino JA & Shah YM (2018) Hepatic hepcidin/intestinal HIF-2α axis maintains iron absorption during iron deficiency and overload. *J Clin Invest* 129: 336–348

Schwörer S, Berisa M, Violante S, Qin W, Zhu J, Hendrickson RC, Cross JR & Thompson

CB (2020) Proline biosynthesis is a vent for TGFβ-induced mitochondrial redox stress. *EMBO J* 39: 1–20

Seeley TW, Sternlicht MD, Klaus SJ, Neff TB & Liu DY (2017) Induction of erythropoiesis by hypoxia-inducible factor prolyl hydroxylase inhibitors without promotion of tumor initiation, progression, or metastasis in a VEGF-sensitive model of spontaneous breast cancer. *Hypoxia* Volume 5: 1–9

Seixas E, Gozzelino R, Chora Â, Ferreira A, Silva G, Larsen R, Rebelo S, Penido C, Smith NR, Coutinho A, *et al* (2009) Heme oxygenase-1 affords protection against noncerebral forms of severe malaria. *Proc Natl Acad Sci* 106: 15837–15842

Shah YM, Matsubara T, Ito S, Yim S-H & Gonzalez FJ (2009) Intestinal Hypoxia-Inducible Transcription Factors Are Essential for Iron Absorption following Iron Deficiency. *Cell Metab* 9: 152–164

Shah YM & Xie L (2014) Hypoxia-Inducible Factors Link Iron Homeostasis and Erythropoiesis. *Gastroenterology* 146: 630–642

Shih H-M, Wu C-J & Lin S-L (2018) Physiology and pathophysiology of renal erythropoietin-producing cells. *J Formos Med Assoc* 117: 955–963

Shimamura T & Morrison AB (1975) A progressive glomerulosclerosis occurring in partial five-sixths nephrectomized rats. *Am J Pathol*

Shiozawa Y, Jung Y, Ziegler AM, Pedersen EA, Wang J, Wang Z, Song J, Wang J, Lee CH, Sud S, *et al* (2010) Erythropoietin Couples Hematopoiesis with Bone Formation. *PLoS One* 5: e10853

Silva M, Grillot D, Benito A, Richard C, Nunez G & Fernandez-Luna J (1996) Erythropoietin can promote erythroid progenitor survival by repressing apoptosis through Bcl-XL and Bcl-2. *Blood* 88: 1576–1582

Silvestri L, Nai A, Dulja A & Pagani A (2019) Hepcidin and the BMP-SMAD pathway: An unexpected liaison. In *Vitamins and Hormones* pp 71–99. Elsevier Inc.

Silvestri L, Pagani A & Camaschella C (2008a) Furin-mediated release of soluble hemojuvelin: a new link between hypoxia and iron homeostasis. *Blood* 111: 924–931

Silvestri L, Pagani A, Nai A, De Domenico I, Kaplan J & Camaschella C (2008b) The Serine Protease Matriptase-2 (TMPRSS6) Inhibits Hepcidin Activation by Cleaving Membrane Hemojuvelin. *Cell Metab* 8: 502–511

Smith K (2003) The cardiovascular effects of erythropoietin. *Cardiovasc Res* 59: 538–548

Soares MP & Hamza I (2016) Macrophages and Iron Metabolism. *Immunity* 44: 492–504

Socolovsky M, Fallon AEJ, Wang S, Brugnara C & Lodish HF (1999) Fetal Anemia and Apoptosis of Red Cell Progenitors in Stat5a−/−5b−/− Mice. *Cell* 98: 181–191

Soofi S, Cousens S, Iqbal SP, Akhund T, Khan J, Ahmed I, Zaidi AK & Bhutta ZA (2013) Effect of provision of daily zinc and iron with several micronutrients on growth and morbidity among young children in Pakistan: a cluster-randomised trial. *Lancet* 382: 29–40

Soranzo N, Spector TD, Mangino M, Kühnel B, Rendon A, Teumer A, Willenborg C, Wright B, Chen L, Li M, *et al* (2009) A genome-wide meta-analysis identifies 22 loci associated with eight hematological parameters in the HaemGen consortium. *Nat Genet* 41: 1182–1190

Souma T, Yamazaki S, Moriguchi T, Suzuki N, Hirano I, Pan X, Minegishi N, Abe M, Kiyomoto H, Ito S, *et al* (2013) Plasticity of Renal Erythropoietin-Producing Cells Governs Fibrosis. *J Am Soc Nephrol* 24: 1599–1616

Spence PJ, Cunningham D, Jarra W, Lawton J, Langhorne J & Thompson J (2011) Transformation of the rodent malaria parasite Plasmodium chabaudi. *Nat Protoc* 6: 553–561

Spence PJ, Jarra W, Lévy P, Reid AJ, Chappell L, Brugat T, Sanders M, Berriman M & Langhorne J (2013) Vector transmission regulates immune control of Plasmodium virulence. *Nature* 498: 228–231

Sukumaran A, Venkatraman A & Jacob M (2012) Inflammation-induced effects on iron-related proteins in splenic macrophages and the liver in mice. *Blood Cells, Mol Dis* 49: 11–19

Thorp ML, Johnson ES, Yang X, Petrik AF, Platt R & Smith DH (2009) Effect of anaemia on mortality, cardiovascular hospitalizations and end-stage renal disease among patients with chronic kidney disease. *Nephrology* 14: 240–246

Unger EF, Thompson AM, Blank MJ & Temple R (2010) Erythropoiesis-Stimulating Agents — Time for a Reevaluation. *N Engl J Med* 362: 189–192

Verga Falzacappa MV, Vujic Spasic M, Kessler R, Stolte J, Hentze MW & Muckenthaler MU (2007) STAT3 mediates hepatic hepcidin expression and its inflammatory

stimulation. *Blood* 109: 353–358

Vogiatzi MG, Macklin EA, Fung EB, Cheung AM, Vichinsky E, Olivieri N, Kirby M, Kwiatkowski JL, Cunningham M, Holm IA, *et al* (2009) Bone Disease in Thalassemia: A Frequent and Still Unresolved Problem. *J Bone Miner Res* 24: 543–557

Wallace DF (2005) First phenotypic description of transferrin receptor 2 knockout mouse, and the role of hepcidin. *Gut* 54: 980–986

Wan L, Zhang F, He Q, Tsang WP, Lu L, Li Q, Wu Z, Qiu G, Zhou G & Wan C (2014) EPO Promotes Bone Repair through Enhanced Cartilaginous Callus Formation and Angiogenesis. *PLoS One* 9: e102010

Wang M, Xin H, Tang W, Li Y, Zhang Z, Fan L, Miao L, Tan B, Wang X & Zhu YZ (2017) AMPK Serves as a Therapeutic Target Against Anemia of Inflammation. *Antioxid Redox Signal* 27: 251–268

Warnecke C, Zaborowska Z, Kurreck J, Erdmann VA, Frei U, Wiesener M & Eckardt K (2004) Differentiating the functional role of hypoxia-inducible factor (HIF)-1α and HIF-2α (EPAS-1) by the use of RNA interference: erythropoietin is a HIF-2α target gene in Hep3B and Kelly cells. *FASEB J* 18: 1462–1464

Watowich SS (2011) The Erythropoietin Receptor. *J Investig Med* 59: 1067–1072

Wei K, Yin Z & Xie Y (2016) Roles of the kidney in the formation, remodeling and repair of bone. *J Nephrol* 29: 349–357

Weiss G, Ganz T & Goodnough LT (2019) Anemia of inflammation. *Blood* 133: 40–50

Weiss G & Goodnough LT (2005) Anemia of Chronic Disease. *N Engl J Med* 352: 1011–1023

Wenger RH & Kurtz A (2011) Erythropoietin. In *Comprehensive Physiology* pp 1759–1794. Wiley

West AP, Bennett MJ, Sellers VM, Andrews NC, Enns CA & Bjorkman PJ (2000) Comparison of the Interactions of Transferrin Receptor and Transferrin Receptor 2 with Transferrin and the Hereditary Hemochromatosis Protein HFE. *J Biol Chem* 275: 38135–38138

White NJ (2018) Anaemia and malaria. *Malar J* 17: 371

WHO Anemia. *https://www.who.int/health-topics/anaemia#tab=tab_1*

WHO (2021) Word Malaria Report 2021

Yang H-C, Zuo Y & Fogo AB (2010) Models of chronic kidney disease. *Drug Discov Today Dis Model* 7: 13–19

Yeh T-L, Leissing TM, Abboud MI, Thinnes CC, Atasoylu O, Holt-Martyn JP, Zhang D, Tumber A, Lippl K, Lohans CT, *et al* (2017) Molecular and cellular mechanisms of HIF prolyl hydroxylase inhibitors in clinical trials. *Chem Sci* 8: 7651–7668

Yokozawa T, Oura H & Okada T (1982) Metabolic effects of dietary purine in rats. *J Nutr Sci Vitaminol (Tokyo)* 28: 519–526

Zhang H & Sun S-C (2015) NF-κB in inflammation and renal diseases. *Cell Biosci* 5: 63

Zimmermann MB, Troesch B, Biebinger R, Egli I, Zeder C & Hurrell RF (2009) Plasma hepcidin is a modest predictor of dietary iron bioavailability in humans, whereas oral iron loading, measured by stable-isotope appearance curves, increases plasma hepcidin. *Am J Clin Nutr* 90: 1280–1287

Zivot A, Lipton JM, Narla A & Blanc L (2018) Erythropoiesis: insights into pathophysiology and treatments in 2017. *Mol Med* 24: 11